Alma Mater Studiorum – Università di Bologna
in cotutela con École Nationale Supérieure d'Arts et Métiers

DOTTORATO DI RICERCA IN

INGEGNERIA BIOMEDICA, ELETTRICA E DEI SISTEMI

Ciclo XXXIII

Settore concorsuale: 09/E2

Settore Scientifico Disciplinare: Sistemi Elettrici per l'Energia (ING-IND/33)

AGING ASSESSMENT OF POLYETHYLENE-BASED INSULATED LOW-VOLTAGE CABLES FOR NUCLEAR APPLICATIONS

Presentata da: Simone Vincenzo Suraci

Coordinatore Dottorato

Prof. Daniele Vigo

Supervisore

Prof. Davide Fabiani

Supervisore

Prof. Xavier Colin

Esame finale anno 2021

Mutat enim mundi naturam totius aetas,

Ex alioque alius status excipere omnia debet,

Nec manet ulla sui similis res: omnia migrant,

Omnia commutat natura et vertere cogit.

For time changes the nature of the whole world,
and one state of things must pass into another,
and nothing remains as it was: all things move,
all are changed by nature and compelled to alter.

De Rerum Natura, Tito Lucrezio Caro

TABLE OF CONTENTS

ABSTRACT

This thesis aims at investigating the evolution of physico-chemical and electrical properties relevant to low-voltage power cables for nuclear application when subjected to typical nuclear power plant (NPP) environments i.e., to gamma radiation and high temperature.

This research is part of the European Project Horizon 2020 TeaM Cables, which aims at providing a novel methodology for efficient and reliable NPP cable aging management to NPP operators.

The analyzed samples consist of both coaxial and twisted pair cables with different polymeric compounds used as primary insulation. Insulating materials are based on the same silane cross-linked polyethylene matrix with different additives and fillers. In particular, two kinds of antioxidants (primary and secondary antioxidants) and flame retardants (alumina try-hydroxide) with different amounts have been added to the base polymer.

In order to characterize the material response to the environmental stresses, various experimental techniques have been used. These characterizations range from the microscale chemical response e.g. by FTIR, OIT and DSC, to the macroscale electrical and mechanical behavior.

A significant part of this Thesis is given to the correlation of the response to aging among the different measured properties. It has been shown that it could be possible to connect both the chemical and mechanical properties of the investigated XLPE cables with the electrical ones. In particular, the high-frequency dielectric response allows an effective monitoring of both the early periods of aging, controlled by the antioxidant consumption kinetics, and then the subsequent oxidation of the polymer matrix. Therefore, dielectric spectroscopy showed to be capable of assessing the LV cable aging state and, consequently it might be used as an aging marker for cable diagnostic.

The last part of the manuscript focuses on the building of a predictive modelling approach of LV cable conditions subjected to radio-chemical aging. It resulted into obtaining a lifetime curve which relates the aging factor to which the cable is subjected to, namely the dose rate, with the limit value of the considered electrical property ($\tan\delta$).

This could be considered a significant step forward for cable aging assessment as it permits an evaluation of the cable aging state not only through non-destructive techniques. In

particular, if the cable is in good health and can fulfill its role, the measured tan δ value is lower than the limit value given by the lifetime curve.

CHAPTER 1

STATE OF THE ART ON NUCLEAR POWER PLANTS CABLES

1.1 INTRODUCTION

Nowadays, low voltage cables are extensively used inside nuclear power plants (NPPs) for power transmission, control of equipment and communication of signals and data. It has been estimated that each NPP may own up to 1600 km of low voltage cables.

Low voltage cables play a very important role in guaranteeing a safe and effective operating life of the NPPs. Early failure of a low voltage cable could lead to unexpected power stops, lack of communication and, in the worst case, to a nuclear accident. For this reason, nuclear cables are designed and qualified to withstand possible nuclear accidents e.g. loss of coolant accidents (LOCAs).

Depending on their location inside the NPP, these cables are subjected to a wide range of environmental conditions and stresses such as high temperature, radiations, moisture and mechanical stresses. All these stressors contribute to an early degradation of cables. In particular, environmental conditions can be particularly harsh in the reactor containment area, leading to accelerated aging of cable components.

Since most of the NPPs built during the '70s and '80s are now reaching their end-of-life, electric utility companies are trying to extend the NPPs operating life up to other 20, possibly 40, years. This can be achieved only if the installed cables can guarantee their functionality during this further application time.

Due to the significant number of those cables, it is difficult to assess the health of the installed cables through commonly used techniques like, e.g., mechanical or chemical tests. To face these needs, new condition monitoring techniques have to be properly developed. These ones need to be ideally reproducible, non-destructive and representative of the entire cable under test.

Moreover, latest advances in polymer aging research have revealed important limits in current methods for estimating the lifetime of NPP cables. These are related to the lack of representativeness of accelerated aging tests and the lack of consideration of the polymer composition (e.g. fillers, additives, antioxidants) in cable aging models. Chemical composition of polymers can deeply influence the cable aging development usually delaying the degradation phenomena e.g. oxidation to occur.

In this Chapter a wide range of the most commonly low voltage cable types used inside NPPs, their chemical composition and properties are reported and discussed. Moreover, the effects of the degradation stressors on the aging of cables are described.

1.2 Extruded low-voltage (LV) cables inside NPPs

Any electrical cable consists of one or several conductors, insulation and jacket systems [1]–[5]. Electric conductors, usually made of metals, deliver electric current to the considered device or instrument. Cable insulation protects one inner conductor from another one and/or from the ground in order to avoid any discharge among them. Finally, jacket systems are usually made of elastomeric compounds and protect the cable from mechanical damage during installation and keep the initial cable configuration. They can also provide protection against ultraviolet (UV) rays by using specific additives.

Cables used inside nuclear power plants (NPPs) may be classified in various groups:

1. Instrumentation cables
2. Control cables
3. Power cables.

It has been estimated by [6] that a typical boiling water reactor (BWR) owns about 100 km of power cables, 80 km of control cables and 400 km of instrumentation cables. About 1600 km of cables are present inside a pressurized water reactor (PWR) power plant.

The three abovementioned groups of cables own different designs, materials, and application, which deeply influence the way they behave and age during their application time. Power cables, in particular, are further divided depending on the voltage they can deliver. Hence, it is possible to distinguish:

1. Low-voltage (LV) cables (rated voltage <2kV and operating voltage <1kV)
2. Medium-voltage (MV) cables (rated voltage <5kV and operating voltage <4kV)
3. High-voltage (HV) cable (rated and operating voltage higher than MV ones).

This Thesis focuses on low-voltage cables used in NPPs, therefore not all the technical discussion and conclusions can be applicable to other kinds of cable because the designs of NPPs cables may differ from others, e.g. the ones used in distribution systems.

1.2.1 Instrumentation cables

Instrumentation signals may be subjected to electromagnetic interference and noise inside NPPs. For this reason, instrumentation cables are usually shielded allowing the draining of electrical distortions to ground. The most common instrumentation cables designs are twisted pair and coaxial ones.

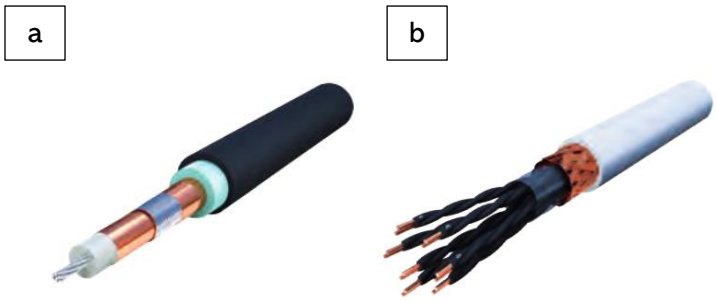

Figure 1 Structure of typical instrumentation cables used in NPPs. (a) Coaxial cable, (b) Multiconductor cable. Courtesy of Nexans.

1.2.2 Control cables

Control cables have simple designs in which an insulated conductor is grouped with one or more additional cables under an outer jacket. In some cases, an additional rubber jacket layer is added over the single cable wires in order to assembly the multiconductor setup before jacketing. The insulation thickness is usually less than 1 mm thick (around 0.8mm) and it is made commonly by the mean of crosslinked polyethylene (XLPE), ethylene-propylene rubber (EPR), ethylene vinyl acetate (EVA) or polyvinyl chloride (PVC). These insulation systems can easily bare up to 90°C for continuous periods of time. However, the entire cable is not suitable to work at this high rated temperature. This because jackets usually can withstand 75°C or less without any damage.

One of the main causes of control cable degradation is thermal stress. Due to the very low voltages of these cables, ohmic heating is not a concern. However, other thermal stressor can come from the adjacent environment such as high temperature valves and piping or hot lighting fixture.

Figure 2 Structure of a typical multiconductor control cable used in NPPs. Courtesy of Nexans.

1.2.3 Low-voltage power cables

LV power cables are characterized by basically the same design of control cables. One difference can be found in the necessity to delivery higher power so that the conductor size can be bigger thus requiring thicker insulation.

1.3 MATERIALS USED INSIDE LV CABLES

1.3.1 Conductor

Copper is the most used conductor thanks to its high electrical and thermal conductivity, good ductility and reasonable price. Copper conductors can easily bear rated temperature at 150°C. It is usually coated with tin, tin-lead alloy, pure lead, nickel or silver to minimize oxidation, enhance solderability and allow operation at higher temperature. Inside NPPs, the most common one is the tinned copper.

Aluminum is also used as a conductor, even if its electrical conductivity is lower than the copper one (by a factor of 40%). Aluminum is used mainly in large-size conductors since its ductility and flux flow characteristics may cause morphological damages to the conductor if this latter has little dimensions.

1.3.2 Insulating material

Polymers are the most common materials used as primary insulation inside cables. They guarantee a high resistivity and breakdown voltage together with enough protection against environmental stressors, such as chemicals, moisture, heat and radiation. In order to ensure these requirements, pure polymers are not suitable for a long-term application, for this reason different kinds and amounts of additives are put inside the main polymer matrix to improve their electrical and physical properties.

As already presented, the most common polymeric materials used are XLPE, EVA, EPDM and PVC. The percentage distribution of these materials inside NPPs cables is reported in Figure 3 [6].

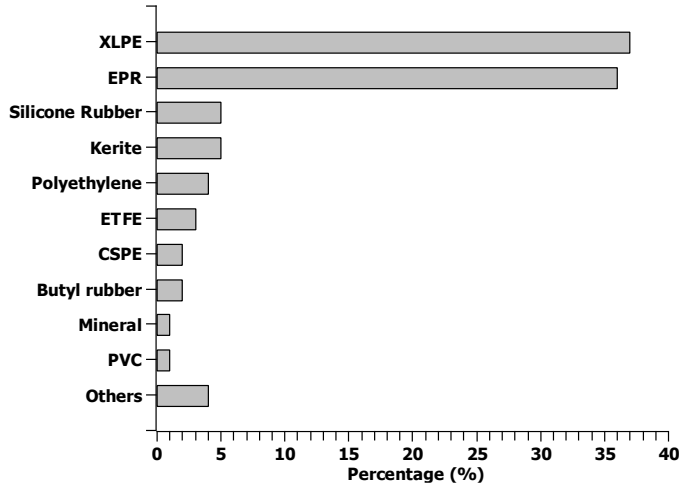

Figure 3 Percentage distribution of polymeric materials used as electric insulation inside NPPs cables

Among the most common additives used there are: antioxidants, plasticizers, vulcanizers and flame retardants. It has been estimated that LV cables may own up to 60% of fillers, reducing the effective insulating material.

It is evident that the high presence of additives can have an impact on both the physical-chemical and on the electrical properties.

Plasticizers

Plasticizers aim at improving the flexibility and mechanical endurance of the polymer. These low-weight molecular compounds are used as spaces between polymer chains, enhancing the flexibility and other physical and mechanical properties of the polymer.

Lubricants

Lubricants are additives which aim at reducing the friction and the viscosity of the polymer making it more processable. External lubricants are placed between the polymer and the mechanical parts of the e.g. extruder, to reduce the friction, while the internal lubricants ensure an easier filling of additives inside the polymer matrix.

Flame retardants

Inflammable polymers require particular fillers which inhibit combustion and smoke in order to guarantee the safety of these materials [7]–[11]. These fillers are known as flame retardants or smoke suppressants. They can reach up to 50% of the polymer total mass.

These fillers are divided into non-halogen and halogen-containing flame retardants.

- *Flame retardants phosphorus-based and hydrate compounds*, e.g. Alumina trihydrate (ATH) and Magnesium hydroxide ($Mg(OH)_2$). These molecules can stop the pyrolysis of the material since they pyrolyze, through endothermic reactions, faster than the polymer, turning themselves into inert matter and reducing the inflammable gas coming from the polymer and preventing the rapid increase of temperature [12].
- *Halogen flame retardants.* These molecules interfere with the ignition phase of the combustion. They showed to be more effective than the previous ones [7], but they release complex radical compounds which can worsen base polymer properties.

Antioxidants

Antioxidants (AOs) are chemical additives which prevent or delay the polymer degradation by oxidation [13]–[19]. Depending on the kind of antioxidants, they can act in different phases of the oxidation process [20]. Antioxidants can be divided into primary and secondary antioxidants.

Primary antioxidants, such as phenolic antioxidants and secondary aromatic amines, are radical scavengers. They interrupt the oxidative degradation reaction chain by scavenging the radicals. The most common radical scavengers in polymer science are the phenolic antioxidants. These

molecules convert peroxy radicals into hydroperoxides and convert themselves into phenoxy radicals. These latter are suspected to participate in a second act of stabilization. A simplified reaction scheme is reported in Figure 4. It is worth commenting that phenoxy radicals could abstract a hydrogen atom from the main polymer chain giving the possibility to start over the oxidative process. In order to minimize and prevent this phenomenon, phenolic antioxidants usually own two tertiary butyl groups. As a result, phenoxy radicals are stabilized by resonance.

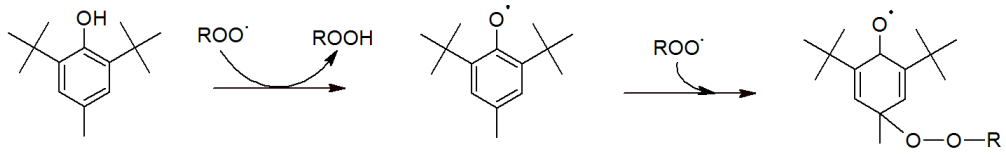

Figure 4 Phenol antioxidant reaction scheme

Secondary antioxidants turn hydroperoxides (ROOH) into non-reactive products before they decompose into alkoxy and hydroxy radicals. These stabilizers are often used in combination with the primary antioxidants in order to achieve a synergistic inhibition effect. Important classes of secondary antioxidants are organic phosphides and thioethers. The thioethers are effective stabilizers because their oxidation products act as long-term heat stabilizers [18], [20]. A simplified reaction scheme of thioethers is reported in Figure 5.

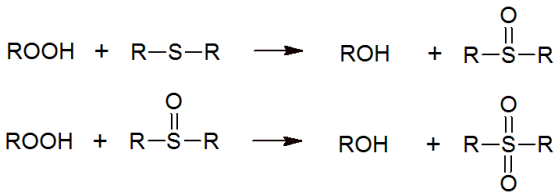

Figure 5 Thioether antioxidant reaction scheme

1.3.3 Shielding

Inside instrumentation cables, the shielding permits the reduction of electromagnetic interference, in order to ensure the correct transmission of signals. Mechanically, the shield can stop the formation of cracks from the sheath to the primary insulation, physically dividing the two materials, hence the cable mechanical properties (e.g. ductility) are enhanced. The most common material used as a shielding system is copper in forms of wire braid or foil.

1.3.4 Sheath

The sheath is the outermost layer of the LV cable systems. It protects the cable from mechanical and chemical stresses, and it has an active protection against fire. Due to this wide protection aims, the sheath materials are usually polymers with a high amount of fillers and additives (e.g. smoke suppressants).

The most common materials used as cable sheaths are Neoprene, Hypalon and polyvinyl chloride (PVC). However, this latter is not used inside the reactor containment area since it can release halogens (chloric acid) in case of fire [21].

Among all the components of the LV cables, the primary insulation and sheath are the most degradable materials since they are prone to degradation by the environmental stressors. Aging can deeply affect the physical-chemical and electrical properties of the material which can lead to the breakdown and the failure of the analyzed cable.

1.4 Degradation mechanisms of polymeric insulation inside NPPs

As presented, NPPs cables are exposed to a wide range of environmental conditions and stresses, depending on their location and application inside the power plant. As an example, these stresses can be particularly harsh inside the containment area.

Material aging or degradation is defined as the irreversible change of at least one of the properties of a material submitted to its environment during its operational life. Aging always results from a change of physico-chemical properties of the material.

The stresses leading to the degradation of the cable may be divided into three groups [2], [20], [22]:

- **Environmental**: radiation, heat, chemicals, moisture, etc.
- **Operational**: high voltages, electrical transients, ohmic heating, mechanical stresses.
- **Design:** related to non-efficient design phase.

Among these stressors, the most significant ones for LV cables inside NPPs are heat and radiation. In the case of BWR plants also moisture content has to be taken into account [6].

In particular, it has been showed by [6] that LV cables application life inside NPPs can be summarized into three scenarios:

1. **Service conditions**. 0.2-1 MGy and 60°C. Usually the service temperatures are between 35 and 60°C and between 0.2 and 1 MGy as absorbed dose.
2. **High temperature conditions.** 0.2-1 MGy and 75-100°C. These conditions are typical of PWR power plants next to the pressurized heaters.
3. **High radiation and temperature conditions.** 2000 MGy and 75-125°C. These conditions can take place nearby the reactor or on cables related to the safety of the reactor. The cables used in such conditions are not discussed in this Dissertation.

All these stressors may lead to various degradation mechanisms. Focusing on the polymeric insulating materials, the main chemical aging mechanisms are:

- **Scission of macromolecular chains**: two new shorter polymer chains are created from an initial bigger one. The chain scission causes the reduction of the average molecular weight of the polymer and a worsening of the mechanical properties of the material.
- **Cross-linking of macromolecular chains**: it is the formation of a covalent bond between two adjacent polymer chains. The higher the number of cross-linking bonds, the stiffer the resulting material. Unfortunately, if the crosslinking extent exceeds a given threshold value, the polymer can also become brittle and not suitable for some applications.
- **Oxidation**: it is the main cause of degradation of polymeric materials. This can be catalyzed by the effect of high temperatures and radiations and create free radicals which lead to the degradation of the material.

These degradation mechanisms are usually correlated each other. A lot of research works focused on the understanding the structure/property relationships of polymeric materials and how these relationships vary during aging. As a result, it has been demonstrated that the changes in microscopical physical-chemical properties cause the modification of the macroscale properties e.g. the mechanical ones. As an example, the following causal chain was established for linear polyethylene [23] (Figure 6):

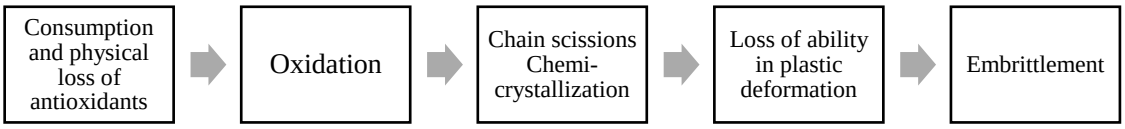

Figure 6 Proposed degradation chain for PE

1.4.1 Thermo-oxidative degradation

Many thermooxidative degradation mechanisms have been widely reported in literature for many kinds of plastics [14], [17], [24]. An example of thermooxidative degradation mechanism often reported for polyolefins is shown in Figure 7. As a chain reaction scheme, the thermo-oxidation can be divided into different steps:

1. **Initiation reaction.** Free radicals are created by the effect of heat. In this step, a covalent bond in the polymer chain (RH) is dissociated and creates a radical and one hydrogen.

$$\text{Polymer (RH)} \rightarrow 2R^{\circ} \text{ (polymer radicals)}$$

2. **Propagation reaction**. The polymer radical R° reacts with oxygen and generates a peroxy radical (ROO°).

$$R^{\circ} + O_2 \rightarrow R\text{-}O\text{-}O^{\circ} \text{ (peroxy radical)}$$

This radical is extremely unstable, and it extract an hydrogen from the polymer generating an hydroperoxide (ROOH) and another radical R°.

$$R\text{-}O\text{-}O^{\circ} + R\text{-}H \rightarrow R\text{-}O\text{-}OH \text{ (hydro-peroxide)} + R^{\circ}$$

3. **Chain branching**. Hydroperoxide radicals decompose and generate alkoxy and hydroxy radicals: alkoxy radical decomposes resulting into chain scission and oxidation products (carbonyl groups, alcohols).

$$ROOH \rightarrow RO^{\circ} + HO^{\circ}$$

$$RO^{\circ} \rightarrow \text{Chain scission (carbonyl, alcohol)}$$

4. **Termination.** Radicals deactivate in ROOR inside the material.

$$2R^{\circ} \rightarrow R\text{-}R$$

$$ROO^{\circ} + R^{\circ} \rightarrow ROOR$$

$$2\ ROO^{\circ} \leftrightarrow ROOR + O_2$$

If inside the polymer antioxidants molecules are present, then the termination reactions are replaced by stabilization reactions:

$$ROO^{\circ} + AO \leftrightarrow R\text{-}O\text{-}O\text{-}X + AY$$

where AY designates antioxidant products

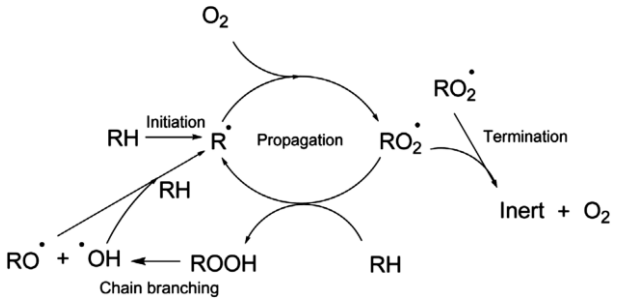

Figure 7 Thermo-oxidation mechanism for polyolefins.

1.4.2 Radio-oxidation

Ionizing radiations generate a huge amount of energy inside the irradiated polymer, which is orders of magnitude higher than the mean chemical bond strength [25]–[27].

The processes given by the interactions between the radiation and the material may be divided into three stages:

1. Absorption of the radiation energy in the material (physical stage)
2. Energy transfer among intermediates (physicochemical stage)
3. Restoration of the chemical equilibrium (chemical stage).

A schematic of the processes occurring during the interaction is reported in Figure 8.

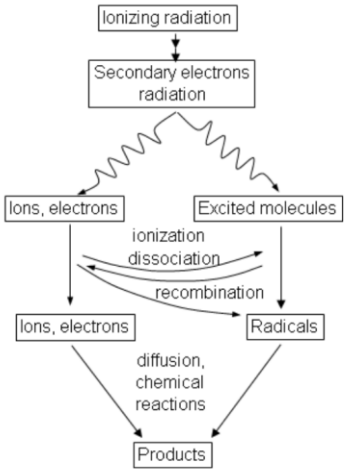

Figure 8 Succession of radiation-chemical processes [26].

During the physical stage, the radiation energy is distributed among atoms and molecules inside the polymer. This phenomenon brings to the generation of high-energy electrons which can excite and ionize the polymer molecule. However, the interaction time is very short and does not permit chemical reactions to take place. As a result, a big number of activated molecules are formed inside the polymeric matrix. The distribution of these radicals depends on the property of the material and on the irradiation characteristics. The secondary electrons, given by the previously activated molecules, may ionize and collide with the neighboring atoms which can give birth to reactive volumes made up of ions, radicals and excited atoms and molecules [26].

In the physical-chemical stage, the excited molecules transfer energy through molecular collisions and chemical reactions. As a result, new ions, radicals and excited atoms are created. Finally, the chemical equilibrium is reached once these radicals chemically react with the environmental oxygen or by each other (chemical stage). This latter stage behaves similarly to the thermo-oxidative chain reactions.

Hence, the molecular modifications induced by the ionizing radiation can be summarized as [28]:

- *Crosslinking*. This forms new C-C covalent bonds between adjacent polymer chains
- *Chain-scission.* The breaking of a long chain into two smaller ones
- *Changes in the nature and number of double bonds*
- *Oxidation*.

In a semi-crystalline polymer, radiations create free radicals in both the crystalline and amorphous phases. It is evident that the oxidation occurs mainly in the amorphous area due to an easier mobility of oxygen molecules and radicals. Indeed, the diffusion coefficient in the

amorphous region are several orders of magnitude higher than the in crystalline phase ones, resulting into an easier movement of chemical compounds in the amorphous phase.

For this reason, radicals in the amorphous region are able to bond each other or with oxygen. On the contrary, radicals formed in the crystalline region remain trapped for a certain period of time after irradiation. These trapped radicals can cause some reactions inside the crystalline area, yielding to a significant variation of both physical and chemical properties of the material. Moreover, due to diffusion phenomena, these radicals slowly migrate to the interface of the crystalline part where they are free to bond with the environmental oxygen leading to further oxidative degradation even when no irradiation source is on. This phenomenon is known in literature as post-irradiation effect, and can significantly change the physical-chemical properties of the material even after radiation is no longer applied to the polymeric matrix [28]–[30].

This phenomenon is particularly significant inside NPPs. Indeed, due to this, it is important to evaluate the health of the insulation, not only immediately after the shutting down of the environmental stressors but even after several time since polymer degradation can evolve even years after the removal of external stressors.

1.4.3 Combined effect of thermal and radiative stressors

Very often the two abovementioned environmental stressors act at the same time inside typical NPP environments. In particular, temperature and radiation may have a synergistic effect on the aging of the cable insulations. Depending on the external conditions, there will be a more predominant degradation process over the other, which would be the main cause of the material degradation.

Figure 9 reports the predominance diagram of the mechanisms of degradation during radiation and thermal aging in radiation environment.

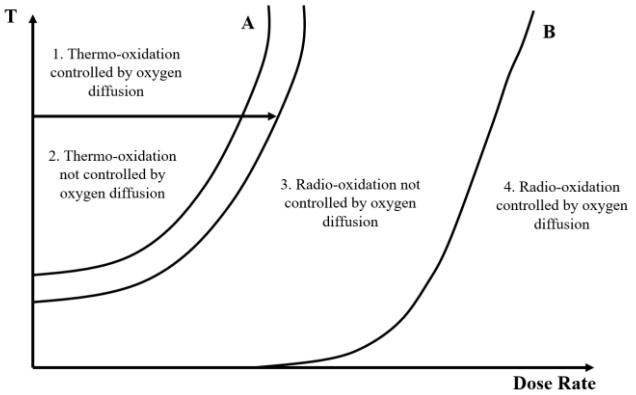

Figure 9 Predominance diagram of the mechanisms of degradation during radiation and thermal aging in radiation environment

This graph depicts four zones:

I. Oxygen diffusion controlled thermo-oxidation
II. Thermo-oxidation not controlled by oxygen diffusion
III. Radio-oxidation not controlled by oxygen diffusion
IV. Radio-oxidation controlled by oxygen diffusion

The A curve in the graph represents the separation between thermal-oxidation and radio-oxidation, while the B curve depicts the separation between the area led by the oxygen diffusion and the area not led by the oxygen diffusion in the radio-oxidation area.

Oxygen diffusion can become determinant if the oxygen present in the material bulk is consumed by reaction with free radicals (generated by the irradiation) faster than the oxygen that is replaced by diffusion from the atmosphere. When this happens, material degradation results to be more significant on the outer layer of the insulation (inhomogeneous degradation), since oxygen cannot successfully penetrate inside the bulk of the material. This phenomenon is known in literature as Diffusion Limited Oxidation (DLO) [21], [31]–[37] and it is significant when high dose rates are applied to the polymeric insulation. Indeed, these yield to a non-homogenous oxidation of the polymer. As presented, radiation catalyzes the oxidative reactions which require oxygen from the surrounding environment. If the amount of oxygen is not enough to bond with radicals made by high radiation dose rates, oxygen molecules cannot migrate to the inner part of the insulation and remain trapped in the outermost layers (Figure 10.a). Simultaneously, given the same concentration of oxygen molecules, thicker insulation can face DLO effects since available oxygen bonds to the polymer outer layer, leading to inhomogeneous aging throughout the thickness. Macroscopically, this behavior results in a brittle external layer of the cable and formation of cracks which can yield to an abrupt reduction of the mechanical properties and, consequently, to the failure of the cable according to the available condition monitoring technique, as it will be discussed in the following. A sketch of the effect of DLO phenomenon is reported in Figure 10.

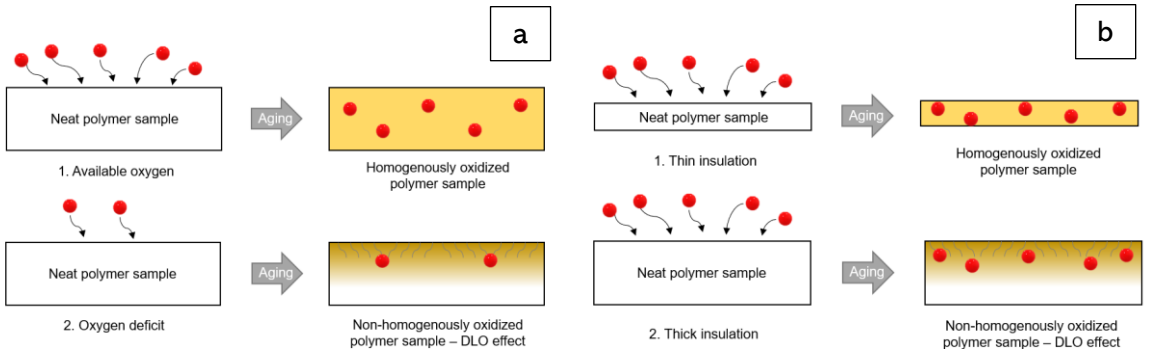

Figure 10 Sketch of diffusion limited oxidation (DLO) phenomenon
a. Change in oxygen concentration. b. Change in polymer thickness.

Identifying the predominance of one environmental stressor over the other (Figure 9) is of utmost importance in order to better understand the evolution of some material properties and to overcome actual limitations of available testing procedures e.g. mechanical ones, which are not directly referred to the actual cable applicability. For this reason, a wide range of testing techniques have to be evaluated in order to better assess the cable health condition.

1.5 The TeaM Cables Project

This P.h.D. thesis has been carried out in the framework of a Euratom H2020 Project called TeaM Cables (www.team-cables.eu).

TeaM Cables aims at providing NPP operators with a novel methodology for efficient and reliable NPP cable ageing management by developing:

- cable aging models and algorithms, which are based on multi-scale studies and can be tailored to cover variations in fillers, additives and degrees of crosslinking,
- methodologies for non-destructive testing techniques and their associated criteria identified from multiscale relations,
- a novel "open access" tool which aims at integrating all the models developed and providing the residual lifetime of cables by crossing non-destructive measurements with predictive models and knowledge of cable exposure conditions (wiring network in the NPP). Cable lifetime estimation accuracy will be greatly improved as current models only distinguish the type of polymer (e.g. EPR or XLPE) and therefore can describe only one parameter of the polymer.

Figure 11 The H2020 TeaM Cables Project logo.

In the project, the study of polymers with growing formulation complexity allows the identification of the role of each component during the polymer aging. Cable materials are subjected to both normal conditions, i.e. soft accelerated aging, representative of normal conditions inside a reactor building, and abnormal conditions, i.e. exposure to design basis event and/or severe accidents. On the one hand, experimental characterizations are carried out at different scales to collect and analyze aging mechanisms and effects. On the other hand, new models are developed trying to correlate the different scale experimental responses with aging.

The capability of a cable system to fulfill its application is strictly related to the degradation of the polymeric insulation. Hence, in order to define a cable end-of-life criterion, it is mandatory to know the evolution of its physical-chemical properties with aging. This is achievable through the development of multiscale kinetic models which take into account the causes of polymer aging e.g. thermal and radiation stressors and their consequences on the polymeric matter.

The validation of these models is obtained through the experimental results coming from the accelerated aging on the project cable samples. A schematic representation of this approach is reported in Figure 12.

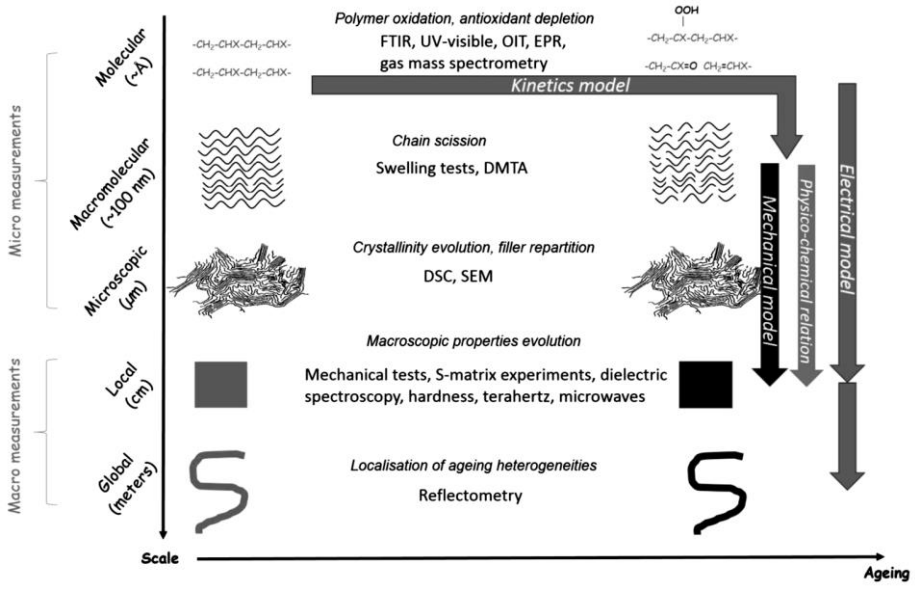

Figure 12 Schematic of the multiscale approach applied in the TeaM Cables Project.

Once known the end-of-life criterion, it would be possible to develop testing procedures for cable diagnostics (e.g. based on electrical measurements) which are needed to be non-destructive, in order to verify the health of the cable and schedule its replacement or extend its operating life.

1.6 Aim of this Thesis

The main aim of this Thesis is to analyze and investigate how the typical aging stressors inside NPPs, i.e. radiation and high temperatures, can modify the physical-chemical and electrical properties of the extruded instrumentation and control low-voltage cables used in this type of power plants.

The main objectives can be summarized as follows:

- Investigate the evolution of the physical-chemical and electrical properties of LV cables for nuclear application subjected to radio-chemical and thermal aging

- Find possible aging markers based on the electrical properties which can be used for the definition of an end-of-life criterion based on electrical measurements
- Correlate and model the changing of the polymeric material properties from the microscale (e.g. chemical) to the macroscale (e.g. electrical and mechanical)
- Develop a non-destructive condition monitoring technique which can be suitable to be used onsite.

In this Thesis, great attention will be paid on the multiscale modelling, focusing mainly on the electrical response of the aged materials. A schematic of the experimental and modelling process is reported in Figure 13.

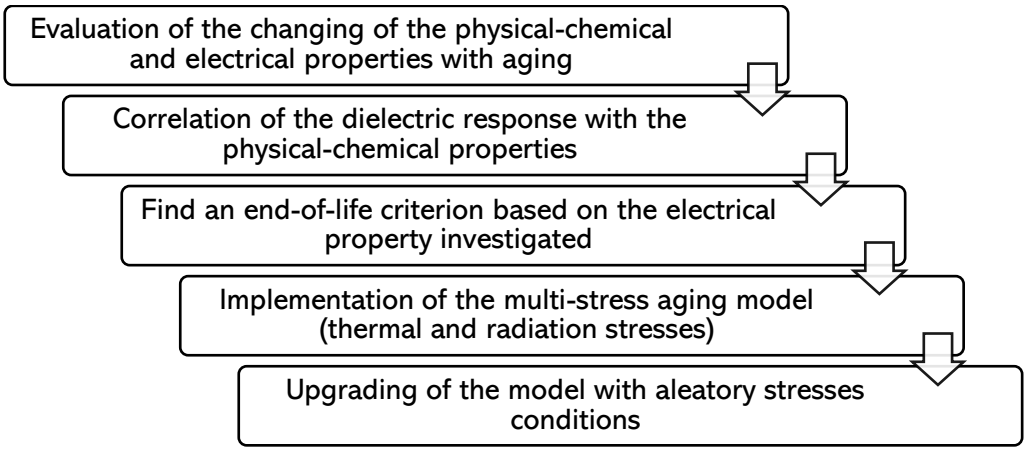

Figure 13 Schematic of the multiscale modelling for electrical measurements

Finally, the verification of the applicability of the end-of-life criterion through available nondestructive on-site testing technique is performed.

CHAPTER 2

CONDITION MONITORING TECHNIQUES FOR LV CABLES

2.1 INTRODUCTION

Cables are essential components of a power plant because they connect system components and deliver data used to ensure efficient work of the plant. All these equipments, hence, need to be qualified to ensure good performance both under normal operating conditions and under accidental conditions e.g. loss of coolant which could occur during their operational life inside NPPs.

Nowadays, qualification of I&C cables important to safety are based on international standards such as IEC-780, IEEE-323, IEEE 383 [38] or national standards such as French National Codes RCC-E and RCC-M and German Safety Standards KTA 3501-3503 and 3505. All these standards have in common the demonstration of the cable ability to withstand a design-based event (DBE) after exposure to normal operating conditions during their planned service life, which is usually about 40 years. As an example, one of the most used technique for cable qualification is reported in the following paragraph.

Currently, the possibility to extend the actual NPP operational life to other 20 years raises the challenge to guarantee that the actual I&C cables can perform safely without any failure. In this background the necessity of nondestructive technique (NDT) for condition monitoring (CM) which can be performed in situ is a key issue to be addressed.
Condition monitoring is defined as the procedure of measuring quantities related to cable insulation status, aiming at evaluating the level of aging degradation of electric cables [39].
Up to now, several condition monitoring techniques have been developed, which are described inside this Chapter. However, none of them succeeded in the establishment of a unique end-of-life criterion beyond which the cable needs the replacement. Indeed, copious research studies are moving towards a combination of different NDTs in order to keep into account the strengths and weaknesses of each technique [40], [41].

In order to efficiently utilize a CM technique, it is important to initially obtain a condition indicator (CI), which represents the maximum (or minimum) value of the measured property at the end of the cable qualified life before a successful DBE test. The aim of the CM is to verify that the qualified condition has not been exceeded. In other words, if the property measured through the CM technique is lower (or higher) than the CI value, the cable may be able to withstand a DBE, hence, it is still under its qualified life.

2.2 CABLE QUALIFICATION PROCEDURE

The initial qualification is a mandatory step prior to the setup of the cable inside the power plant. According to IEEE-383 [38], the qualification can be achieved through different methods: type testing, operating experience or analysis. The most common one is the type testing technique whose goal is to verify the capability of the cable to fulfill its functions throughout its operating life and after a possible LOCA.

As stated in the introduction, there are several standard procedures depending on the type of cable to be qualified (safety or non-safety cables), on the country, and on the place of the cable application inside the NPP. However, a common procedure for cable qualification can be summarized as follows [42], [43]:

1. Visual inspection
2. Measurement of initial functional properties
3. Simulation of ageing in normal operation (pre-ageing)
4. Testing of functional properties
5. Simulation of the accident and post-accident period
6. Measurement of final properties
7. Final visual inspection

These testing procedures have to be performed in the specific order. In the end, the detailed procedure and the followed testing techniques have to be reported in the Test specification document which has to be approved by the Technical Safety Organization (TSO), NPP owner and Country authority.

Specimens to be tested are obtained from the splitting of the entire cable into its components, namely: insulated wire, insulation and sheath. On the contrary, coaxial cables are tested as a whole.
The length of each sample must be higher than 3.05 m, according to IEEE-383 [38].
Sample materials are then subjected to accelerated aging in order to simulate the normal operating life of those cables. Being in an NPP environment, aging is performed both under radiation and high temperatures. Radiation aging is usually achieved through a ^{60}Co irradiation source, keeping into account that the dose rate could impact the final property change. Therefore, common dose rates used for accelerated aging usually do not exceed 110 Gy/h per 1 mm insulation thickness.

Accelerated thermal aging is performed using the Arrhenius approach, according to which short-term simulation of aging at high temperatures causes the same long-term reduction of cable lifetime at operating temperature. However, the aging temperature has to be chosen according to the chemical limitation of the polymeric compound used. Generally, for common

polyethylene plastics, temperatures higher than the PE melting temperature (around 120°C) are not allowed due to the change in the morphology inside the material.

Accelerated aged specimens are then subjected to a Design-basis Accident (DBA) which consists of further irradiation with accident dose and simulation of thermodynamic profile of DBA and post-DBA (Figure 14). The accident dose rate can be up to 10 kGy/h, common values are around 2.5 kGy/h at room temperature. The thermodynamic profile is made up of various temperature ramps in a steam environment at different pressures. In addition, a chemical spray can be inserted, if required. During DBA, cables can be energized in the case of power cables (both voltage and current) or communication cables (only voltage usually equal to 50 V_{rms}).

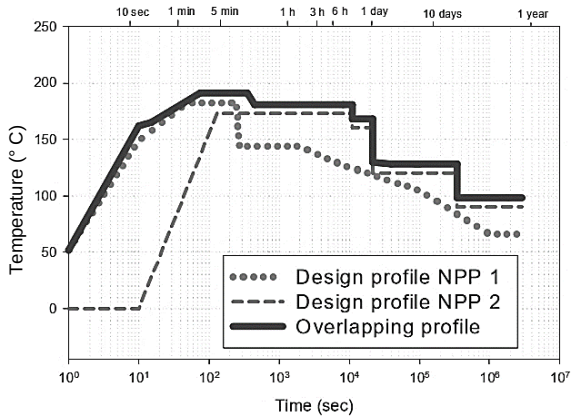

Figure 14 Example of thermodynamic profile of DBA simulation [42].

After DBA simulation, specimens are tested in order to verify that their properties show acceptable values. The properties usually tested are electrical and mechanical ones. Among the electrical ones, common testing techniques are insulation resistance and breakdown voltage. Tensile stress technique is the one used for assessing the mechanical properties. In addition to that, samples have to be coiled around a mandrel in order to verify the mechanical resistance of the analyzed cables to bending.

Acceptance criteria are the main issues related to the qualification of nuclear cables. Indeed, there is no absolute *a priori* criterion available for cable qualification but some common measurable functional properties are available, e.g., elongation-at-break or insulation resistance measurements. Criteria are usually the limit values of properties beyond which the degree of deterioration is considered to reduce the ability of the cable to withstand stresses encountered in normal service, and during accidents.
A typically recommended threshold value for the mechanical properties is 50% of the absolute elongation-at-break. This value showed to guarantee sufficient safety margins to the qualified cable, and it is widely used as an acceptance criterion.

Referring to electrical measurements, the insulation resistance is usually the quantity to be measured. This must be sufficiently high to exclude the possibility of activation of the current protection systems at the NPP for the specific installation. This means that there is a maximum leakage current a cable can deliver. As an example, for a 100 m cable, the leakage current shall not exceed 25 mA for cables with a conductor size of 1.5 mm^2.

In conclusion, if the analyzed cable passes all the above required conditions and tests, it is considered qualified for 40 years, and no condition monitoring is required during its qualified life. However, as a better understanding of the aging behavior of polymeric materials has been achieved during the last years, new concerns about the original approach to qualification raised. For this reason, the development of new effective condition monitoring techniques is becoming more and more a key issue for the management of nuclear cables. In the following, various available condition monitoring techniques are presented and discussed, focusing on their applicability on site and their industrial availability.

2.3 Available Condition Monitoring techniques

2.3.1 Visual inspection

The first condition monitoring technique is clearly the visual inspection. It has been shown that a change in color of the cable jacket can be considered as an indicator of aging. The change of color in polymers are usually related to the formation of double bonds (due to e.g. antioxidant degradation products or unsaturated irradiation products) which, in the case of polyethylene, give the polymer a yellowish texture [44]. In the case of black rubbers, on the contrary, the polymer color changes into a grey-white form. Anyway, no evidence is reported claiming that the intensity of the color change can be correlated to the amount of degradation. For this reason, the changing in color can be used only as a warning alarm on the actual degradation of the cable but no information about the degradation stage can be extracted.

2.3.2 Tensile stress

Among the mechanical tests, the tensile test is, with no doubt, the most common and widely accepted condition monitoring technique for NPPs cables.

A typically accepted rule among NPP regulators is that if the elongation-at-break (EaB) of the cable primary insulation and jacket is higher than 50% absolute elongation, the cable may still fulfil its required function under normal operation and it could withstand a DBE without damage (§ 2.2). This criterion was proposed in a report issued by EPRI [45] in 2005. In this report, dozens of extruded LV cable specimens have been aged and mechanically tested before and after a DBE simulation. It has been demonstrated that all the cables which withstood a DBE simulation owned an EaB equal or higher than 50% absolute value.

It is established that this criterion is not representative of the entire cable degradation due to the fact that it is made on a small portion of the insulation (usually around 5 cm) and it can be affected by huge error displacements. Moreover, different polymeric materials can show very different initial EaB values, e.g. for polyethylene initial EaB can be around 400% or 200%, depending on its additives content, while rubbers can have much higher EaB initial values (more than 1000%).

Nevertheless, the use of this method over many years and its very good correlation with polymer degradation level brought to the general acceptance of this method as a good condition monitoring technique for cables [46]–[54].

The tensile method is a destructive technique, standardized in the IEC 60811-501:2012 [55], which consists of applying a constant elongation force to the specimen until it breaks. The maximum elongation value at break is called Elongation-at-break (EaB). The specimen shape is a dumb-bell shape (Figure 15), with an initial section A_0 and length l_o, to which is applied a constant longitudinal force F that causes the elongation of the specimen itself (Δl_0).

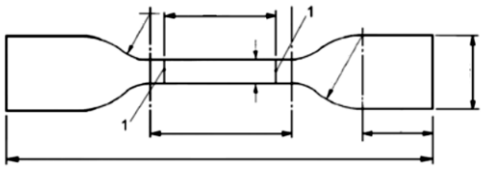

Figure 15 Dumb-bell shape for tensile tests (from IEC 60811-501)

Hence, the stress σ can be defined as:

$$\boldsymbol{\sigma = \frac{F}{A_0}\ (Pa)} \tag{1}$$

While the elongation-at-break is defined by:

$$\boldsymbol{EaB(\%) = \frac{(l - l_0)}{l_0} \cdot 100} \tag{2}$$

where l_0 and l are the initial and breaking useful lengths of the specimen, respectively.

The instrumentation acquires at the same time the stress and the strain to which the specimen is subjected, building the stress-strain curve, as seen in Figure 16.

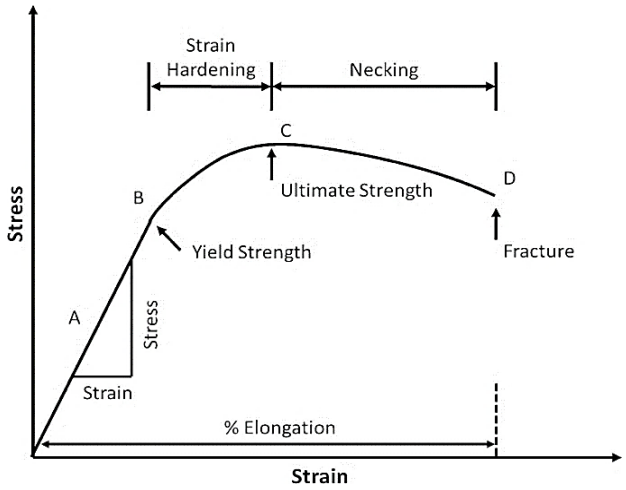

Figure 16 Typical polymer stress-strain curve

The curve can be divided into two zones corresponding to two different mechanical behaviors of the polymer:

- **Elastic behavior** (linear trend). Deformations occurring in this phase are reversible. If the specimen is unloaded, it can recover its initial shape without any damage;
- **Plastic behavior** (non-linear trend). Deformations occurring in this phase are only partially reversible. The specimens change their shape and they will not be back to their initial form.

2.3.3 Indentation measurements

Microindentation hardness testing (MHT) provides information about the compressive modulus of the material under controlled conditions. A diamond indenter of specific geometry is pushed towards the surface of the material under test using a known applied force (load). The most common indenters are the Knoop and Vickers one (Figure 17) and the applied force usually ranges from 9.8×10^{-3} to 9.8 N [56]–[58]. The testing procedure is standardized in the ASTM E384 Standard, published in 2017 [56].

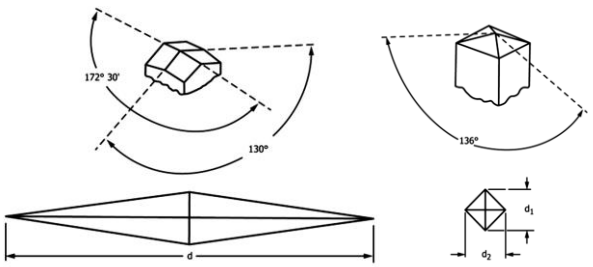

Figure 17 Knoop (a) and Vickers (b) indenters morphologies

During the test, the applied force produces a local displacement on the surface of the sample, this local displacement is characterized by a penetration depth caused by the applied load. All these quantities are acquired by the instrumentation so that the force-displacement curves are

obtained in both the loading and unloading phases (Figure 18). The slope of the unloading phase allows the evaluation of the local Young's modulus of the material.

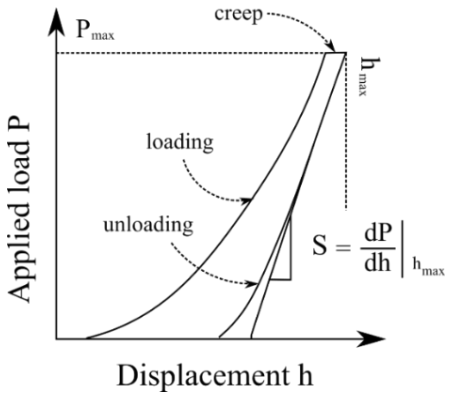

Figure 18 Schematic of the loading and unloading phases of the indentation test

The reduced modulus (E_r) is given by the initial slope of the discharging curve, according to the following:

$$\mathbf{E_r} = \frac{\sqrt{\pi \mathbf{S}}}{2\beta\sqrt{\mathbf{A_c}}} \tag{3}$$

where S is the initial slope of the discharge curve, β is a form factor dependent on the type of indenter (β = 1.012 in the case of a Vickers indenter) and A_c is the proposed contact area, which depends on the type and geometry of the indenter.

Finally, the Young's modulus is given by:

$$\mathbf{E} = \frac{\mathbf{1}}{\frac{\mathbf{1-\vartheta^2}}{\mathbf{E_r}} - \frac{\mathbf{1-\vartheta_i^2}}{\mathbf{E_i}}} \tag{4}$$

ϑ is the Poisson coefficient of the sample ($\vartheta_{XLPE\ Silane}$ = 0.42). ϑi and E_i are the Poisson coefficient and Young's modulus of the diamond indenter, equal to 0.07 and 1147 GPa, respectively.

It has been demonstrated that the more severe the degradation of the cable, the higher the Young's modulus. Indeed, it is known that degradation causes the embrittlement of the polymer resulting into the increase of the Young's modulus. The microindentation technique is quite commonly used inside NPPs since various portable devices have been commercially available for several years. This technique shows to be appropriate on EPR cable, well correlating with the aging and degradation of the material. On the contrary, very little changes of the modulus are appreciable on XLPE cables [59], [60]. Against its ease-of-use and commercial availability of this instrumentation, it must be taken into account that this measure is very sensitive to temperature changes and, since it is a local measurement, the testing spots can be non-representative of the entire cable system health.

2.3.4 Differential scanning calorimetry (DSC) measurements

The Differential Scanning Calorimetry (DSC) analysis measures the difference in heat flow (in mW) between a sample and a reference, in an inert atmosphere, during a set temperature change [61], [62]. DSC analyses give both quantitative and qualitative information about the physical and chemical transformations which imply heat exchange and variation of heat capacity (Figure 19) occurring inside the material under test. Hence, through DSC is possible to investigate the nature and temperature of exothermic and endothermic reactions (e.g. polymer melting).

From the DSC analysis thermograms, it is possible to determine the enthalpy of melting as the integral of the endothermic peak. Indeed, during melting, polymer acquires heat from the environment in order to melt the crystalline phase (endothermic reaction).

In particular, it is possible to evaluate the ratio of crystallinity (χ_c) of the material under test by the following equation:

$$\chi_c = \frac{\Delta H_m}{\Delta H_{m,\infty}} \tag{5}$$

where ΔH_m is the enthalpy of melting of the sample (J.g^{-1}), and ΔH_∞ is the enthalpy of melting of the PE crystal (commonly used value for ΔH_∞ is 290 J.g^{-1} for PE).

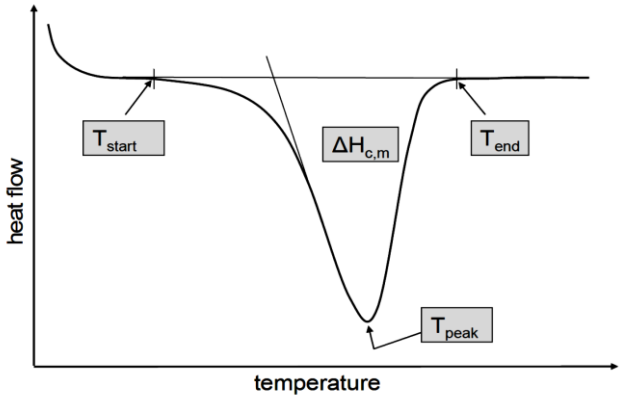

Figure 19 Typical polymer thermogram obtained by DSC measurements

Crystallinity ratio is not commonly used as an aging indicator but it has been demonstrated by several authors [23], [63], [64] that aging may cause the detachment of short macromolecular fragments from the amorphous phase, which might migrate up to the surface of the pre-existing crystals to thicken them. This phenomenon in known as chemicrystallization [23]. Anyway, the quantitative study of the chemicrystallization is often complicated by various phenomena e.g. the loss of small molecules by evaporation, the change of density of the polymer chain due to oxidation and the effect of radiation and thermal stressor which can influence in different ways the changes in the crystallinity ratio.

2.3.5 Oxidation induction time (OIT) measurements

This technique, based on the DSC instrumentation setup, allows the evaluation of the time required to induce oxidation inside the material under a controlled flux of oxygen. In the case of stabilized polymers, OIT measurements could give a quantitative assessment of the degree of stabilization of the material since the OIT can be also defined as the time required for consuming all the stabilizers inside the specimen.

The OIT procedure is standardized by the ASTM D3895-19 [59], [65], [66] and it is made up of three steps:

- Rapid ramp under nitrogen from room temperature to testing temperature (around 200°C)
- Temperature equilibration (around 5 mins)
- Switching of the furnace atmosphere from nitrogen to pure oxygen
- Isotherm at testing temperature until an exothermic peak appear in the thermograph (Figure 20).

The exothermic peak is related to the oxidation reactions in the polymer under test.

The time at which the switch of gas flow occurs is defined as t_1, while the time at which the exothermic peak appears is t_2. This latter is graphically obtained by the tangent-method, namely it is the intersection of the baseline with the steepest tangent of the reaction peak. The difference between these two values of time is defined as oxidation induction time (OIT).

$$\mathbf{OIT = t_1 - t_2} \tag{6}$$

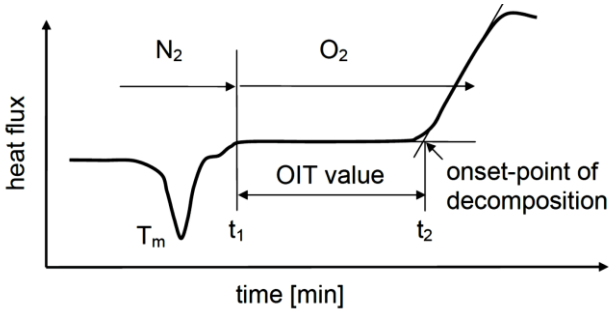

Figure 20 Graphical scheme of a typical OIT thermograph

It is evident that the more severe the degradation state of the material the lower its resistance to oxidation, hence the OIT value. For this reason, OIT can be considered a suitable condition monitoring technique for certain kinds of insulating polymer.

Indeed, OIT measurements proved to be appropriate for materials based on PE, in particular XLPE. For other materials, very few examples are reported requiring special knowledge about the material composition and properties [46]–[48], [67], [68].

This method is, up to date, not so commonly used inside NPPs because the DSC instrumentation is a laboratory machine but sampling can be done on site and since very low amount of material is needed (usually around 5-10 mg) the test can be considered as non-destructive. On the other side, this method is only suitable on materials filled with antioxidants or other types of stabilizers and it does not provide any information about the cable functionality itself.

2.3.6 Thermo-gravimetrical analysis

Thermo-gravimetrical analysis (TGA) is a chemical technique which records the weight of the material sample as a function of the increase of temperature in a controlled atmosphere. This technique is standardized by the ASTM D6370 reapproved in 2019 [69]. The thermograms (Figure 21) given by the instrumentation provide the mass loss over the specified temperature range from which it is possible to obtain a compositional analysis of the sample. In particular, it is possible to evaluate the concentration of fillers e.g. flame retardants and plasticizers.

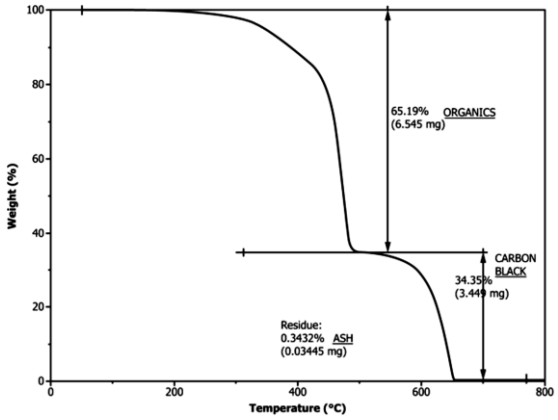

Figure 21 Typical thermogram for rubber-based polymers

For this reason, this test is typically used for the analysis of degradation of polymers based on PVC, which can lose their plasticizers during aging, and on rubber polymers like, e.g., EVA and chlorosulfonated polyethylene (CSPE), whose degradation state is directly proportional to the hydrogen atoms replacement in the polymer main chain with other functional groups [47], [49], [67].

2.3.7 Fourier Transform Infrared (FTIR) Spectroscopy

FTIR (Fourier Transform Infrared) spectroscopy is a non-destructive technique based on the interaction of infrared radiation with the analyzed material. The reference standard for this technique is the ASTM E168 published in 2016 [70].

It is known that, when a light beam impresses a material, some part of the beam passes through, the other part is reflected from or is absorbed by the material under test. Essentially, the amount of light absorbed by the sample is the difference between the incident radiation *(I_0)* and the transmitted radiation *(I).* This amount of absorbed light can either be expressed in transmittance *(T)* or in absorbance *(A).* Transmittance and absorbance can be expressed as follows:

$$\mathbf{T} = \frac{\mathbf{I}}{\mathbf{I_0}} \tag{7}$$

$$\mathbf{A} = -\log(\mathbf{T}) \tag{8}$$

Absorption of light can cause a transition from an initial energetic state to a higher one. The nature of the transitions depends on the energy of the photon but also on the chemical nature of the interacting compound. As a result, a change of the molecular dipole moment occurs. The molecule vibrates or rotates to dissipate the excess of energy and restore the initial equilibrium. In doing so, the instrumentation records the peak related to the excited molecule, a number of those giving birth to the so called FTIR spectrum (Figure 22).

The vibration frequency of chemical bonds is directly related to the chemical nature of the involved atoms, but also on their chemical environment. Characteristic wavenumbers for several chemical bonds are often available from literature [71]–[74].

Additionally, the intensities of the bands are proportional to the concentration of the chemical functional group involved. Hence, FTIR spectroscopy can also be used as a quantitative technique. In particular, the oxidation reactions give raise to new carbonyl groups (C=O) whose peaks appear at around 1720 cm^{-1}. Since the oxidation is reported to be the main cause of degradation of the polymeric materials, the increase of the intensity of the carbonyl peak is often used as an aging marker for extruded cable systems [60], [73], [75]–[77].

Unfortunately, this measurement requires laboratory equipment which is usually a non-portable device. Moreover, the carbonyl band can be also overlapped by non-oxygen related molecules e.g. phenolic antioxidants or other additives, so that the suitability of this technique for cable diagnostics has to be evaluated once known the exact composition of the cable under test.

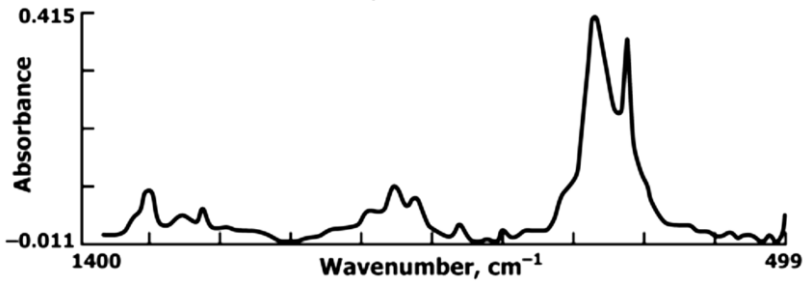

Figure 22 Example of FTIR spectrum

2.3.8 Dielectric spectroscopy

Dielectric spectroscopy (DS, sometimes called impedance spectroscopy) measures the dielectric response of a medium subjected to an external alternating electric field as a function of frequency [78]–[81].

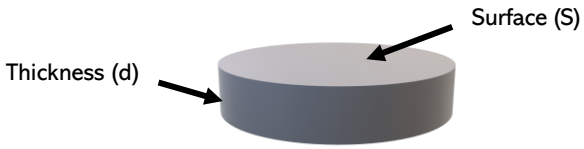

Figure 23 Parallel-plate capacitor dimension scheme.

This technique measures the impedance of a system over a range of frequencies, and therefore the frequency response of the system. Namely, the electrical properties of a dielectric placed in a parallel-plate capacitor, with surface *S* and thickness *d* (Figure 23), under the effect of an alternating voltage with frequency *f*, is described by measuring its capacitance *(C)* and conductance *(G),* defined as follows [80]:

$$\mathbf{C}(\boldsymbol{\omega}) = \boldsymbol{\varepsilon}_0 \boldsymbol{\varepsilon}'(\boldsymbol{\omega}) \frac{\mathbf{S}}{\mathbf{d}} \tag{9}$$

$$\mathbf{G}(\boldsymbol{\omega}) = \boldsymbol{\varepsilon}_0 \boldsymbol{\omega} \boldsymbol{\varepsilon}''(\boldsymbol{\omega}) \frac{\mathbf{S}}{\mathbf{d}} \tag{10}$$

where ε_0, ε', ε'' are respectively the permittivity in vacuum, the real and imaginary parts of permittivity of the analyzed dielectric material. Therefore, the complex permittivity can be defined as follows:

$$\dot{\boldsymbol{\varepsilon}} = \boldsymbol{\varepsilon}'(\boldsymbol{\omega}) - \mathbf{j}\boldsymbol{\varepsilon}''(\boldsymbol{\omega}) \tag{11}$$

The real part of permittivity is defined as the ability of the dielectric medium to store energy while the imaginary part of permittivity defines the energy losses of the material.

The trend of the complex permittivity as a function of frequency gives birth to the so-called dielectric spectrum representing the various polarization phenomena occurring inside the material under test (Figure 24). The spectrum is given by a convolution of various peaks related to the various molecular species which are inside the material under test. Indeed, when the applied field owns a frequency similar to the opposite of the characteristic relaxation time of the considered molecule, the spectrum exhibits a peak related to the relaxation of the molecule [80].

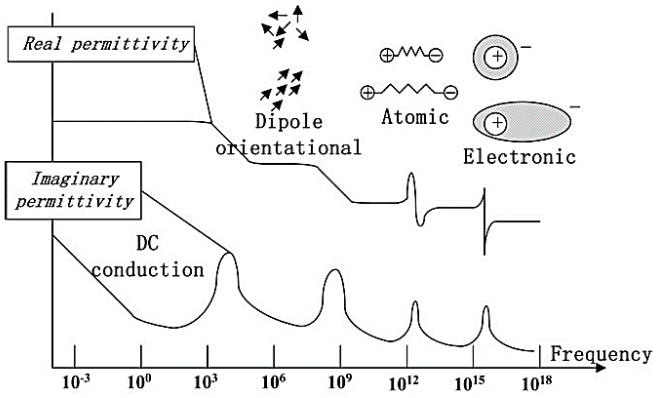

Figure 24 Schematic presentation of the frequency dependences of complex permittivity with the different polarization processes

There are four polarization phenomena depending on the analyzed frequency region. Namely:

1. **Electronic polarization**. This polarization mechanism is occurring in all the solids and it consists of the displacement of the electronic cloud in the opposite direction of the electric field. Characteristic frequency is around 10^{15} Hz.
2. **Atomic polarization**. According to this polarization mechanism, the applied electric field modify the atom displacement inside the molecule, modifying the length of the chemical bonds between atoms. Characteristic frequencies are 10^{12}-10^{13} Hz.
3. **Dipolar polarization**. This polarization occurs in materials made up of polar molecules. Molecular dipoles can modify their spatial orientation and tends to align themselves according to the applied electric field. This polarization mechanism is dependent on temperature due to the changing of the molecular kinetics with heating. Characteristic frequencies are 10^{12}-10^{3} Hz.
4. **Interfacial polarization**. Also known as the Maxwell–Wagner–Sillars polarization, it occurs in heterogeneous systems and it is favored when the electrical characteristics (i.e. permittivity and conductivity) of the constituent phases significantly vary. An applied external field forces unbounded charges, which could be present from the stage of the composite manufacturing, to migrate at the interface of the phases, forming large dipoles. These induced dipoles exhibit enhanced inertia and require enough time (low field frequency) and thermal agitation (high temperatures) to follow the alternation of the applied field. Characteristic frequencies are < 10^{2} Hz.

In addition, the dielectric losses can also be reported in the form of tanδ, also called dissipation factor (DF) which is defined as follows:

$$\tan\delta = \frac{\sigma/\omega + \varepsilon''}{\varepsilon'} \sim \frac{\varepsilon''}{\varepsilon'} \text{ (at high frequencies)} \quad (12)$$

where σ is the conductivity of the material and ω is the angular frequency of the wave. At high frequencies, as reported in equation (12), the contribution given by the conductivity becomes negligible ($^{\sigma}/_{\omega} \to 0$).

Dielectric analysis of co-existent processes underlines correlations between molecular spectroscopy, which examines the properties of individual constituents, and the techniques characterizing the bulk properties of the material under investigation e.g. FITR and EaB. In particular, the DS technique is very sensitive to the change of polarity inside the polymer chain, since polar molecules e.g. C=O and C-OH are deeply influenced by the external field applied to the material under test [82], [83].

As presented, the abovementioned dipolar molecules are the main products of the thermo-oxidative degradation, for this reason, DS showed to be suitable to follow the degradation grade of the analyzed cable. In particular, DS appears to be appropriate for apolar materials e.g. polyethylene, since its dielectric spectra is not influenced by the external applied field due to the absence of polar species. Hence, degradation mechanisms, which can give birth to oxidized products (e.g. C=O), results into the enhancement of the dipolar properties of the material causing the rise of a relaxation peak in the dielectric spectrum. The intensity of these peaks is directly dependent on the concentration of the considered molecule, so that dielectric spectroscopy can be considered as a quantitative technique.

The correlation of relaxation signals with molecular movements is a result of enough knowledge about composition and morphology of the specimen under test and of further information from nondielectric investigations e.g. FTIR or OIT.

In the last years, the dielectric spectroscopy technique has gained more and more importance in the field of condition monitoring technique thanks to its ability to follow the aging and degradation of the material under test, its ability to assess the actual electrical application of the cable, in addition to its non-destructiveness and possibility to be used on site.

As a matter of fact, at the industrial scale, several setups are available for the evaluation of dissipation factor on site. However, through these devices only few frequencies can be investigated resulting into a non-significant description of the electrical relaxation phenomena of the molecules inside the material.

2.3.9 Charging and Discharging current (CDC) measurements

Insulating materials are used to isolate components of an electrical system from each other and from ground, as well as to provide mechanical support for the components. For this purpose, it is necessary to have the insulation resistance as high as possible, together with acceptable mechanical, chemical, and heat-resisting properties.

Insulation resistance and conductivity are characteristic electrical properties of the material. These quantities can be derived by charging and discharging (CDC) current measurements. It is widely known [84]–[89] that the degradation of the insulation matter causes a reduction of insulation resistance and, consequently, an increase of conductivity (or conduction current). For this reason, insulation resistance measurements can be used as a condition monitoring technique for cables. This method is a non-destructive technique and it is standardized in the ASTM D257 published in 2014 [90]. The setup used for this kind of measurements will be described in the following Chapter.

The charging and discharging current (CDC) measurement procedure is made up of two phases (Figure 25):

1. **Polarization phase:** the DC voltage is switched on and the polarization process begins. An electrometer acquires the measured current (usually nA) as a function of time
2. **Depolarization phase:** the DC voltage is switched off and the specimen is short-circuited. The depolarization current is registered until it reaches nearly 0 as a value of current.

The polarization phase is characterized by a sum of different currents:

- **Capacitive currents**, corresponding to the current that charges the insulation as a pure capacitor. It is the main responsible for the very high initial value of currents during CDC measurements. It rapidly reaches zero.
- **Polarization current**, corresponding to the current generated by the alignment of polar molecules in the applied DC electric field orientation. Once all the molecules are oriented in the electric field direction, this value of current reaches zero.
- **Conduction current,** corresponding to the current that continuously flow through the specimen. It raises with the increase of the degradation state of the polymer.

From the conduction current value, it is possible to obtain the conductivity value of the material under test. It can be derived according to:

$$\sigma = \frac{J_c}{E} \ (S/m) \tag{13}$$

where J_c is the conduction current density and E is the applied electric field.

The depolarization phase allows the evaluation of the very low-frequency (LF) dielectric response (e.g. complex permittivity) through the Fourier Transform [80], [87]. The LF complex permittivity, in particular, is related to the interfaces inside the polymer matrix, e.g., the interface between the crystalline and the amorphous phases in semi-crystalline polymers.

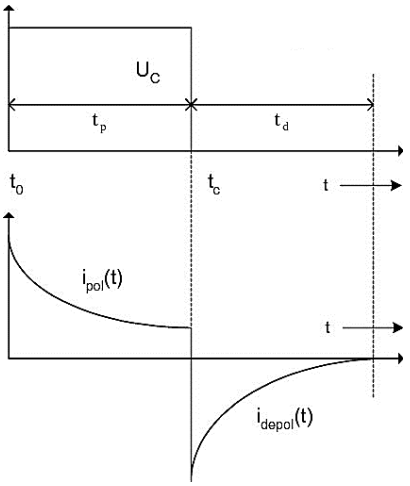

Figure 25 Typical diagram of polarization and depolarization currents

Using the Fourier Fast Transform (FFT), the complex electric susceptibility can be derived from this measurement. This indicates the degree of polarization of a dielectric material in response to an applied electric field. The higher the electric susceptibility, the greater the ability of a material to polarize in response to the field, and thereby reduce the total electric field inside the material (and store energy).

The response of the dielectric system in the time domain is obtained directly from the depolarization current:

$$\mathbf{g(t)} = -\frac{\mathbf{J_d(t)}}{\boldsymbol{\varepsilon_0 E}} \tag{14}$$

where: J_d is the measured depolarization current caused by the polar species returning to the casual distribution, ε_0 is the permittivity in vacuum; E is the electric field.

Applying the FFT to g(t), the response in the frequency domain (complex susceptibility) $\chi(\omega)$ can be derived through:

$$\begin{aligned} \boldsymbol{\chi(\omega)} &= \boldsymbol{\chi'(\omega) - j\chi''(\omega)} \\ &= \int_0^{+\infty} \mathbf{g(t)\,\exp(-j\omega t)\,dt} \\ &= \int_0^{+\infty} \mathbf{g(t)\cos(\omega t)\,dt - j\int_0^{+\infty} g(t)\sin(\omega t)\,dt} \end{aligned} \tag{15}$$

This expression is related to the complex permittivity through the following formula:

$$\boldsymbol{\chi'} = \frac{\boldsymbol{\varepsilon' - \varepsilon_0}}{\boldsymbol{\varepsilon_0}} \tag{16}$$

$$\chi'' = \frac{\varepsilon''}{\varepsilon_0} \tag{17}$$

This allows the evaluation of the complex permittivity in the low frequency range (up to 1 Hz) [80].

It has been demonstrated in literature that this low-frequency response can be related to the aging of the material since the oxidized species could present huge interfaces whose dielectric response can be investigated through this technique [91]–[93]. Up to now, this technique is used for MV and HV cables but not in LV cables. It is worth noting that this kind of test can be done only on non-energized cables so that measurements have to be coordinated with the maintenance work scheduled for the system.

2.3.10 Space charge measurements protocol using the Pulse Electro Acoustic (PEA) method

The PEA method is a non-destructive technique for profiling space charge accumulation in polymeric materials. A sequence of high-voltage pulses of very short time length (5-30 ns) is applied to an insulation specimen interposed between two electrodes. Each pulse produces an electric force displacing internal charges and generating pulsed acoustic pressure waves in correspondence of each charge layer in excess with respect to neutrality. The resultant pressure pulse is detected by a piezoelectric transducer, so that the charge distribution in the specimen under test can be obtained from the output voltage of the transducer. The output signal is then amplified and registered by a digital oscilloscope. The analysis of space-charge profiles is restricted to one dimension: this assumption imposes to consider that space charge density, electric field distribution and acoustic wave propagation can vary only along the specimen thickness (z-coordinate) [2], [94].

A sketch of the PEA system is reported in Figure 26.

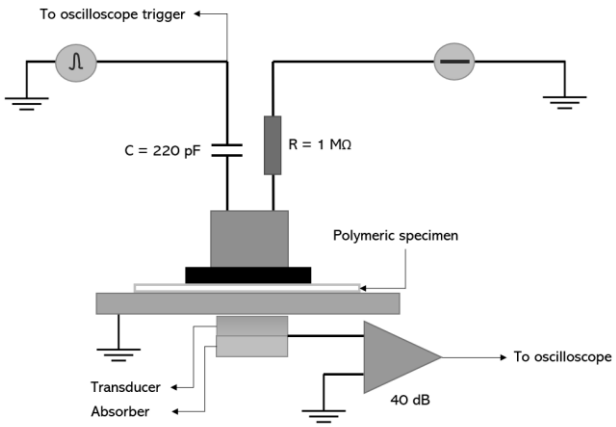

Figure 26 PEA schematic representation

A quantity associated with the space charge accumulation in the insulation bulk is the absolute stored charge density q_S which represents the absolute value of the charge accumulated in the bulk at a chosen depolarization time. It can be obtained from the space charge profiles after polarization at field E applying the following equation [95], [96]:

$$\mathbf{q_s(E, t_d) = \frac{1}{l}\int_0^l |q(x, E, t_d)|dx} \tag{18}$$

where l is insulation thickness and t_d is the depolarization time, $q(x,E,t_d)$ is the space charge profile detected at time t_d. The maximum absolute stored charge density, q_{SM} is evaluated at the beginning of depolarization (t_d = 2 s).

In order to investigate the charge dynamic, the trap-controlled mobility μ can be estimated from depolarization characteristics $q_S(E,t_d)$ with t_d in the range 0-3600 s, according to the following simple, but approximate, expression [95], [96]:

$$\mathbf{\mu = \frac{2 \cdot \varepsilon}{q_s^2} \cdot \frac{dq_s}{dt}} \tag{19}$$

where ε is the electric permittivity of the insulating material.

Space charge formation and accumulation is one of the main causes of faults in HV or MV cable systems, since it can cause the distortion of the electric field in the insulation bulk. On the contrary, space charge accumulation does not constitute a problem for the insulation of low voltage cables. A typical graph representing the charge distribution as a function of the cable thickness is reported in Figure 27 [97].

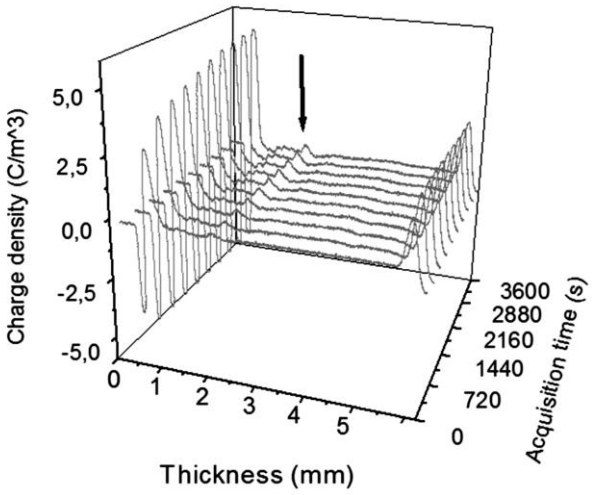

Figure 27 Space charge distribution as a function of the sample thickness and acquisition time [97].

The change in the space charge distribution and accumulation is reported to be related to the degradation of the polymer insulating material since aging causes the modification of distribution of both chemical and physical traps.

Chemical traps are characterized by chemical species inside the polymer matrix, e.g. antioxidants, contaminants, cross-linking by-products and fillers. Physical traps can be linked to morphological inhomogeneities of the polymeric chains, particularly at the interface between the crystalline and amorphous phase or between the polymer and the inorganic fillers. Oxidation together with other degradation phenomena e.g. chain scissions and free radical formation may alter trap density and depth, usually increasing the number or the depth of charge traps [89], [94], [98]–[100].

For these reasons, the space charge measurements can be suitable for the evaluation of the cable health condition on-site. In particular, the test can be performed when the cable is in operation, if it operates in DC, since the application of an external DC electric field is needed in order to inject charges inside the material. The impulse voltage, in addition, together with the piezoelectric sensor can mobilize the space charges which can be finally recorded by the instrumentation [94]. Moreover, several portable devices are commercially available and used on HV and MV cables.

2.3.11 Time domain reflectometry (TDR)

The degradation of the polymeric insulation matter is reported to cause a variation of the characteristic impedance of the cable [22], [41]. Hence, it is possible to use this quantity as a condition monitoring technique for cable diagnostics.

The time domain reflectometry (TDR) is a testing technique which measures reflections of an impulse signal along a single conductor to detect and locate any changes in the cable impedance. If the cable owns a homogenous impedance, there will be no reflection between the initial peak and the final peak (i.e. open circuit). On the contrary, if the cable shows any variation of impedance, part of the initial signal will be reflected back to the source, resulting in little peaks on the acquired spectrum. The reflected signal can be linked to distance along the cable and its peak amplitude allows the estimation of the impedance change [101]–[103]. Under these circumstances, TDR tests are capable to assess the condition of the entire cable, but very little information are referred to changes in the insulation.

TDR is also used to analyze local aged spots since the spectrum can show variations as a function of the cable length (Figure 28). For this reason, recent works focused on the possibility to couple a portable dielectric spectroscopy measurement device together with a TDR-capable VNA. This setup can provide an in-depth assessment of the health of the cable system in a non-destructive way. In fact, an initial evaluation through dielectric spectroscopy allows the

definition of the global status of the cable insulation and its capability to fulfill its role without any damage to the system. An additional test through TDR setup permits the evaluation and identification of local aging defects and cable weak points.

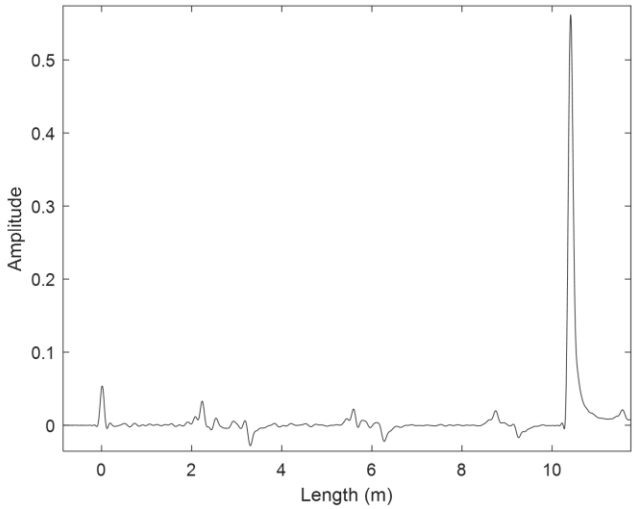

Figure 28 Typical TDR measurement spectrum as a function of cable length [40].

2.4 Modelling

In addition to the various condition monitoring technique, modelling of the different material properties with aging and application life of LV cables can provide useful tools for maintenance scheduling and, in case, the replacement of the considered cable.

The aim of predictive modelling is to estimate either the residual life of in-service cables or the expected life of new cables as accurately as possible. Predictive modelling is based on the simulation of in-containment environmental conditions by accelerated tests, allowing extrapolation to much lower aging conditions, like the ones inside NPP.

Numerous methods are available for the modelling of the behavior of cables undertaking radiation and thermal aging. In particular, the most common method used for thermal aging is the application of the Arrhenius law, which describes the relationship among the rate of degradation, the aging temperature and the exposure duration [2], [35], [104]–[107].

The Arrhenius law assumes that the rate of the thermal aging mechanism decreases with the inverse of temperature (in a log scale). Namely, it claims that the short-term simulation of thermal aging at higher temperature causes the same degradation as the service long-term aging at lower temperature. In a first approach, degradation can be described by a single reaction of rate constant *k,* which is defined as:

$$\mathbf{\ln k = \ln A - \frac{E_a}{RT}} \tag{20}$$

where A is pre-exponential factor, E_a is the activation energy for the process analyzed, R is the perfect gas constant and T is the absolute temperature.

Therefore, if the reaction rate is plotted against the inverse of temperature in a log/log diagram, a straight line is obtained whose slope is the activation energy. This plot allows the extrapolation of test data to lower or higher temperature than the ones used to perform the accelerated aging. Unfortunately, it is sometimes possible to have a *break point* which determines a change in the kinetic regime. Hence, the activation energy is not the same over the whole temperature domain. As an example, XLPE polymers show, in DSC thermographs, a melting peak between 90 and 120 °C. If accelerated aging is performed in such conditions, when the polymer is entirely in the amorphous phase, it is not possible to extrapolate the behavior of the material at lower temperatures (semi-crystalline phase), like the ones used for the actual application for cable systems. This occurs due to the fact that the morphology of the material would deeply influence degradation mechanisms occurring during aging. For this reason, the use of the activation energy value related to complete amorphous polymer could lead to wrong estimation of the real service life of the insulation system.

An example of an Arrhenius plot is reported in Figure 29.

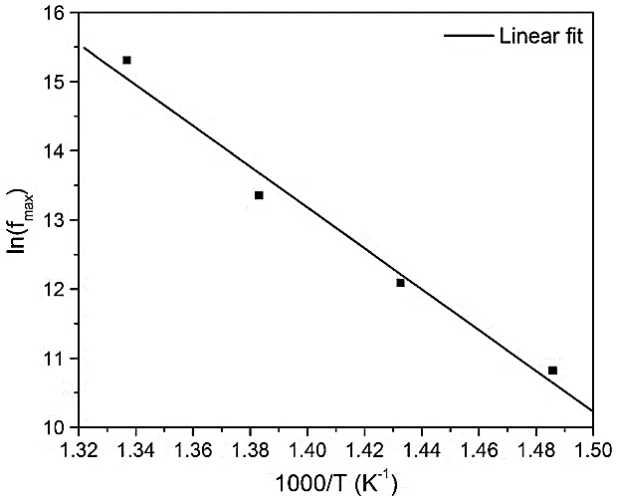

Figure 29 Arrhenius plot for a generic thermal degradation mechanism

Focusing on the radio-chemical aging modeling, the most used approach is based on the power law extrapolation method [104], [108].

This method is based on the extrapolation of test data obtained under isothermal conditions in air over a range of dose rates. The test data obtained at different dose rates are used to determine end point criteria which are extrapolated graphically to the service dose rate.
In order not to face diffusion limited oxidation and, consequently, the premature mechanical failure of the analyzed material, the maximum dose rate at which homogeneous oxidation occurs must be assessed. Once established, at least two (preferably 3) dose rates should be

selected, each dose rate preferably being one order of magnitude lower than the previous value.

This modeling procedure, which showed to be feasible on elastomers and thermoplastics, is based on the evaluation of the elongation at break with aging. To establish the end-of-life dose value at each dose rate, the relative elongation EaB/EaB_0 is plotted against absorbed dose (EaB_0 is the initial value of the elongation at break).

Usually, a commonly accepted end-of-life criterion, also proposed in the IEC 60216-2, is equal to the 50% of the initial value of the property.

Obviously, the real on-site aging conditions must be initially assessed in order to enable the end point criterion at each dose rate to be established without extreme extrapolation.

The dose at which the end point criterion is reached, namely the dose to equivalent damage (DED), is then plotted against the dose rate in a log/log plot (Figure 30). This plot is found to be linear in some materials e.g. some polyolefins, enabling extrapolation to lower dose rates. The end point dose is then given by:

$$\mathbf{DED} = \mathbf{K} \cdot \mathbf{DR^n} \qquad (21)$$

where *DR* is the dose rate; *K* and *n* are empirical constants specific to the material tested. The constant *n* is usually ranged between 0 and 0.3.

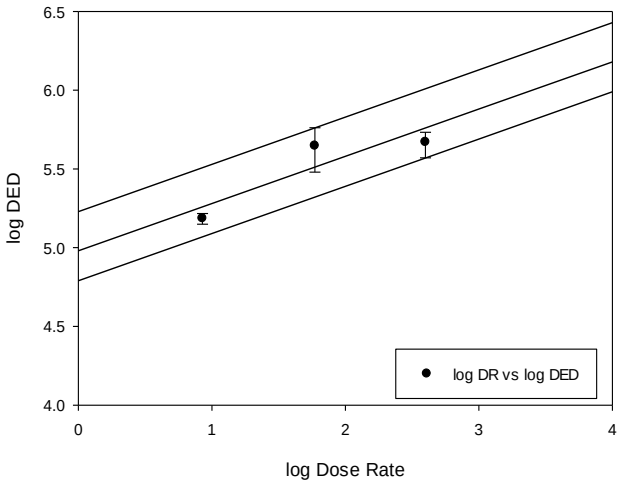

Figure 30 Example of the application of the power law extrapolation method

This method permits the evaluation of polymer behavior with aging at very low dose rates. However, the breakdown point, at which the radiation effects become dominant over the thermal aging effects, must be assessed. On a log/log plot (DED versus dose rate) obtained through the power law extrapolation method, the thermal-dominant area would be represented by a line with slope equal to 1 (Figure 31). However, the extrapolation of DED values within the thermal dominated region would be in certain cases too high. Hence, often two sets of

data are used (thermal and radiation aging data) depending on the dominant stressor in the investigated region.

A more detailed description of this modelling approach is reported in Chapter 6 Modelling of cable aging, where it is applied to the materials analyzed in this Thesis.

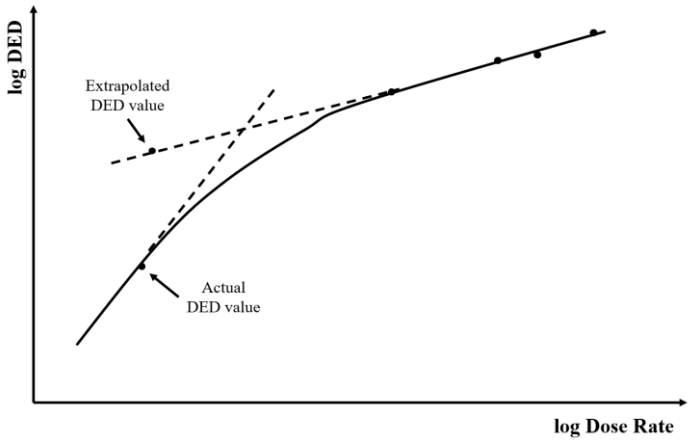

Figure 31 Extrapolation of DED near the thermal aging limit

CHAPTER 3

MATERIALS AND METHODS

3.1 INTRODUCTION

In the following section the materials and methods used in this Thesis are described and commented. In particular, the cable properties and the accelerated aging performed are reported in sections 3.2 and 3.3, respectively. Moreover, the experimental setup for electrical (3.4.1) and physical-chemical (3.4.2-3.4.5) testing is described.

3.2 CABLE SPECIMENS

The cable specimens analyzed in this Thesis are those provided in the framework of the H2020 TeaM Cables project. The project focuses its research on the insulating materials given that the insulation of the cable is the essential part for guaranteeing the cable electrical functionality. Indeed, the primary insulation is the part most affected by aging. In addition, the current end-of-life criteria of nuclear cables are based on the assessing of the health of insulating materials.

The project cable materials are limited to two types of insulating polymers:

- Cross-linked Polyethylene (XLPE) is the most used low voltage cable in Gen III reactors
- Ethylene propylene diene terpolymer (EVA-EPDM) is commonly used for systems important to safety.

In this Thesis, only the results coming from the tests on cross-linked polyethylene are reported and discussed.

3.2.1 Polymeric compound

Nowadays, cross-linked polyethylene is the most common insulating material for cable applications. It is characterized by a three-dimensional network structure made through intermolecular chemical bonds. This polymer is produced from linear polyethylene (PE) through a cross-linking process during which the PE macromolecules bond each other, giving birth to a 3D structure. This crosslinking process requires reactive groups along the PE macromolecules, allowing the formation of new chemical bonds between carbon atoms or between silanol groups. There are three main cross-linking process commercially available:

- Crosslinking through peroxide (e.g. DCP)
- Crosslinking through silanes
- Crosslinking through radiation

Inside this Thesis, the polymer matrix is obtained by the crosslinking through silanes which is the most common XLPE compound used for low-voltage cable because it is the fastest and cheapest technology for crosslinking.

As a result, the polymer network takes the chemical structure reported in Figure 32.

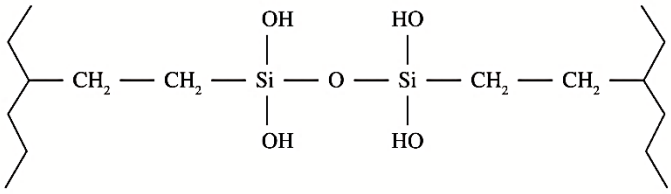

Figure 32 Silane cross-linked chemical structure

In order to investigate the contribution of additives and fillers inside the polymer, the compounds used for cable manufacturing are based on the same silane XLPE matrix but with different kinds and amounts of additives. The additives types and concentrations used inside the TeaM Cables project are reported in Table 1.

Table 1 Concentrations and amounts of additives used in the project materials. Phr: per hundred resin.

Type of additive	Commercial compound	Concentration
Primary antioxidants	Irganox® 1076 [109]	1 phr
Secondary antioxidants	Irganox® PS802 [110]	1 phr
Flame retardants	Alolt 60 LDS [111]	50 phr

The analyzed compounds are:

- Compound #1: Silane XLPE + Primary Antioxidants + Secondary Antioxidants
- Compound #2: Silane XLPE + Both Antioxidants + Flame retardants

3.2.2 Specimens geometries

In order to investigate the contribution of the geometry on the aging of the primary insulation, the polymeric compounds have been prepared in three forms, characterized by an increasing complexity, from the simplest polymer-only tape to the most common twisted pair cable geometry (Figure 33).

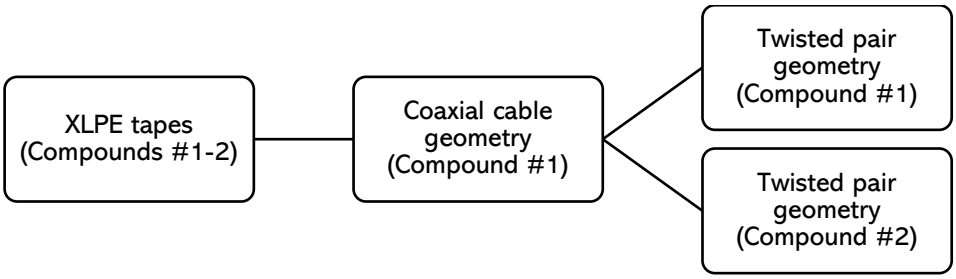

Figure 33 TeaM Cables specimen geometries

3.2.2.1 Coaxial cables

The geometry of the coaxial cables investigated is reported in Figure 34. These cables are made up of five concentric parts:

1. Conductor: copper, solid wire, diameter: 0.88 mm
2. Primary insulation: Silane XLPE (compound #1), thickness 1.05 mm
3. Shielding: Copper wire braid
4. Sheath: Low smoke zero halogen rubber, thickness 0.7mm

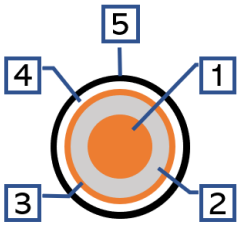

Figure 34 Multilayer structure of coaxial cables under investigation. (1) Conductor – Copper, (2) Primary insulation – XLPE, (3) Polymeric film – PET, (4) Shielding – Copper wire braid, (5) Sheath – Low smoke zero halogen rubber

3.2.2.2 Twisted pair cables

The geometry of the investigated twisted pair cables is reported in Figure 35. These cables are made up of three twisted pairs with three different insulation compounds in addition to the shielding and external sheath. In particular:

1. Conductor: copper multiwire, 28x0.208mm
2. Primary insulation
   a. Silane XLPE (compound #1), thickness 0.7 mm
   b. Silane XLPE (compound #2), thickness 0.7mm
   c. EVA/EPDM, thickness 0.7mm
3. Shielding: Copper tape
4. Inner sheath: Low smoke zero halogen rubber, thickness 1.6mm
5. Collective screen: copper wire braid
6. Outer sheath: Low smoke zero halogen rubber, thickness 1.6mm

Figure 35 Multilayer structure of twisted pair cables under investigation. (orange) Conductor – Copper, (grey) Primary insulation, (orange) Shielding – Copper wire braid, (black) Sheath – Low smoke zero halogen.

3.3 Accelerated aging conditions

In order to investigate the evolution of the physical-chemical properties of the primary insulation of the analyzed material, accelerated aging has been performed on project samples. The aim of the accelerated aging is to simulate the typical aging conditions inside NPPs. In the Team Cables project, in particular, seven different aging conditions (4 radio-chemical and 3 thermal-only) have been chosen. Aging conditions and withdrawal times are reported in Table 2.

Table 2 Aging conditions used in the project

Aging condition	Temperature (°C)	Dose rate (Gy/h)	Sampling time	Max. aging time
Low dose rate	47°C	8	2880 h	14415 h
Medium dose rate	47°C	60	860 h	4810 h
High dose rate	21°C	400	167 h	835 h
Combined aging	87°C	8	2880 h	14415 h
Thermal aging (87)	87°C	-	~3 months	~2 years
Thermal aging (110)	110°C	-	~3 months	~1.5 years
Thermal aging (130)	130°C	-	~3 months	~1.3 years

3.3.1 Radio-chemical aging

The accelerated radiation aging has been performed by UJV Rez a.s. (www.ujv.cz/en), one of the project's partners in Prague (Czech Republic). The irradiation facilities are two ^{60}Co γ-irradiation sources, with the cobalt placed in the center of a cylindrical irradiation chamber (Figure 36).

In both cases, the cables to be aged have been placed around stainless-steel cylinders and placed around the irradiation source. A dose gradient is expected within the samples since the actual dose depends upon the distance from the cobalt source.

To perform combined aging conditions, a thermobox has been incorporated inside the Panoza facility. In this way it has been possible to obtain a temperature around 87°C next to the irradiation facility.

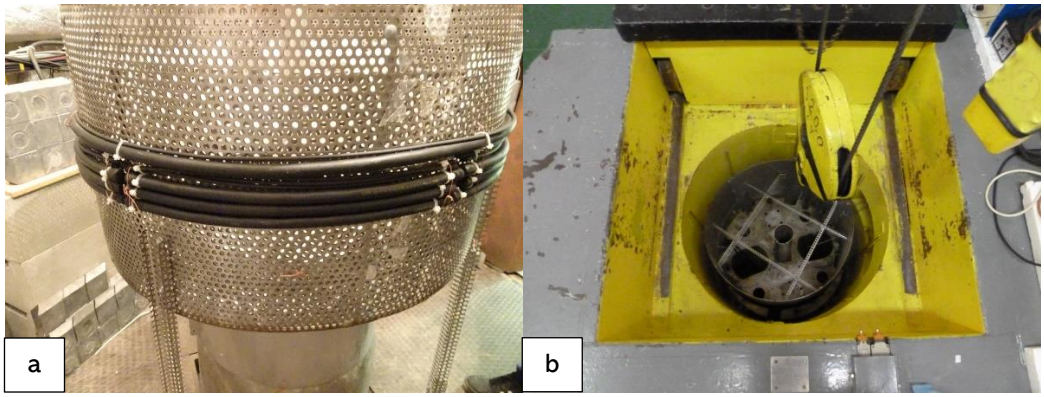

Figure 36 UJV Rez irradiation facilities (a) Panoza (b) Roza. Courtesy of UJV.

3.3.2 Thermal aging

Thermal aging has been performed by PIMM laboratory at ENSAM (pimm.ensam.eu), one of the project's partners in Paris (France). The thermal aging facilities are several ovens (Figure 37) set at different temperature according to the project's purposes (87, 110 and 130°C).

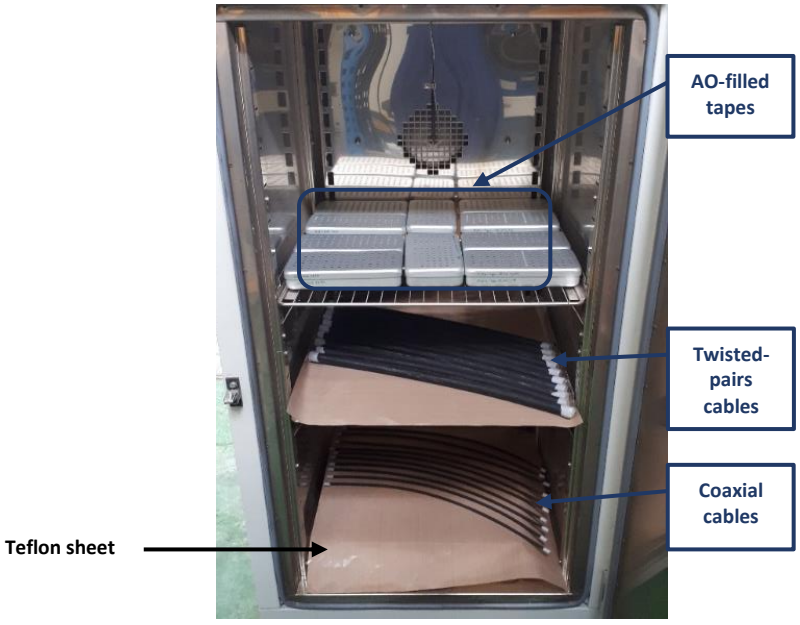

Figure 37 Air-ventilated oven used for thermal aging conditions

The different materials have been aged in separate ovens according to their formulation in order to avoid any exchange of additives (e.g. antioxidants) due to physical migration which could deeply influence the oxidation kinetics of the different materials.

3.4 EXPERIMENTAL SETUP

In the following sections, the experimental setup used for the investigation of the aging of the materials under test is presented. Electrical tests have been performed at LIMES laboratory in Bologna while Chemical tests have been performed at PIMM laboratory in Paris.

3.4.1 Dielectric spectroscopy

The dielectric spectroscopy measurements have been performed by the mean of the Novocontrol Alpha Dielectric Analyzer v2.2 (Figure 38).

As presented in the previous Chapter, this experimental setup allows the evaluation of capacitance, dissipation factor (tanδ) and complex permittivity (ε' and ε''); in the frequency range between 10^{-2} -10^{6} Hz.

Figure 38 The Novocontrol Alpha dielectric analyzer v2.2 used for the tests

This instrument consists of two major components:

- a **frequency response analyzer** with a sine wave and DC-bias generator and two AC voltage input channels. Each input channel measures the AC voltage amplitude of an applied sine wave. In addition, the phase shift between the sine waves applied to both inputs are detected. In particular, each channel measures the amplitude and phase angle of the harmonic base wave component of a signal applied to the input. The harmonic base wave component is measured at the frequency of the AC sine wave generator. Most other signal components are suppressed. In addition, higher harmonics may be measured.
- a **dielectric (or impedance) converter** with a wide dynamic range current-to-voltage converter and a set of precision reference capacitors.

A voltage *V* with fixed frequency $\omega/2\pi$ is applied to the sample capacitor. *V* causes a current *I* at the same frequency in the sample. In addition, there will generally be a phase shift between current and voltage describe by the phase angle φ (Figure 39). δ angle is defined as follows [80]:

$$\boldsymbol{\delta = 90° - \varphi} \tag{22}$$

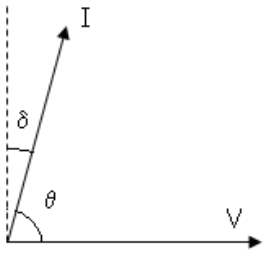

Figure 39 Dissipation angle representation

Under these circumstances, the δ angle is described as the dissipation angle since it is referred to the energy dissipated during the polarization process. The tangent of the δ angle (tanδ) is defined as the dissipation factor, as already presented in the previous Chapter (§ 2.3.8).

A schematic representation of the dielectric spectroscopy measurements setup and its sample holder are reported in Figure 40.

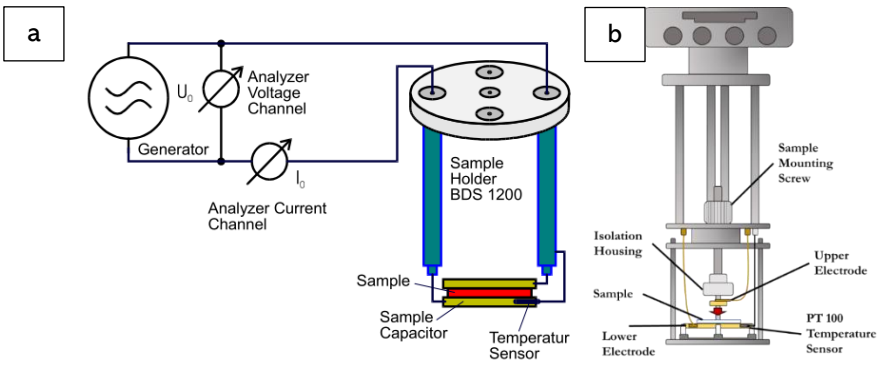

Figure 40 Schematic of the dielectric spectroscopy measurements system (a) and its sample holder (b)

The equipment was set using the following test parameters:

- Applied voltage: 3 V_{rms}
- Frequency range: 10^{-2} – 10^{6} Hz
- Temperature: 50°C (in oven).

For coaxial cables, input voltage was applied to the inner conductor through a BNC plug and output signal was obtained through the copper wire braid shielding. In the case of twisted pair cables, the input voltage was applied to one of the two conductors while the output signal

was obtained connecting the second conductor with the shielding and finally to the output BNC cable. Cables and BNC connections are shown in Figure 41.

The presented setup is designed for testing flat specimens, hence the required reference capacitance in vacuum needs be evaluated by reducing the coaxial cable geometry to a plane capacitor. Equivalent capacitor diameter D_{eq} was calculated through the following equation:

$$D_{eq} = \sqrt{\frac{8 \cdot d \cdot L}{\ln\left({}^{R_2}/_{R_1}\right)}} \tag{23}$$

where: d is the thickness of the insulation, L the length of the metallic mesh, and R_1 and R_2 the inner and outer radius of the electrical insulation, respectively.
Finally, the reference capacitance C_0 was calculated through:

$$C_o = \varepsilon_0 \frac{\pi\left(\frac{D_{eq}}{2}\right)^2}{d} \tag{24}$$

where: ε_0 is the permittivity in vacuum.

The use of 50°C as a test temperature has been chosen since it has been observed that this temperature allowed easier test repeatability and a reduction of environmental noise.

In the case of twisted pair cable, a finite element method (FEM) modeling is required in order to obtain a reference capacitance value. Modeling was performed through COMSOL® Multiphysics software. For the twisted pair cables analyzed, with length of about 50 cm, the reference capacitance obtained by the simulation resulted to be equal to around 25 pF.

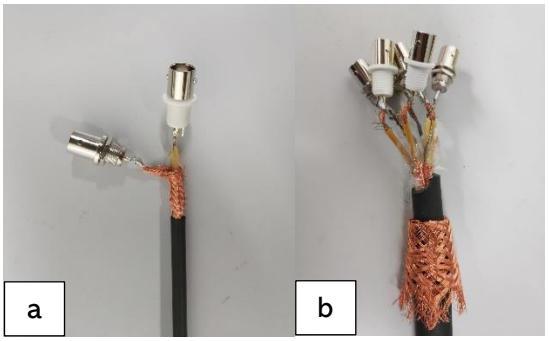

Figure 41 Photographs of cable connections. (a) coaxial cable, (b) twisted pair cable.

3.4.2 Differential Scanning Calorimetry (DSC) measurements

DSC measurements was performed using a TA instruments Differential Scanning Calorimeter Q1000 (Figure 42).

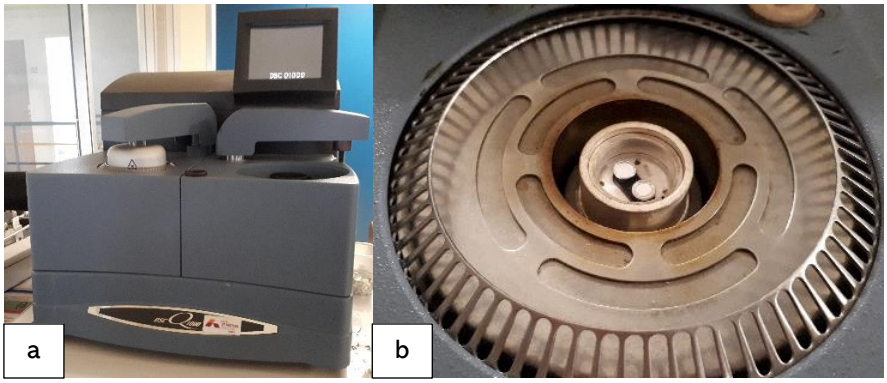

Figure 42 Photo of the TA DSC Q1000 (a) and its furnace (b)

Before each measurement campaign the instrumentation was calibrated through an Indium reference.

Samples with mass between 5 and 10 mg have been placed inside aluminum pans while as a reference an empty closed aluminum pan has been used.

The procedure used is made up of an initial equilibrium at low temperatures and two runs under 50 mL/min flow of pure Nitrogen, in particular:

1. Equilibrium at -80°C
2. Isothermal for 2 mins at -80°C
3. **First run**: heating rate up to 200°C at 10°C/min
4. **Second run**: cooling rate down to -80°C at 10°C/min

In order to keep into account measurement uncertainties, tests have been performed at least two times. Once obtained the thermograms, the value of crystallinity ratio is obtained from the first heating run through the method explained in § 2.3.4.

3.4.3 Oxidation Induction Time (OIT) measurements

The instrumentation used for OIT measurements is the same as DSC ones. The main difference lays on the possibility to switch the furnace atmosphere into pure oxygen in order to perform the tests in oxidative environment. For the same reason, the aluminum pans are placed without the lid, hence open, in order to facilitate the oxidative reactions.

The steps used are the following:

1. **Heating** from room temperature to 210°C (heating rate 10 °C/min) under pure nitrogen
2. Isothermal for 5 mins at 210°C
3. **Switch of the gas** from nitrogen to pure oxygen

4. Isothermal at 210°C until the end of the test

The test was considered complete after the entire detection of an exothermal peak assigned to the oxidation reaction of the analyzed material. Once obtained the thermograms, the value of oxidation induction time (OIT) is obtained as described in § 2.3.5.

3.4.4 Fourier Transform InfraRed (FTIR) spectroscopy measurements

The infrared spectra have been recorded by the mean of a Perkin Elmer FTIR Frontier spectrometer in ATR mode (Figure 43).

Figure 43 Photo of the Perkin Elmer FTIR Frontier spectrometer in ATR mode

Due to the cable specimens under test, only ATR (superficial) mode was possible to be performed due to the concavity and reduced thickness of the samples.

In ATR mode, the contact between the analyzed sample and the diamond/ZnSe of the ATR is ensured by screwing a clamp device. Before testing, the background spectrum is registered by the single beam spectrum of the clean and dry ATR element. Once obtained, the FTIR spectra have been imported in the Perkin Spectrum software in order to analyze the different peak heights. Since the FTIR technique can be considered as a quantitative technique, comparing the different peak heights with some reference peaks over different aging periods can be used to investigate the evolution of the concentration of some interesting molecules (e.g. oxidized species) with aging.

In particular, the $-CH_2$ peak related to the crystalline phase of the polyethylene (1472 cm^{-1}) is kept as the reference peak. Among the various peak, as reported in Chapter 2, the peak related to the esters (around 1742 cm^{-1}) is shown in literature to be a good aging marker since it may be related to the oxidation grade of the polymer. Moreover, in the cases here analyzed, ester peaks are also linked to the phenolic antioxidants and their degradation products which exhibit the same bond, making the distinguishing of one phenomenon from the other difficult. The ratio between the two abovementioned absorbance peaks heights is defined as Ester index.

$$\textbf{Ester Index} = \frac{\mathbf{A_{1742cm^{-1}}}}{\mathbf{A_{1472cm^{-1}}}} \tag{25}$$

The trend of the ester index over aging time is quite often used as an aging marker due to its ability to evaluate the oxidation, hence degradation, grade of the material under test in a non-destructive way.

3.4.5 Tensile stress measurements

The tensile stress measurements have been performed by UJV Rez in Prague (Czech Republic). As presented, this technique is the most commonly used for assessing the conditions of cables inside NPPs. For this reason, a number of standards and ease-of-use are present [38], [55], [112]–[114].

The sample used for these measurements should have been, as required by standards, in form of dumbbells. Unfortunately, due to the small diameter of cable jacket and insulation, there is no possibility to obtain the required dumbbells. For this reason, tubular specimens, obtained removing the inner conductor from the cable sample, were used to perform the tests.

The tubular specimens of the minimal total length L of 60 mm have been prepared after transversal cutting the insulated wire samples to pieces with length of about 65 mm. Then, all the other layers were carefully removed paying attention at not damaging the insulation material.

Figure 44 Instron 3366 used for tensile stress measurements

For tensile test, the calibrated Instron 3366 machine (Figure 44) equipped with pneumatic grips with smooth steel surfaces were used. Tubular specimens have been placed between the two gauges and the following test parameters were applied:

a) Testing (cross-head) speed: 50 mm/min
b) Initial grip distance for *tubular* specimens: 30 mm
c) Rate of tensile test data acquisition: 50 mm/min

The test is considered as completed when the breaking of the sample occurs.

As a result, the stress/strain curve was registered and obtained, from this it is possible to obtain the ultimate elongation value (Elongation-at-break) through the equations presented in the previous Chapter (p.21).

CHAPTER 4
RESULTS

4.1 INTRODUCTION

In this Chapter the evolution of the physical-chemical and electrical properties of the investigated materials is reported. Results are obtained from different microscale chemical measurement techniques, i.e., FTIR, DSC analyses and OIT measurements as well as from macroscale electrical and mechanical tests, i.e., dielectric spectroscopy and tensile testing.
Due to the long aging periods considered i.e., low dose rate and combined aging, chemical and tensile stress measurements are performed on a limited number of specimens. Similarly, thermally aged cables are characterized only through electrical measurements (dielectric spectroscopy).

4.2 DIELECTRIC SPECTROSCOPY RESULTS

In this section the results coming from the dielectric spectroscopy measurements are reported for the three cable specimens analyzed.

4.2.1 Coaxial cable

Figure 45-48 depict the behavior of the real and imaginary parts of permittivity vs. frequency, for the different radio-chemical aging conditions considered.

The dielectric spectra show similar behavior among the different radio-chemical aging conditions. In general, both the real and imaginary parts of permittivity increase with aging, as expected. As it has been already presented in Chapter 1, aging causes the formation of polar molecules which deeply influence the electrical behavior, resulting in the increase of the complex permittivity. In particular, the imaginary part of permittivity is the quantity to be analyzed since it is associated to the dielectric losses of the material and thus can be used as an aging marker [2], [59], [83], [115].

However, in all the conditions considered, one can observe, in the early period of exposure, an initial decrease of the imaginary part of permittivity. This peculiar behavior will be described in the discussion section since it could be related to a sudden change in the micro-chemical properties of the material under test.

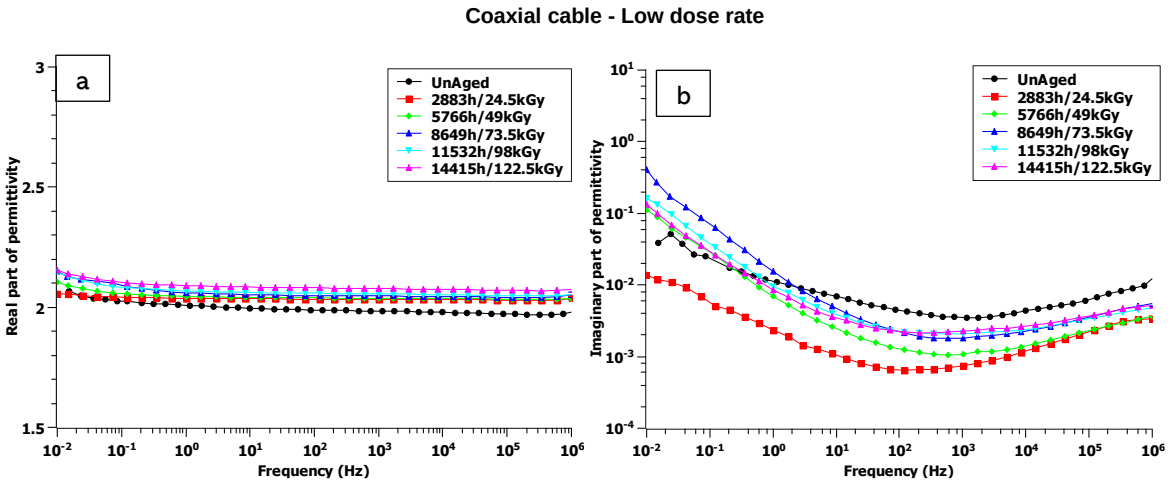

Figure 45 Real (a) and imaginary (b) parts of permittivity for low dose rate aging. Coaxial Cable.

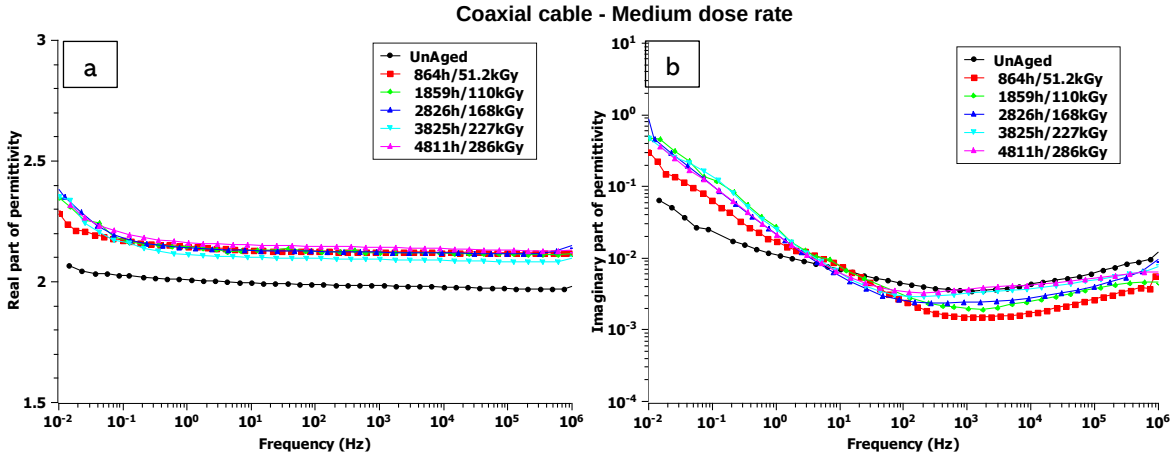

Figure 46 Real (a) and imaginary (b) parts of permittivity for medium dose rate aging. Coaxial Cable.

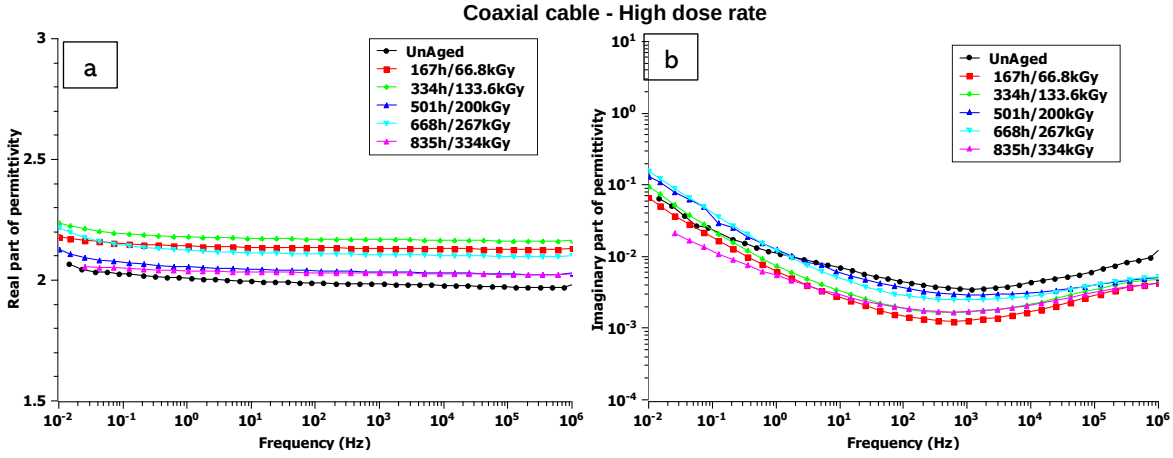

Figure 47 Real (a) and imaginary (b) parts of permittivity for high dose rate aging. Coaxial Cable.

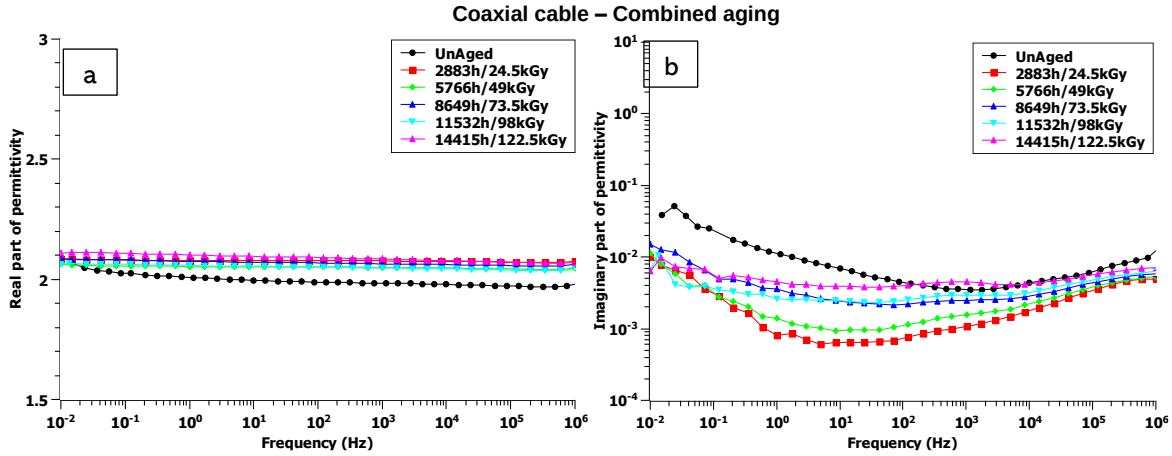

Figure 48 Real (a) and imaginary (b) parts of permittivity for combined aging. Coaxial Cable.

On the contrary, further aging causes the increase of the complex permittivity except for the last aging period of the high dose rate aging. This result may be considered as an outlier given by inhomogeneities related to the specific specimen under test since no similar behavior can be evaluated in any other condition.

The trend over frequency of the imaginary part of permittivity is characterized by one peak at very high frequencies (~10^6 Hz) followed by an almost linear increase of dielectric losses with frequency in the low frequency region (10 – 0.1 Hz). Due to its characteristic frequencies, the former peak may be linked to dipolar polarization phenomenon. The low-frequency increase of the imaginary part of permittivity might be associated with the Q-DC (quasi-DC) conduction phenomenon [116]. In brief, this is obtained by the presence of free ions and/or radicals created during e.g., aging which can move towards the material when it is subjected to a very low frequency AC field, similarly to what occurs during DC conduction. In the dielectric spectra, the Q-DC conduction is characterized by a constant value of the real part of permittivity to which it corresponds a slope equal to -1 in the imaginary part of permittivity trend over frequencies. Figures 45-48 depict the possible presence of Q-DC conduction for the irradiated cables which show a -1 slope in their imaginary part of permittivity trends. In particular, since the complex permittivity behavior is the same among aged and unaged samples, this could be also linked to free radicals coming from incomplete crosslinking process e.g., unbonded silanol groups. However, it must be highlighted that analogous frequencies may be related to interfacial polarization (§ 2.3.8). It can be noticed from Figure 45-48 that both the parts of complex permittivity raise lowering the frequencies, this suggests the presence of a possible interfacial polarization peak, whose higher frequency branch can be evaluated in the analyzed region. This could be imputed to both physical and chemical interfaces inside the material under tests, as it will be discussed in the following Chapter. Nevertheless, it is worth pointing out that the two phenomena just described can be overlapped, hence it is not possible to distinguish the effects of Q-DC conduction and of interfacial polarization in the dielectric

spectra. In the analyzed case, contribution of Q-DC conduction appears to be significantly predominant over the interfacial polarization phenomena due to the very modest increase of the real part of permittivity. Hence, it is not simple to speculate on the kind and number of interfaces created during aging. Nonetheless, the combined aging causes a change of the low-frequency imaginary part of permittivity slope, imputing cable dielectric response at low frequencies only to interfacial polarization mechanism.

In the case of cables, it is usually a good practice to report the trend of the dissipation factor (tanδ) since it is not dependent on the geometry of the cable under analysis. Hence, the use of tanδ can avoid any error coming from empirical or FEM (finite element method) analyses for the calculation of the relative capacitance in vacuum. Given the almost negligible variation of ε' through the investigated frequencies, the dissipation factor (tanδ) is function of the dielectric losses (ε''). At high frequencies, it can be considered as directly proportional to the imaginary part of permittivity, hence it can be itself used as an aging marker (§ 2.3.8).
The trend of dissipation factor for all the conditions considered is reported in Figure 49.

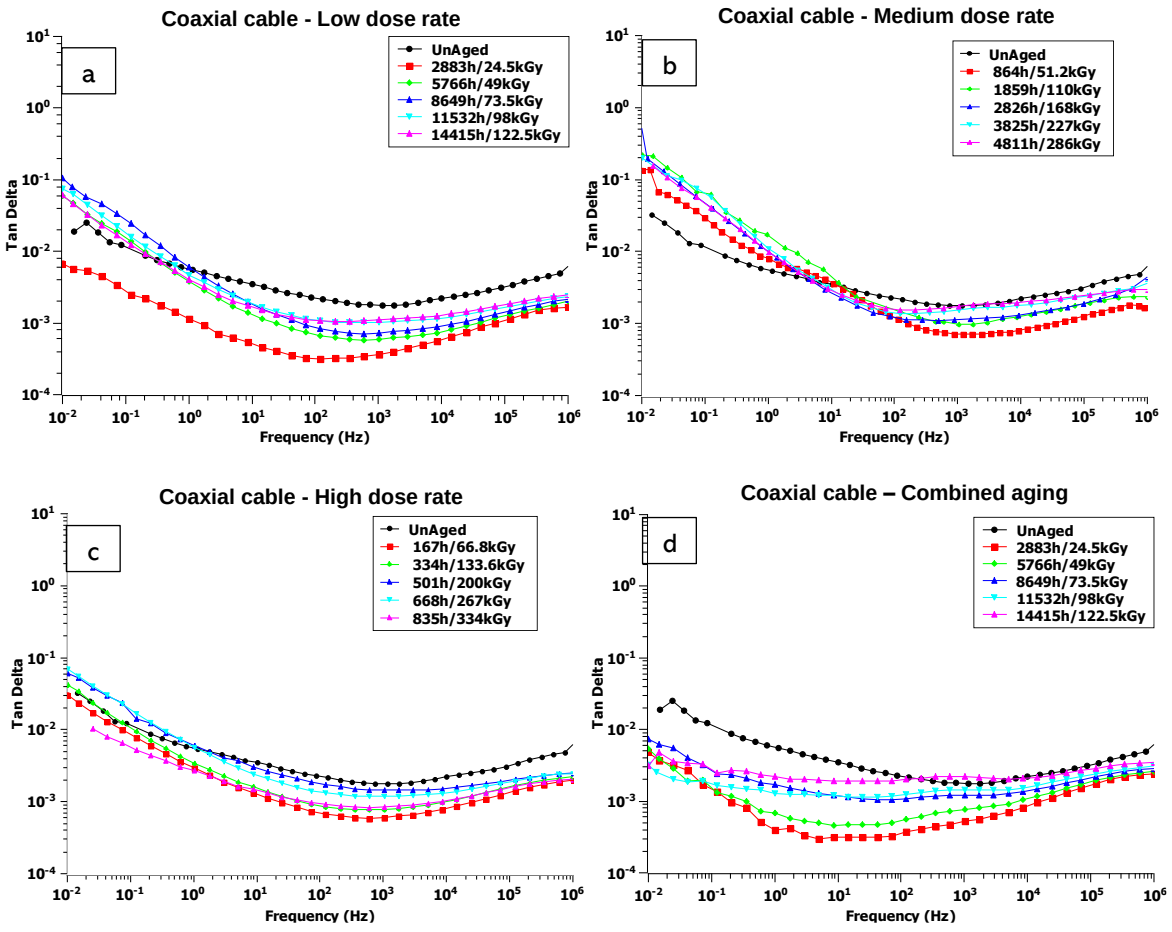

Figure 49 TanDelta as a function of frequency for the different aging conditions analyzed (a) Low dose rate (b) Medium dose rate (c) High dose rate (d) Combined aging. Coaxial Cable.

Here, tanδ depicts the same trend over frequency as the imaginary part of permittivity just discussed. Despite the same tendency, the absolute values are different due to the ratio by the real part of permittivity value and the contribution of conductivity in tanδ equation (§ 2.3.8). In order to better understand the increase of the dielectric losses with aging, the tanδ values at fixed frequencies (100 kHz and 0.1 Hz) are plotted against the aging time for all the conditions analyzed. These frequencies have been chosen since it has been shown in literature [2], [48], [59], [83], [115], [117], [118] to well represent the highest and lowest frequency region analyzed through the dielectric analyzer (10^{-2}-10^{6} Hz), respectively.

Focusing on the high frequencies, as it can be seen in Figure 50.a, different aging conditions lead to different electrical responses of the material under test. In particular, one can observe that the increasing slope of the dielectric losses is directly related to the dose rate which is applied to the material. As a result, the high dose rate aging with time causes a steep increase of the dielectric losses while lower dose rates result into a slower variation of the losses, according to the higher dose rate the faster the degradation rate approach described in § 1.4.

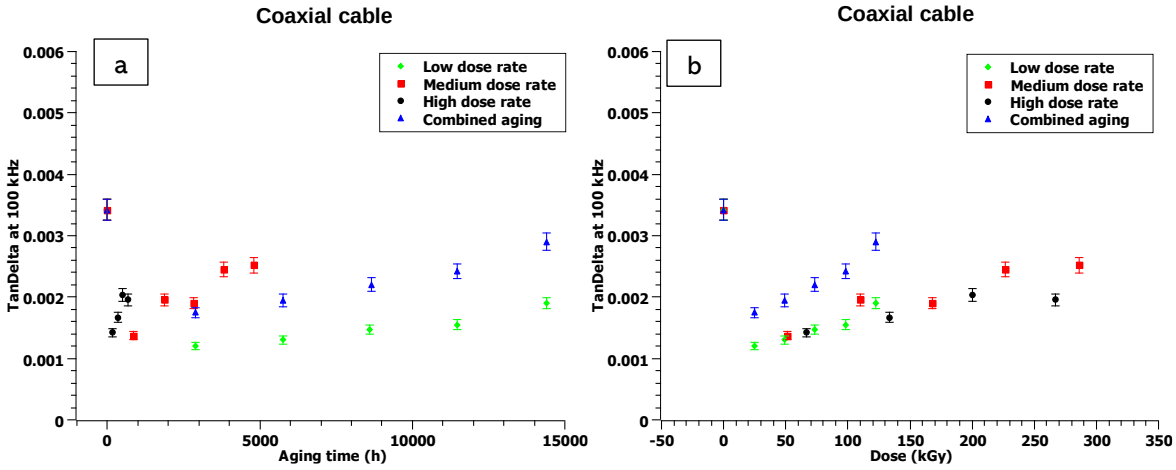

Figure 50 Tan(delta) at 100kHz for the different radio-chemical conditions considered as a function of (a) aging time and (b) total absorbed dose. Coaxial cable.

Referring to the amplitude of the dielectric loss increase, it is shown that the high dose rate condition causes a lower (or negligible) increase of the dielectric losses with aging time. This behavior could be related to the diffusion limited oxidation (DLO) phenomenon [35], [119] and it will be discussed in the following section.

Referring to the increase of losses with dose (Figure 50.b), it is possible to claim that substantially no differences can be appreciated among the different aging conditions before reaching 200 kGy. Further aging causes the divergence of the trends: medium dose rate values continue to increase, while high dose rate ones slightly decrease (DLO effect).

Combined aging, which is realized by the superposition of the thermal stress to the low dose rate, replicates the slope of the low dose rate trend almost perfectly, but tanδ values are higher.

This behavior suggests that, for the analyzed conditions, the slope of the growing of the dielectric losses is only related to the radiation stress, while the temperature results into an upward shift of the dielectric losses.

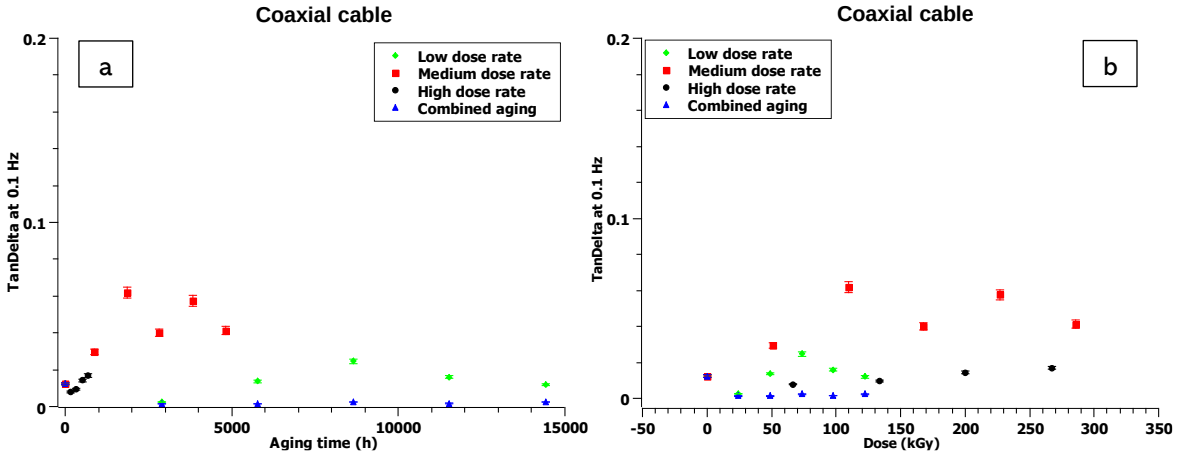

Figure 51 Tan(delta) at 0.1 Hz for the different radio-chemical conditions considered as a function of (a) aging time and (b) total absorbed dose. Coaxial cable.

Focusing on the low frequency domain (Figure 51.a), one can observe a non-homogenous increasing trend for dose rates higher than 70 Gy/h. Lower doses show a monotonous increase of the dielectric losses.

With respect to the dissipation factor amplitude, different dose rates result into different tanδ values. In particular, medium dose rate conditions appear to own the highest dielectric losses in this frequency area.

It is important to recall that this frequency region is related to the Q-DC conduction phenomenon and interface polarization. From the presented results, it is possible to claim that radicals and interfaces created during dose rates <70 Gy/h are significantly more copious than the ones created under high dose rate conditions. However, the non-monotonous increase of tanδ suggests that this frequency region is not feasible for the investigation of the aging evolution of the analyzed cable. Moreover, the considered frequency does not reproduce the rise of the dielectric losses with the increase of the aging conditions severity.

Figure 52 reports the coaxial cable tanδ trend as a function of frequency for the three analyzed aging temperatures. All the displayed spectra are characterized by the trend over frequency similar to the one already described for the combined aging condition. Indeed, the trend at low frequency does not exhibit any behavior imputable to Q-DC conduction. This could be linked to the effect of thermal stresses which rapidly recombine the radicals created during aging. The first aging period results into the reduction of the tanδ trend throughout all the frequency region investigated, as already presented in the case of the radio-chemical aging conditions. This was then imputed to microstructural modifications which weaken the dipolar response, as it will be discussed in the following Chapter. Further aging causes the raise of the

dielectric loss values, whose increase is directly proportional to the aging time. However, very little increasing variations are appreciable for the two lower aging temperatures (87 °C and 110 °C); while a peculiar decrease is revealed in the case of the 130 °C aging condition.

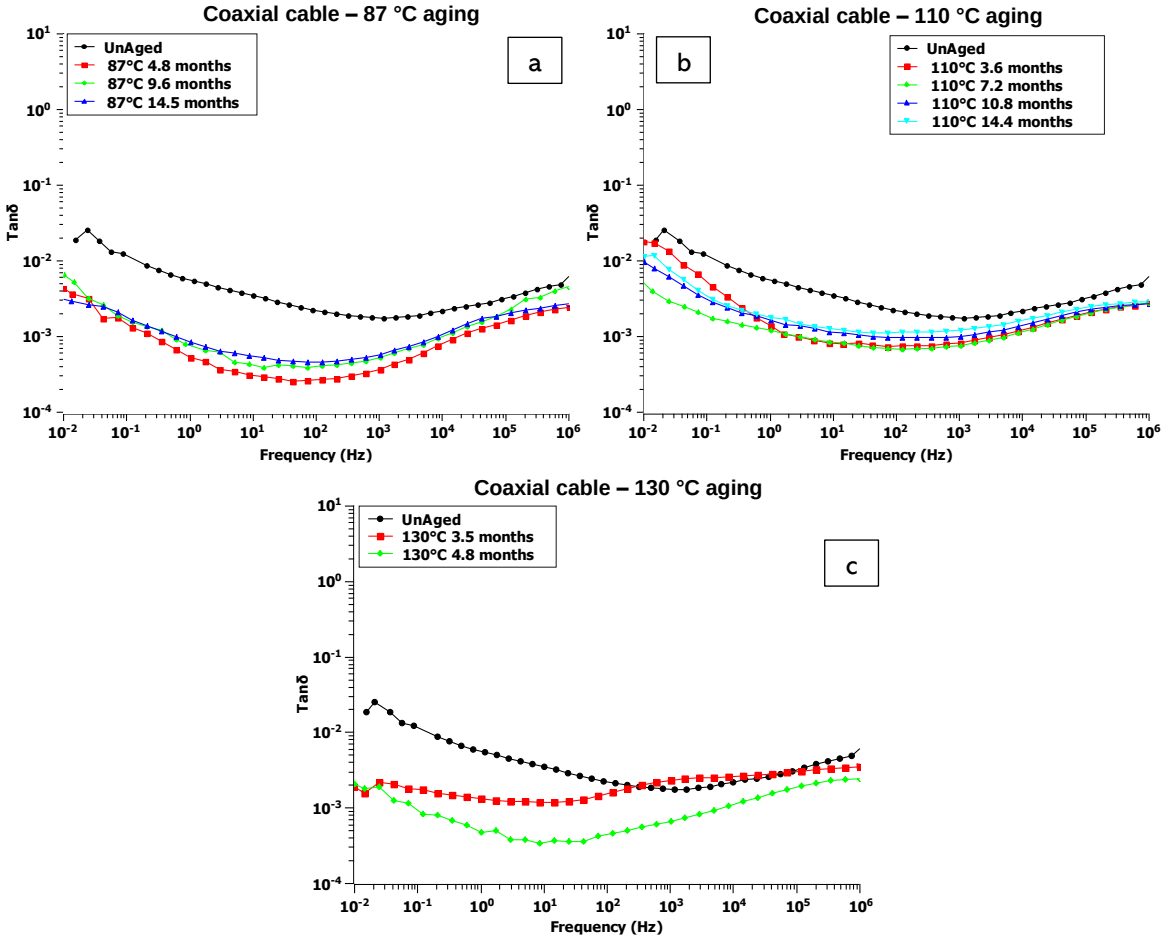

Figure 52 Dielectric losses as a function of frequency for different aging period. (a) 87 °C, (b) 110 °C, (c) 130 °C. Coaxial Cable.

In order to better describe the evolution with aging, the trend of the dissipation factor at 100 kHz and 0.1 Hz is reported in Figure 53.

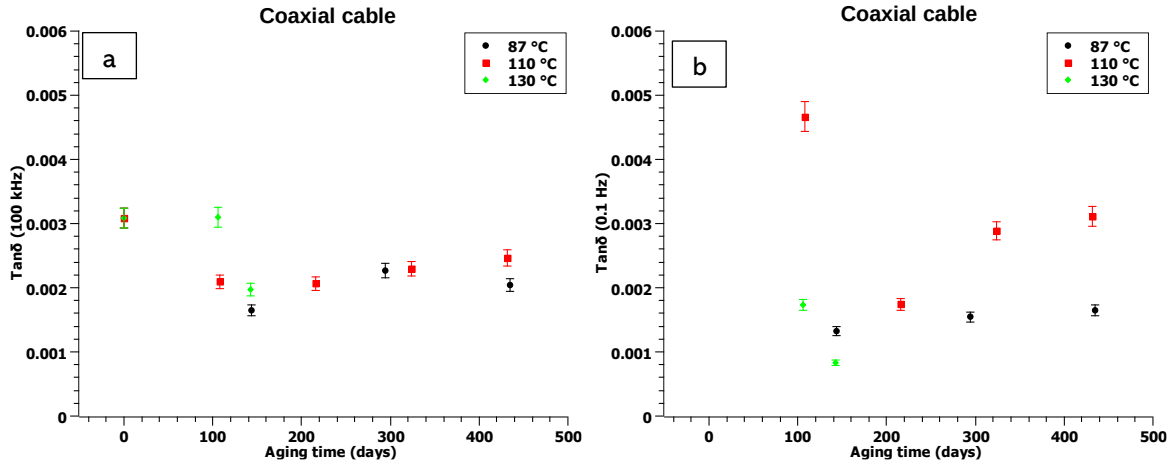

Figure 53 Tan(delta) at (a) 100 kHz and (b) 0.1 Hz for the different thermal aging conditions analyzed. Coaxial cable.

From Figure 53.a it is possible to notice that, at high frequencies, very little increase of the property is appreciable after the initial reduction, as already discussed. In particular, marginal variation can be noticed among different aging temperatures. Moreover, the tanδ values reported are still at very low value, suggesting that no significant concentration of dipolar species e.g. oxidized ones arose. It could be concluded that the presence of the two antioxidants result into a synergistic effect, which essentially makes the tanδ dependent particularly on aging time rather than on the aging temperature.

The low-frequency dielectric response (Figure 53.b) is characterized by a significant decrease of the property during the first aging periods followed by an increase of tanδ. Even in this case, the variation of the values with aging is very reduced, suggesting that the arrangement of interfaces inside the polymer do not substantially vary after the first aging phase.

4.2.2 Twisted pair non-filled cable

For the twisted pair cables, no analytical equation is available for modelling the cable geometry with a simple plane-to-plane capacitor. Hence, in order to avoid any error coming from empirical or FEM (finite element method) analysis for the calculation of the relative capacitance in vacuum, only the trend of the dissipation factor (tanδ) is reported for the twisted pair cables.

Figure 54 represents the behavior of dissipation factor as a function of frequency for all the radio-chemical aging conditions considered.

Even in this case, as expected, the dielectric losses raise with the increase of aging period. The increase can reach up to one order of magnitude in the case of the high dose rate, due to the faster formation of degradation products, which brings to the increase of the dielectric losses. Unlike the previous case, referring to the twisted pair cables, the values of tanδ of the unaged material are lower than the ones related all the aging periods. This could be related to different dipolar properties of the material under test, as it will be discussed in the following Chapter.

The chemical composition of the twisted pair cable under analysis is the same as the previously described coaxial cable. Therefore, the dissipation factor trend with frequency is very similar, thus characterized by the presence of one peak at very high frequencies (~10^6 Hz) followed by, in most cases, a linear increase of the property lowering the frequencies (10 – 0.1 Hz).

It is worth noting that the contribution of interfaces into the electric response over frequency can be significantly higher, in the case of twisted pair cables, due to the measurement protocol used (§ 3.4.1). This takes into account the entire physical interface placed between the two wires, enhancing the low frequency dielectric response related to interfaces.

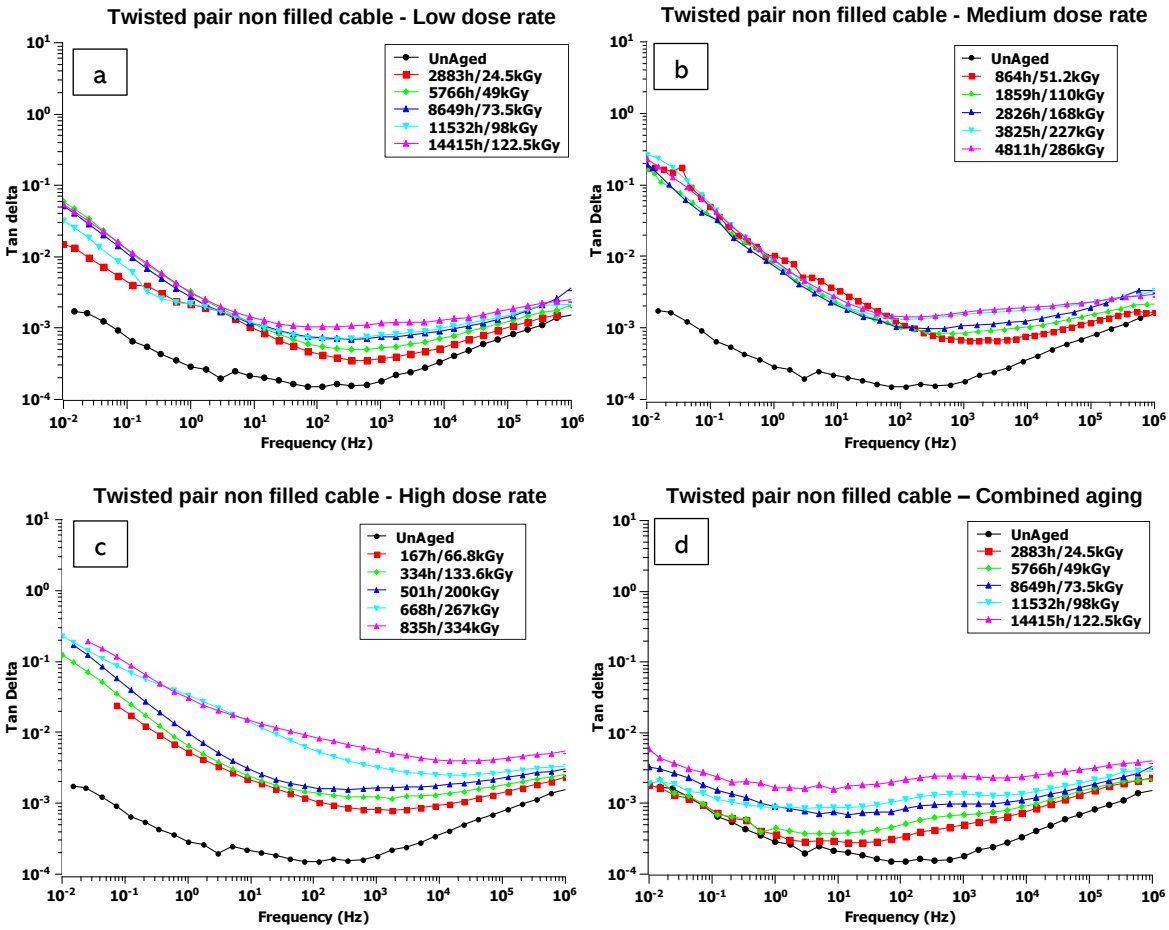

Figure 54 Tan(delta) trend as a function of frequency for (a) Low dose rate (b) Medium dose rate (c) High dose rate and (d) Combined aging conditions. Twisted pair non-filled cable.

Nonetheless, the behavior between the irradiated-only and the combined aging conditions is slightly different at low frequencies. The combined aging condition (Figure 54.d) shows a smaller low-frequency peak, suggesting a lower amount of interfaces inside the polymeric material. On the contrary, in the absence of thermal stress, low dose rate causes a huge increase of the dielectric losses at low frequencies, which is shared among all the other radio-only aged trends. This could be again imputed to possible Q-DC conduction phenomenon together with the creation of wider or copious interfaces, as reported in the case of coaxial cable.

In order to better describe the evolution with aging, the trend of the dissipation factor at 100 kHz and 0.1 Hz is reported in Figure 55.

As expected, the trend of the dissipation factor at 100 kHz follows the typical tanδ increase with aging time. Even in this case, the severity of the aging conditions plays a major role, setting the slope of the increase which is higher as we increase the severity of aging conditions.

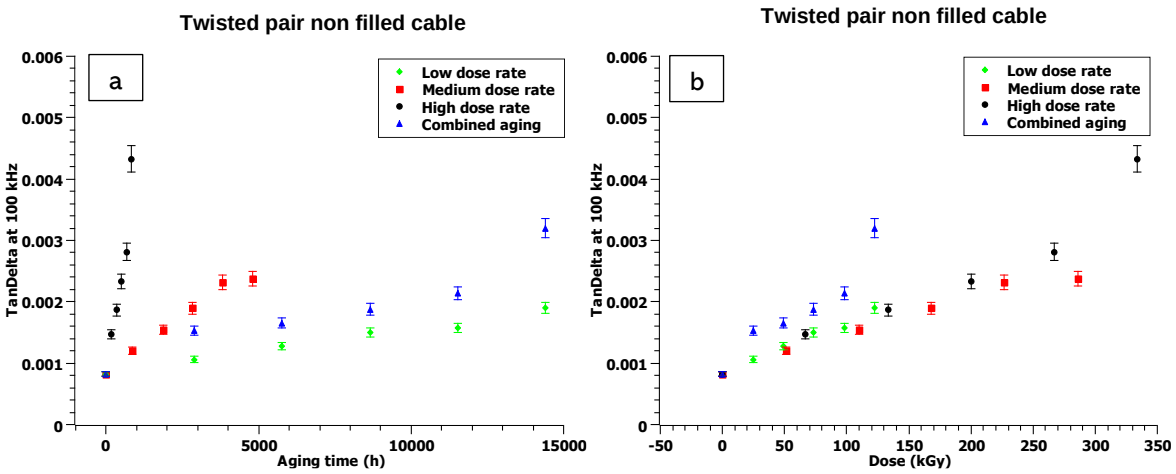

Figure 55 Tan(delta) at 100kHz for the different radio-chemical conditions considered.
Twisted pair non-filled cable

The dielectric losses appear to be larger, in terms of magnitude, than in the case of the coaxial cable. This is probably imputable to the different geometry of the cable or to little microstructural variations inside the polymer compound due to the industrial manufacturing process. However, the trend of the dielectric losses with aging is very similar to the one presented in the case of the coaxial cable. The increase of tanδ for the highest dose rate is very steep, while dose rate reduction results into the flattening of the increase over aging time. Focusing on the trend as a function of the absorbed dose (Figure 55.b), it is possible to point out that the contribution of the different dose rates seems negligible, suggesting that similar absorbed doses cause similar electric behavior, as already presented in the previous case.

This different cable response with aging could be linked to the different layer structure of the twisted pair cable. On the one hand, each cable pair is in contact with air, hence oxygen can affect them. On the other hand, the effective dose rate acting on the primary insulation could be way lower than the one in the case of the coaxial cables. For these reasons, it appears that no oxygen deficit, hence limiting DLO effect, is present in the highest dose rate considered, so that variations of the electrical property could be more significant than in the coaxial cable case (see Figure 10).

Finally, also for the twisted pair cable, the superposition of the thermal stress causes an upward shift of the dielectric losses from the radio-chemical-only aging conditions values both on the time and absorbed dose domains (Figure 55). The last aging period of combined aging shows a significant increase of tanδ probably related to the arising of oxidized species after the running out of antioxidants.

Focusing on the low frequency dielectric response (Figure 56), it is not possible to observe a monotonous increase with aging in all the conditions considered, due to the two concurrent phenomena (Q-DC conduction and interfacial polarization). High dose rate aging exhibits a linear increase of the property with time. Medium dose rate condition results into a negligible

change with aging until the last withdrawal, where a significant increase is registered. Even in this case, combined aging shows a decrease of the dielectric losses in comparison to the radiation-only condition, and a negligible increase with aging time similarly to the low dose rate case.

This behavior suggests that the interfaces created with aging are not directly related to the aging of the material, as other phenomena may be more predominant in this frequency region e.g. conduction, interfacial reorganization.

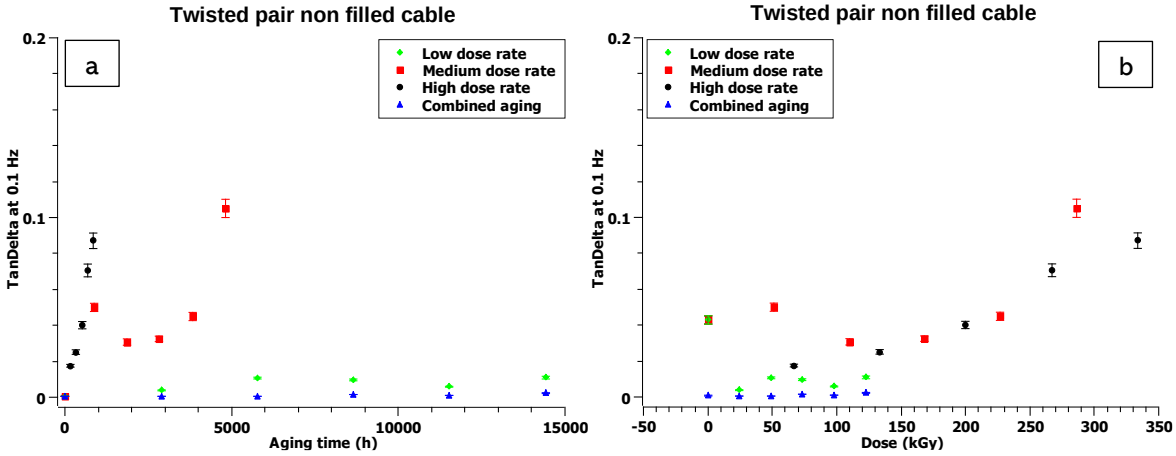

Figure 56 Tan(delta) at 0.1 Hz for the different radio-chemical conditions considered as a function of (a) aging time and (b) total absorbed dose. Twisted non-filled cable.

The frequency spectrum of tanδ as a function of aging time for thermally aged non-filled twisted pair samples is reported in Figure 57. As already presented, the twisted pair non-filled cable owns the same chemical compound as the coaxial cable. Consequently, the trend of the dielectric losses over frequency is very similar to the one described for thermally aged coaxial cables, where the low frequency response has been linked to interfacial polarization phenomena.

Focusing on the electrical response of the 87 °C aging condition, it can be observed that, after an initial increase of the tanδ trend during the first aging period, the remaining curves are almost overlapped one each other. This suggests that the chosen aging temperature and period do not affect the electrical performance of the analyzed material. On the contrary, higher temperatures (110 °C and 130 °C) cause an appreciable variation of the dielectric losses with aging.

The 110 °C aging (Figure 57.b) brings to an increase of the dielectric property throughout all the aging period considered. As it will be discussed in the following, this behavior is more evident in the high frequency region, where one can single out a monotonous increase of tanδ. In contrast, at low frequencies, the curves are almost overlapped, claiming an inappreciable variation of the insulation interfacial arrangement.

Finally, the harshest aging condition (130 °C) shows an abrupt increase of the dielectric losses during the first aging period, followed by a slower increase with aging. However, at this stage, very few withdrawals are available for this aging condition, hence it could be difficult to deliver a complete picture of the microstructural modification occurring in the polymer.

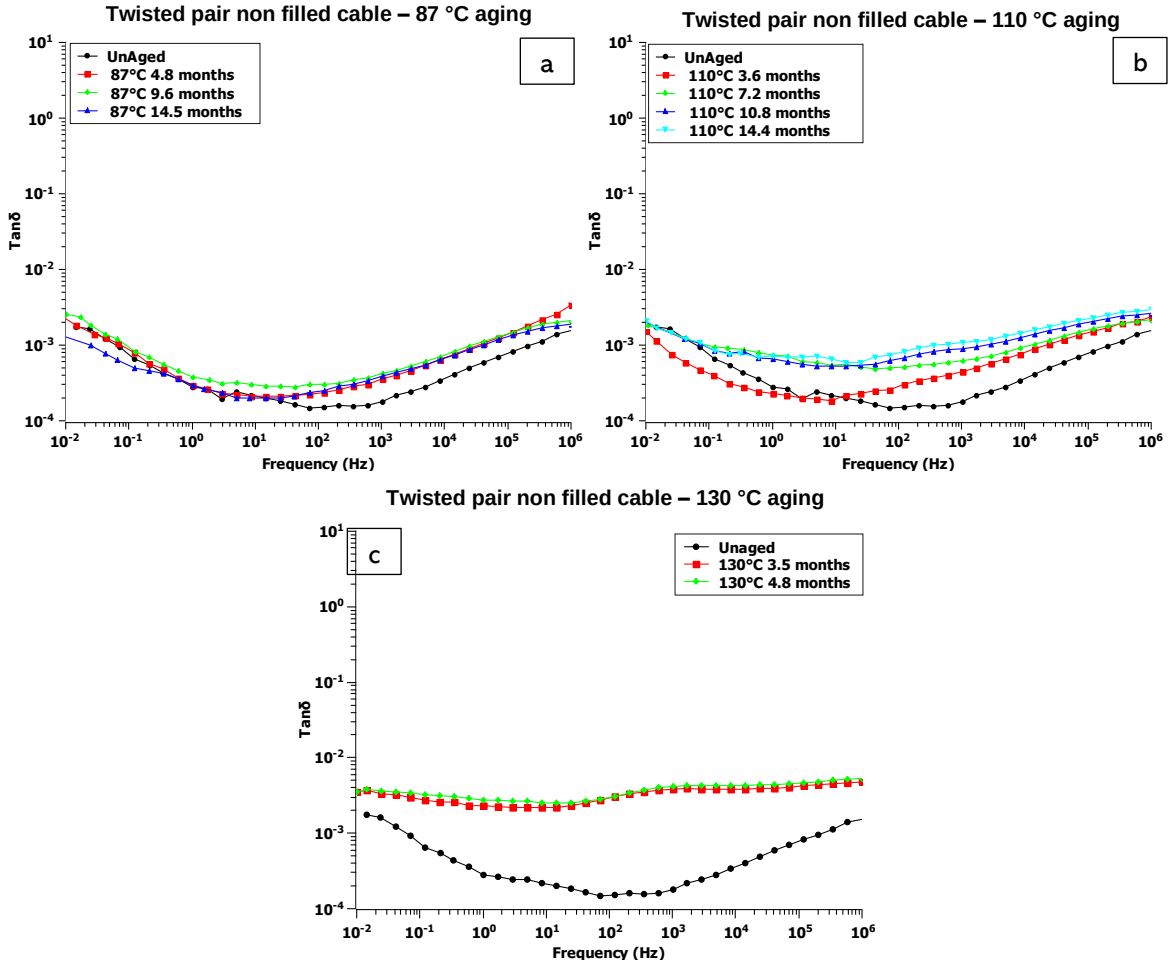

Figure 57 Dielectric losses as a function of frequency for different aging period. (a) 87 °C, (b) 110 °C, (c) 130 °C. Twisted pair non-filled Cable.

Figure 58 depicts the trend over time of tanδ at 100 kHz and 0.1 Hz for the three chosen aging temperatures.

As partially presented above, the response of tanδ at high frequency (Figure 58.a) is characterized by an increasing trend over time for the three temperatures. In particular, the harsher the aging condition, i.e. high aging temperature, the more significant are the increase of the dielectric property over time. It is important to point out that, even if the difference in tanδ values for the two lower temperatures (87 °C and 110 °C) are almost negligible for the first aging periods, sufficiently long aging time leads to the divergence of the two trends. Finally, the 130 °C aging exhibits a very significant increase during the first aging period followed by a slower raise of tanδ value, as reported above.

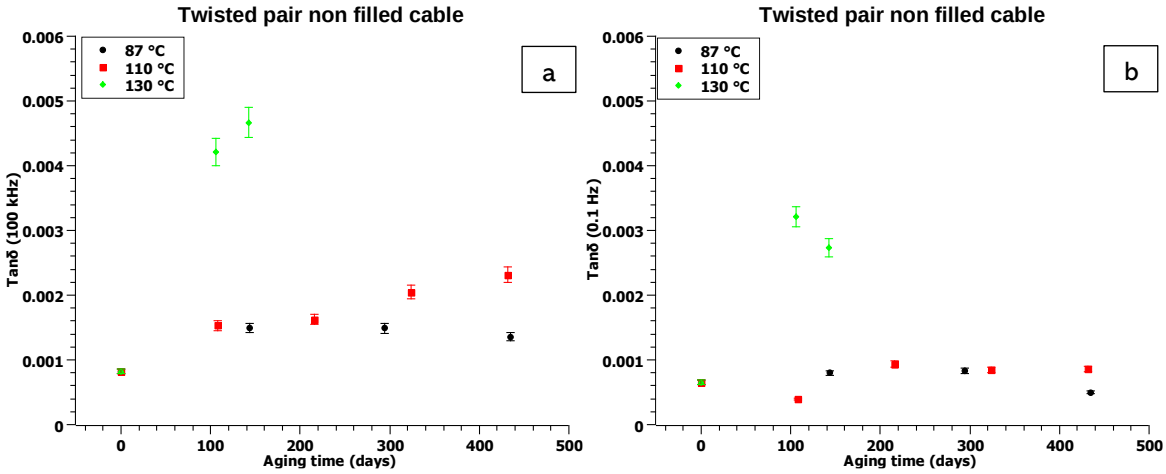

Figure 58 Tan(delta) at (a) 100 kHz and (b) 0.1 Hz for the different thermal aging conditions analyzed. Twisted pair non-filled cable.

Focusing on the low frequency response (Figure 58.b), one can notice an almost constant electrical property with aging, particularly for 87 °C and 110 °C conditions, suggesting a similar arrangement of insulation interfaces with aging. The 130 °C aging, probably due to the very severe condition together with long aging time, brings to the increase of tanδ during the first aging period, which is followed by a slightly reduction of the property.

Under these circumstances, it is evident that the low frequency domain response is not suitable for the evaluation of the aging conditions due to a non-monotonous variation of the property over time.

4.2.3 Twisted pair filled cable

Figure 59 shows the behavior of the dissipation factor as a function of frequency for all the radio-chemical aging conditions considered.

The dissipation factor of the twisted pair cable with compound #2 as primary insulation shows quite different behavior in terms of trend over frequency in comparison to the other two cases described above. Indeed, at least for the irradiated cables, the trend depicts a situation in which the interfacial polarization peak (low frequencies) is enlarged towards higher frequencies. This could be imputed to two main causes: the previous described interfacial peak (as for Compound #1) is broader due to the increase of the size of interfaces or it is due to a convolution of a mid-frequency (around 10^1 Hz) peak which is usually associated with the presence of water molecule bonded to the polymer chain or additives [120], [121].

This last hypothesis may be also confirmed by the fact that ATH molecules are strongly hydrophilic, so that it is possible for the water molecule to permeate inside the polymer bulk and chemically bond at the surface of these fillers.

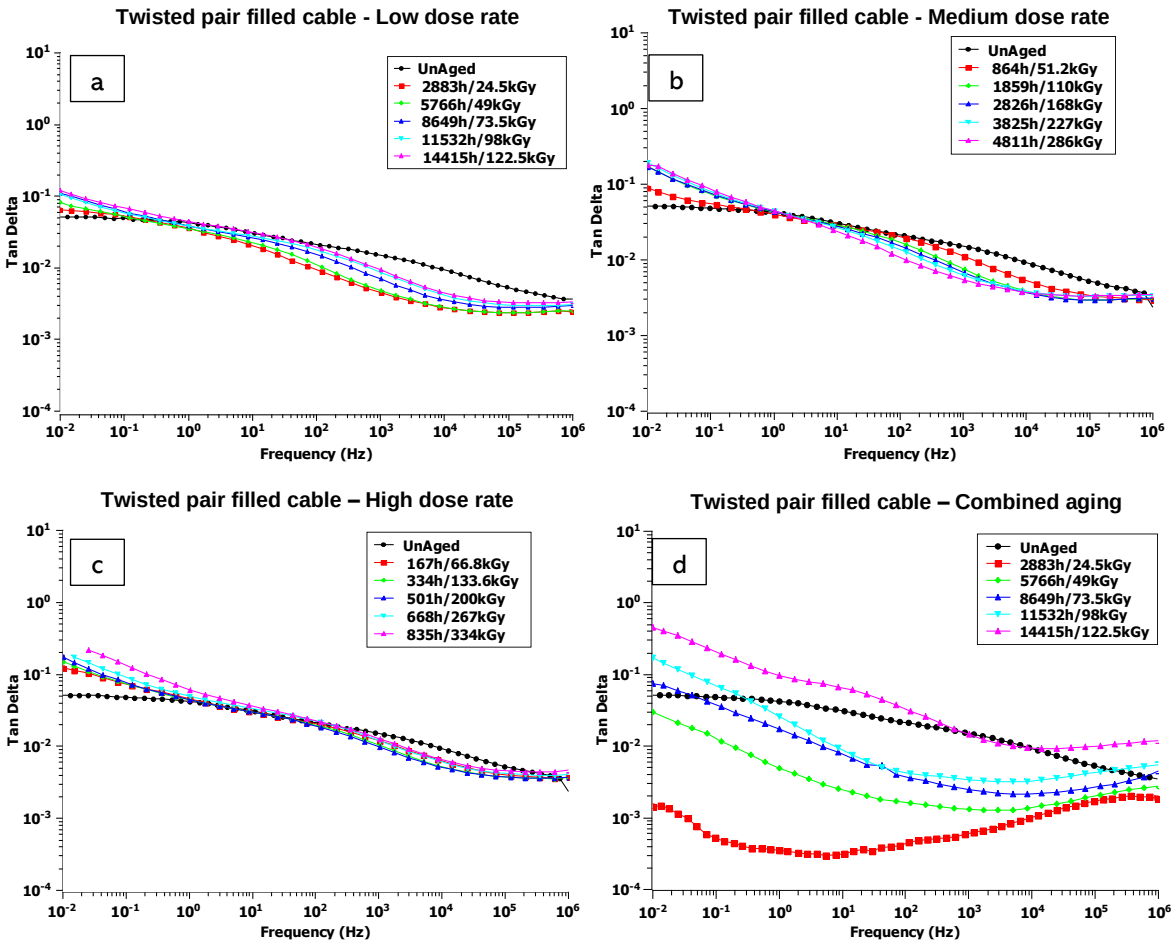

Figure 59 Tan(delta) trend as a function of frequency for (a) Low dose rate (b) Medium dose rate (c) High dose rate and (d) Combined aging conditions. Twisted pair filled cable.

The ATH fillers in such high concentration can easily agglomerate creating wide interfaces whose electrical response is placed in the lowest frequency region among the ones here analyzed. Indeed, very little variations in the low-frequency peak are reported with aging. This might be considered as an indicator that the lowest interfacial peak is related only to the inorganic filler inside the polymer matrix which does not vary throughout aging.

It is worth mentioning that combined aging (Figure 59.d) deeply changes the trend over frequency of the analyzed electrical property. Unlike the radiation-only aging, the addition of thermal stress broads the variation of tanδ both in the high and low frequency regions. In particular, the biggest changes lay in the low frequency domain suggesting that the cable initial interfacial arrangement is deeply modified by aging stresses. Specifically, the values of tanδ in this region varies up to three orders of magnitude indicating a huge increase of interfaces inside the considered compound. This might be possibly related to the action of high temperatures on the weak bonds which usually keep into clusters the ATH fillers. High temperatures and other aging stresses can break these bonds, leading to free ATH molecules

and aged polymeric species. Then, these species can differently arrange themselves causing creation of copious and bigger interfaces, electrically responding in the low frequency region.

The dissipation factor of the twisted pair filled cable does not monotonously follow the increase of aging time. One can observe an initial decrease of tanδ values followed by a little rise in the case of the high and medium dose rates and a continuous increase in the case of the low dose rate and combined aging conditions. The first phase is similar to the case of the coaxial cable, and it could be related to the microstructural modifications occurring in the polymer in the early period of exposure, as it will be presented in the following.

However, the increase of tanδ is not significant for the irradiation conditions here considered. The reason for this could be found again in the filler properties of the insulating material, as it will be discussed in detail in the discussion section. Briefly summarizing, the high dipolar property of ATH can significantly impact on the high frequency spectrum overwhelming the contribution of the other polar species arising with aging, e.g., antioxidants products and oxidized chains. As a result, it would be difficult to single out the contribution of these two dipolar species. Moreover, the non-monotonous increasing behavior could be imputable to the fact that the presence of fillers reduces the actual degradable polymeric matter. Therefore, the same aging stressors cause an enhanced degradation which can effectively cause DLO events also for lower dose rates, e.g., medium dose rate. Under these circumstances, the variation of the dissipation factor for high and medium dose rates is almost negligible at high frequencies. On the contrary, low dose rate condition causes an increase of the dielectric losses as previously discussed for the cases of the other analyzed cables (compound #1), likely imputable to the contribution of longer aging times.

In order to better describe the evolution with aging, the trend of the dissipation factor at 100 kHz and at 0.1 Hz is reported in Figure 60.
Here, the dissipation factor at high frequencies follows the abovementioned behavior. In particular, high and medium dose rates exhibit an initial decrease of the property followed by an increase which is barely noticeable, probably due to not sufficiently enhanced aging inside the polymer. On the contrary, tanδ values for low dose rate and combined aging conditions show an initial decrease until lower values, followed by an almost linear increase with aging. In this case the presence of the thermal stressor causes a downward shift during the first three aging periods probably imputable to the filler response to thermal aging, as it will be discussed

in the following Chapter. Further aging causes an abrupt increase of the property which raise up to one order of magnitude, as seen from the insight in Figure 60.

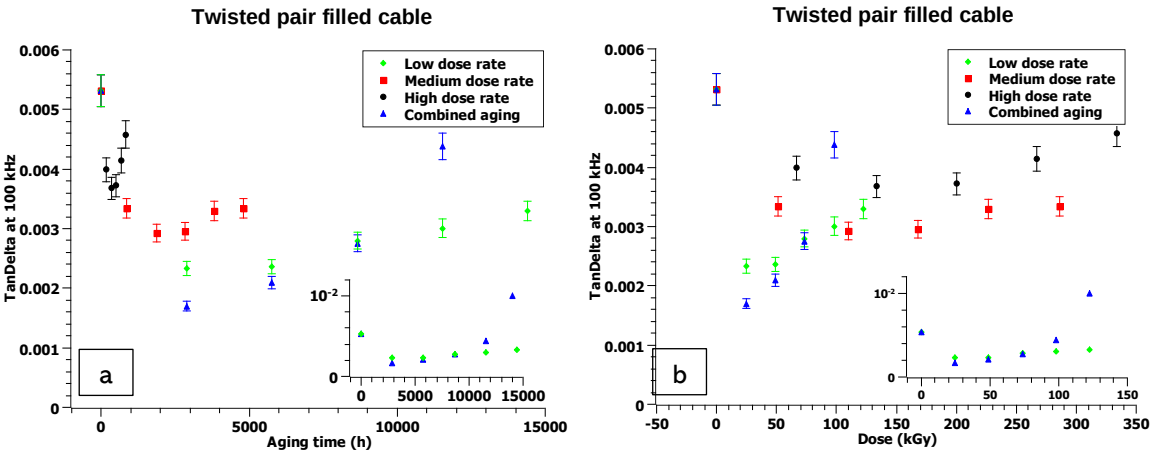

Figure 60 Tan(delta) at 100kHz for the different radio-chemical conditions considered as a function of (a) aging time and (b) total absorbed dose. Twisted pair filled cable.

Referring to the low frequency dielectric response (Figure 61), no homogenous increase with aging can be appreciated. Like the high frequency region just described, it may be seen an initial stabilization followed by a slightly increase of the dielectric losses. As it will be discussed in the following Chapter, this was expected since the presence of fillers and their agglomeration into clusters also rule the lowest frequency region. Hence, it is not possible to consider this frequency region as an aging marker, at least at low doses. As a matter of fact, very high doses bring to the creation of enough aging species which can overcome the filler dielectric response, resulting into an appreciable increase of the dielectric property.

Combined aging condition tanδ evolution behaves like the highest frequency region, increasing the property by almost one order of magnitude. This suggests that combined thermal and radiative stresses also impact on the interfacial arrangement inside the polymer.

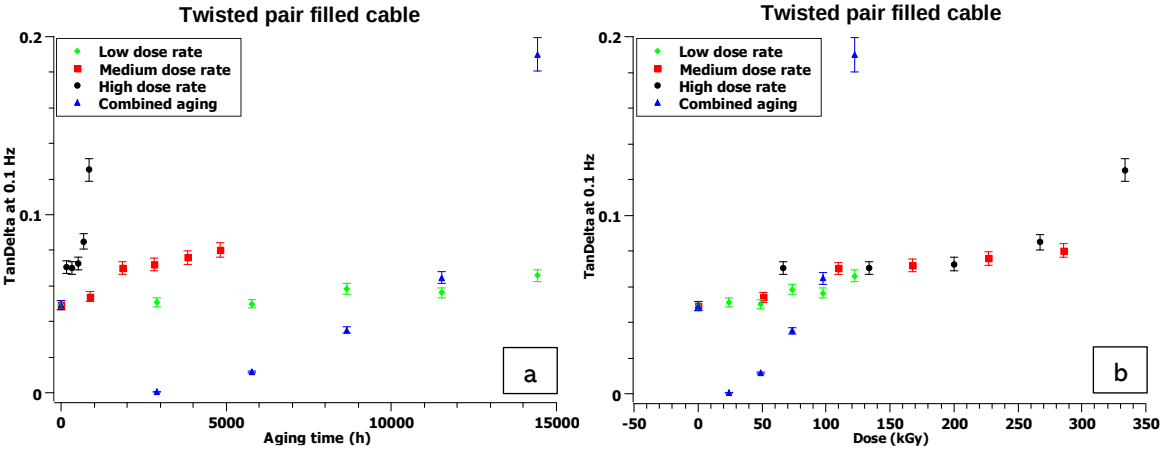

Figure 61 Tan(delta) at 0.1 Hz for the different radio-chemical conditions considered as a function of (a) aging time and (b) total absorbed dose. Twisted filled cable.

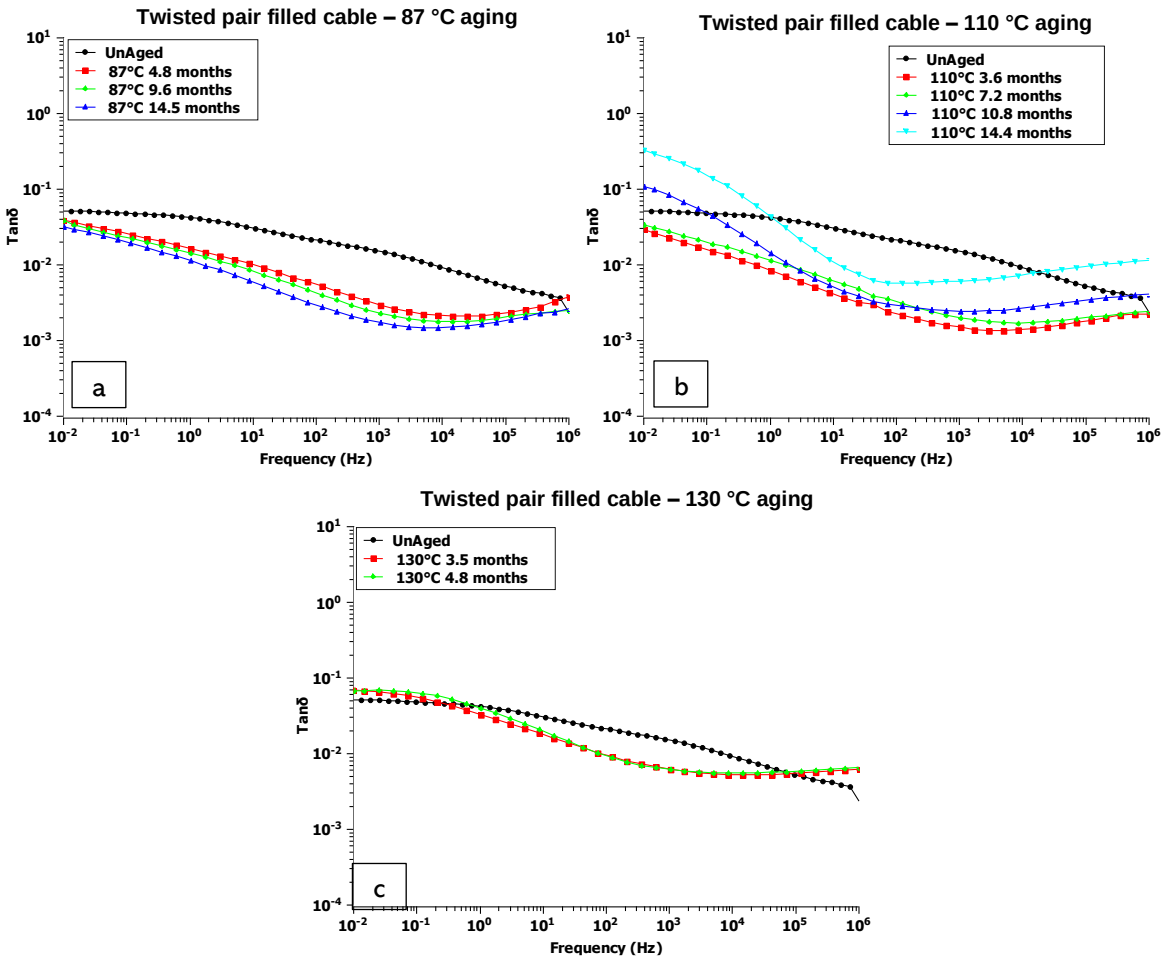

Figure 62 Dielectric losses as a function of frequency for different aging period. (a) 87 °C, (b) 110 °C, (c) 130 °C. Twisted pair filled cable.

Referring to thermal aged cables (Figure 62), the initial aging period causes a reduction of the dielectric losses probably relatable to the consumption of the dipolar antioxidant molecules, as reported above. Together with the reduction in terms of amplitude, the shape of the curve changes, giving birth to a double-peak structure. In particular, it is possible to define a first peak occurring at slightly higher frequencies than the ones here analyzed (likely around 10^8 Hz), and a second peak arising at around 10^{-2} Hz. This second peak, as already discussed, could be linked to the bigger interfaces created by the inorganic fillers which are present in significant high concentration and can agglomerate, enhancing interfacial polarization response.

Focusing on the lowest aging temperature (87 °C), after the abovementioned significant reduction during the first aging period, a slightly shifting downwards of the tanδ curve is appreciable with further aging. However, the registered variation is very little, and it could be also associated with the specimen-related measurement uncertainties.

Harsher aging conditions (110 °C) bring to a significant increase of the dissipation factor with aging time. In particular, very small variations can be observed between 3.6 and 7.2 months of aging, while further aging causes a considerable rise of tanδ in all the analyzed frequencies

(by more than one order of magnitude). It is worth highlighting that the low-frequency peak changes its shape for aging periods longer than 7.2 months, suggesting a different interface arrangement, linkable to bigger interfaces created by aging-related products.
Finally, the 130 °C aging condition is again characterized by a very high initial tanδ value which is then followed by a slower increase, as seen for the twisted pair non-filled cable.

Figure 63 reports the value of tanδ at 100 kHz and 0.1 Hz as a function of aging time for the three different aging temperatures. As already reported, the trend of tanδ between the two considered frequencies is almost the same. However, it could be stated that the variations at low frequencies are more substantial in terms of amplitude for all the three temperatures. This is again referred to the 110 °C aging where after 7.2 months, tanδ values show an abrupt increase associated with the abovementioned arising of interface effect.
Additionally, this suggests that both frequency regions could be suitable for the evaluation of aging conditions of the compound #2 cables.

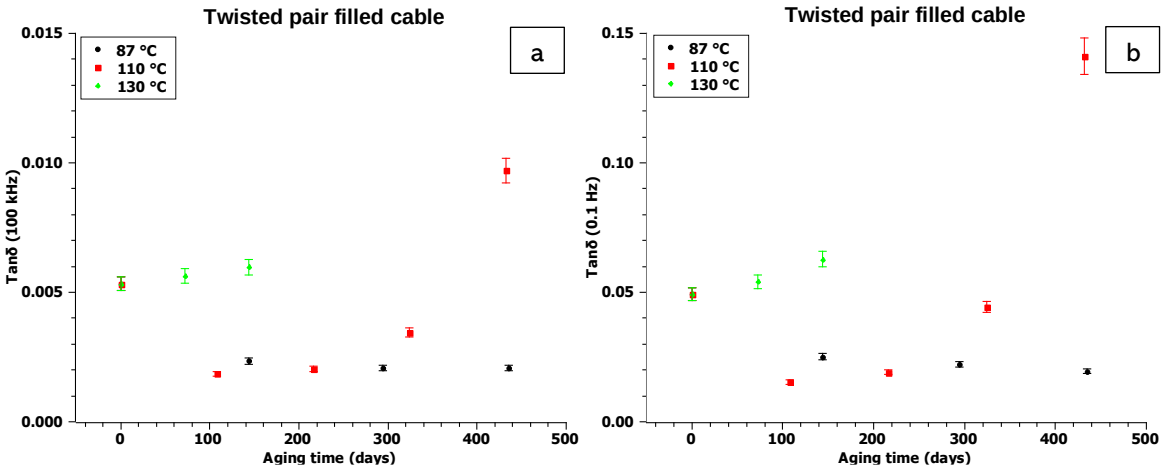

Figure 63 Tan(delta) at (a) 100 kHz and (b) 0.1 Hz for the different thermal aging conditions analyzed. Twisted pair filled cable.

4.3 Differential scanning calorimetry (DSC) measurements

As stated in Chapter 2, the DSC measurements allow the evaluation, among others, of the crystallinity ratio of the polymeric material.

As an example, Figure 64 reports the DSC thermograms obtained for the coaxial cable subjected to the high dose rate.

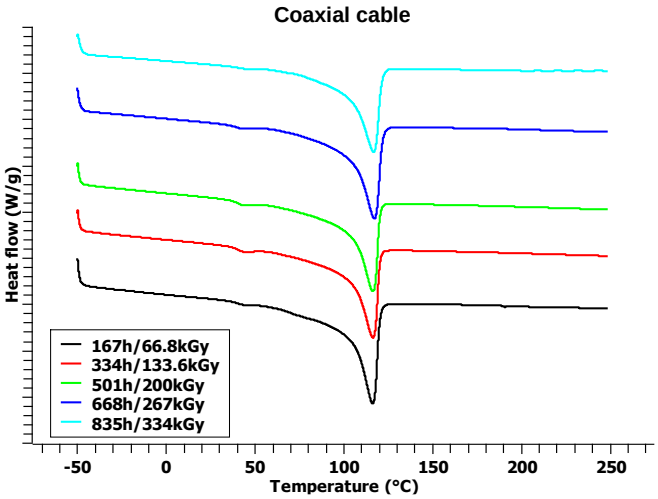

Figure 64 DSC thermograms after different high dose rate aging periods. Coaxial cable.

The thermograms show the presence of two peaks: the first around 50°C and the second around 120°C which are attributable to the melting of the primary antioxidant (Irganox® 1076 [109]) and to the melting of the crystalline phase of the polyethylene, respectively. In order to evaluate the crystallinity ratio, the entire endothermal decreasing phase has to be taken into account. Hence, both peaks contribute to the evaluation of the crystallinity ratio. Moreover, from Figure 64, it is possible to point out that the intensity of the first peak (50°C) is more and more negligible, suggesting a continuous antioxidant depletion during aging. However, due to the very little amplitude of this peak no significant quantitative analysis can be conducted.

Consequently, the main contribution to the crystalline ratio value is given by the polyethylene melting peak. This latter does not significantly vary during aging since very little modifications affect the crystalline phase of the polyethylene under radio-chemical aging at low temperatures.

Due to the large amount of data, only values of crystallinity ratio as a function of the different aging conditions and analyzed materials are reported in the following.

4.3.1 Coaxial cable

Figure 65 depicts the trend and values of the crystallinity ratio as a function of aging time for the different aging conditions considered.

It can be evaluated that no significant variations in the crystallinity ratio with aging occur in the coaxial cable, for all the conditions considered. Variations are very low (less than 3%) and inside the data error bars.

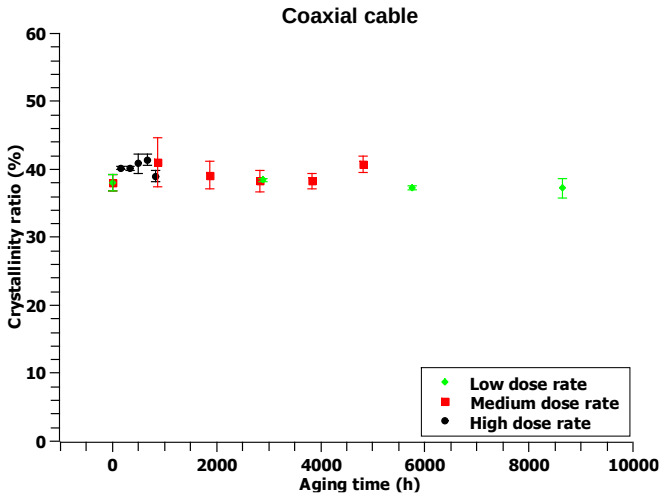

Coaxial cable (compound #1)			
Aging period	**χ_c** High dose rate	**χ_c** Medium dose rate	**χ_c** Low dose rate
Unaged	38	38	38
1	40	41	38
2	40	39	37
3	41	38	37
4	41	38	
5	39	41	

Figure 65 Crystallinity ratio values as a function of the different aging conditions. Coaxial cable.

4.3.2 Twisted pair non-filled cable

Figure 66 shows the trend and the values of the crystallinity ratio for the twisted pair non-filled cable under different aging conditions.

The initial crystallinity value is the same as the one seen in the case of the coaxial cable due to the fact that the analyzed polymeric compound is the same. With aging, the variation of the crystallinity can reach up to 7%. The severer is the aging condition the higher is the variation of the crystallinity ratio. Low dose rate causes no appreciable variation of the crystallinity ratio.

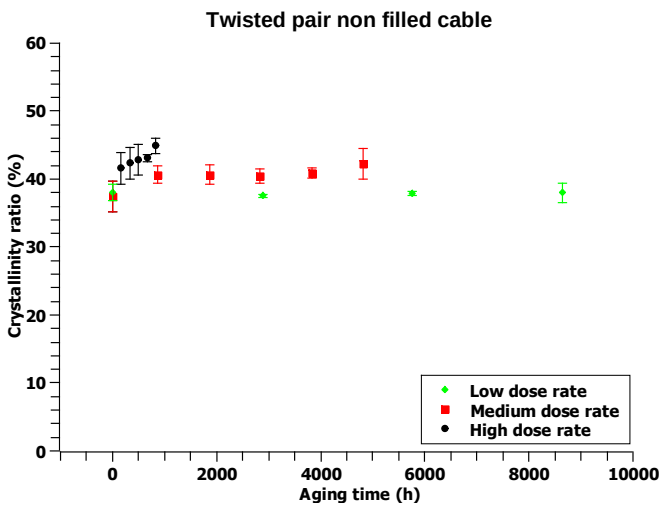

Twisted pair non-filled (compound #1)			
Aging period	**χ_c** High dose rate	**χ_c** Medium dose rate	**χ_c** Low dose rate
Unaged	38	38	38
1	42	41	38
2	42	41	38
3	43	40	38
4	43	41	
5	45	42	

Figure 66 Crystallinity ratio values as a function of the different aging conditions. Twisted par non-filled cable

4.3.3 Twisted pair filled cable

The trend and values of the crystallinity ratio for the twisted pair filled cable (compound #2) are reported in Figure 67.

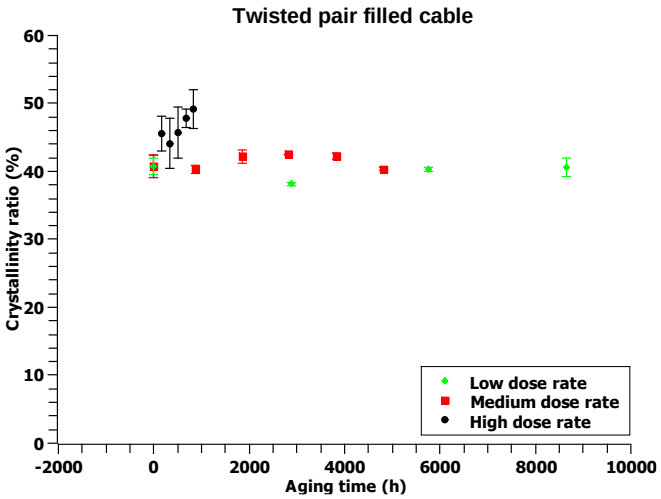

Twisted pair filled (compound #2)			
Aging period	χ_c High dose rate	χ_c Medium dose rate	χ_c Low dose rate
Unaged	41	41	41
1	46	40	38
2	44	42	40
3	46	43	41
4	48	42	
5	49	40	

Figure 67 Crystallinity ratio values as a function of the different aging conditions. Twisted pair filled cable

Here, the initial crystallinity value is slightly higher than in the previous cases (by 3%) probably due to the different compound analyzed. With aging, a substantial increase of the crystallinity ratio (up to 10%) in the case of the high dose rate is noticeable. Lower dose rates cause very little variations ±3% imputable to less severe conditions, hence, to reduced degradation phenomena.

4.4 Oxidation induction time (OIT) measurements

4.4.1 Coaxial cable

In Figure 68 the OIT measurements results and trends as a function of the different aging conditions are reported.

Here, the trend of OIT is quite similar among the different aging conditions. It can be observed that OIT decreases during the radio-thermal aging, which is presumably due to the chemical consumption of antioxidants by specific chemical reactions and/or their migration from the bulk to the insulation surface. The drop in OIT is particularly drastic during the first aging period, for which OIT is reduced by factors up to 6. Then, OIT is still decreasing but slower. The OIT decreasing rate depends on the severity of the aging conditions. It can be seen from Figure 68 that the higher the dose rate the faster is the OIT decay, according to the enhancement of degradation phenomena with higher dose rates. Finally, it reaches a very low but non-null value (2 minutes at least) for all the conditions considered.

It is worth recalling that OIT is considered a quantitative measurement technique for evaluating the concentration of antioxidants inside the material [122]. Hence, as far as the OIT value is not nearly zero, the antioxidants are still present, and no oxidative reaction can take place. However, due to the graphical extrapolation of data (tangent method described in page 49), 2 minutes represents the minimum value recordable by the instrumentation and linkable to the

OIT of a pure XLPE material; so that it is possible to claim that oxidation may start even if the OIT owns a non-zero value (2 mins).

Focusing on the high dose rate aging, one can observe that the OIT value of the last aging time (5th) is higher than the previous one. This behavior, quite unusual, could be related to the inhomogeneity of the sample and referred as an outlier.

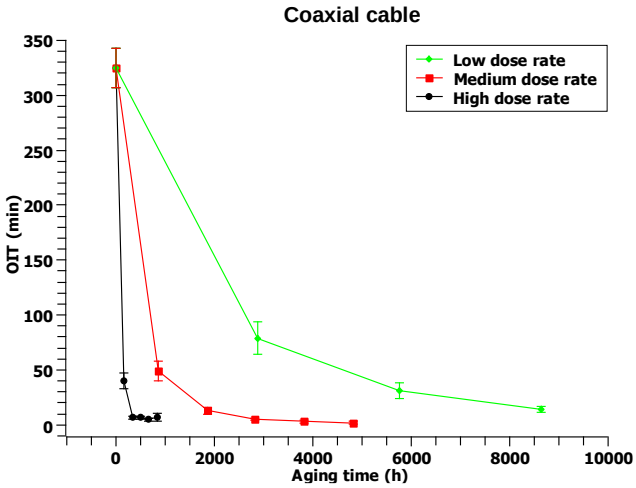

Coaxial cable (compound #1)			
Aging period	**OIT** High dose rate	**OIT** Medium dose rate	**OIT** Low dose rate
Unaged	325	325	325
1	40	49	79
2	7	13	31
3	7	5	14
4	5	3	
5	7	2	

Figure 68 OIT values for the three different aging conditions and material analyzed. Coaxial cable.

4.4.2 Twisted pair non-filled cable

Similarly to the coaxial cable, the trend of the twisted pair non-filled OIT values is characterized by an initial abrupt reduction and followed by a slower decreasing with aging time. However, the initial OIT value is about 50 min lower than the one of the coaxial cables, even if the chemical compound is the same. Given the quantitative property of measurement, this could be imputable to the different real number of stabilizers inserted during the manufacturing process. Therefore, the diminishing phase shows lower values of OIT so that all the conditions considered reached the lowest recordable value (around 2 min). Even in this case the decreasing rate depends on the severity of aging stressors, as discussed for the coaxial cable.

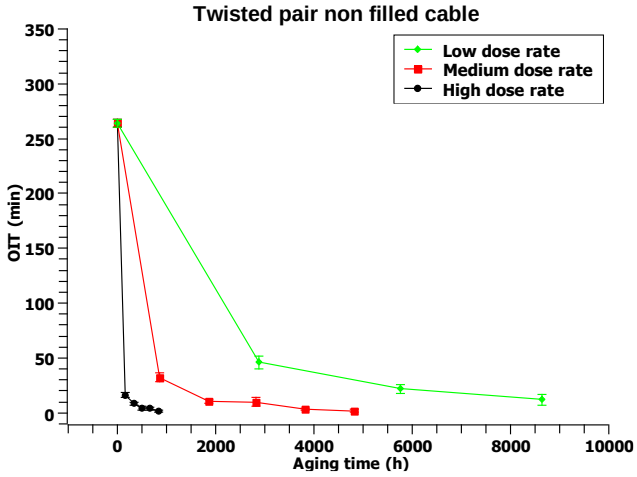

Twisted pair non-filled cable (comp. #1)			
Aging period	**OIT** High dose rate	**OIT** Medium dose rate	**OIT** Low dose rate
Unaged	264	264	264
1	17	33	46
2	9	10	22
3	5	10	12
4	4	3	
5	2	2	

Figure 69 OIT values for the three different aging conditions and material analyzed. Twisted pair non-filled cable.

4.4.3 Twisted pair filled cable

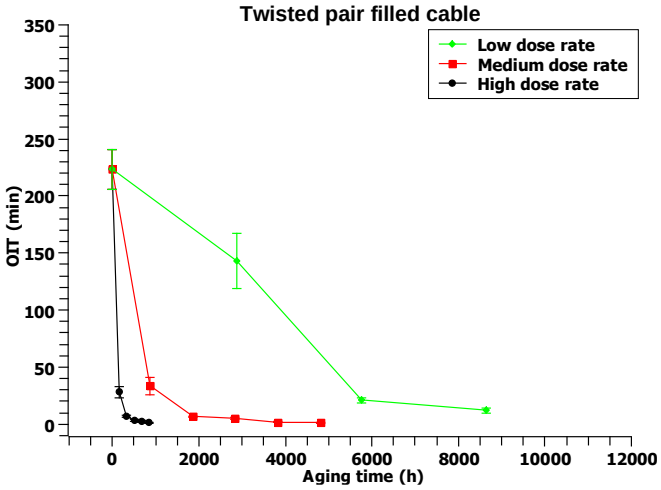

Twisted pair filled cable (comp. #2)			
Aging period	**OIT** High dose rate	**OIT** Medium dose rate	**OIT** Low dose rate
Unaged	223	223	223
1	28	34	140
2	7	7	21
3	3	6	12
4	2	2	
5	2	2	

Figure 70 OIT values for the three different aging conditions and material analyzed. Twisted pair filled cable.

The OIT values for compound #2 (Figure 70) are quite different from the ones just presented. Indeed, the initial value of OIT is way lower than the one of the coaxial cables (about 30% less). This could be imputable again to the different actual amount of stabilizer inside the compound or to the effect of inorganic filler (ATH) which are present in this material.
Indeed, it has been shown that ATH filler can cause a negative contribution to the stabilization of the final material [123], probably due to trapping of antioxidant molecules on the surface of fillers (e.g. hydrogen bonding).

The trend of OIT values with aging is very similar to the one already presented for compound #1 except for the first aging period of the low dose rate. In this latter case, in fact, the value of OIT is not characterized by an abrupt decrease but it is kept quite high, suggesting that the stabilization level of the material, hence antioxidant concentration, is still elevated.
Here again, the decreasing phase is ruled by the severity of the aging stressors. Moreover, it can be reported that all the aging conditions considered reached the ultimate recordable value of OIT (2 mins), suggesting the complete running out of antioxidants and the possible starting of the oxidation process.

4.5 FTIR

In this section the FTIR spectra for the different aging conditions and materials are presented. From this technique, it is possible to obtain much information about the chemical composition of the material. Figure 71 shows the FTIR spectrum of the unaged coaxial cable (compound #1) in the wavenumber range between 4000 and 600 cm^{-1}. Three spectrum regions, reported in the same figure, are interesting for aging evaluation:

a) Carbonyl (C=O) region: 1850-1600 cm^{-1}
b) Hydroxyl (-OH) region: 3800-3500 cm^{-1}

c) Ester (C-O) region: 900-1500 cm^{-1}

These regions are widely investigated as aging-related ones since they represent the oxidized species inside the polymer, which are the main products of the polymer degradation.
However, these regions, and the molecules to which they refer, can show some peaks also in the case of the unaged material. This is imputable, for example, to additives and fillers (e.g. phenolic antioxidants) whose concentration is, in some cases, higher than the one of the oxidized species with aging so that, due to the convolution of different peaks, it is difficult to single out the different contributions and precisely follow the aging.

In order to keep the uncertainties given by the local inhomogeneities, the measurements have been performed at least 3 times in different zones of the specimens.
In this section, FTIR spectra over the entire analyzed wave number domain are reported for cables and aging conditions analyzed. However, in order to obtain an easier and more detailed discussion, only the parts of spectra related to the three abovementioned regions are considered and analyzed.

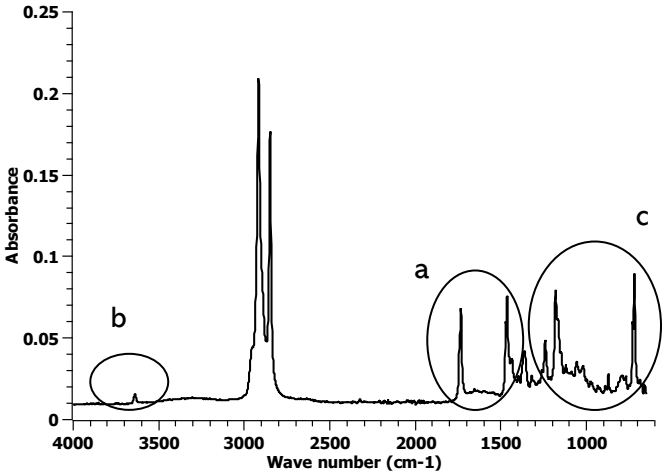

Figure 71 FTIR spectrum of the unaged coaxial cable. Rounds (a) Carbonyl region, (b) Hydroxyl region and (c) Ester region

4.5.1 Coaxial cable

FTIR spectra performed on the surface of coaxial cables as a function of different aging times and conditions are reported in Figure 72.

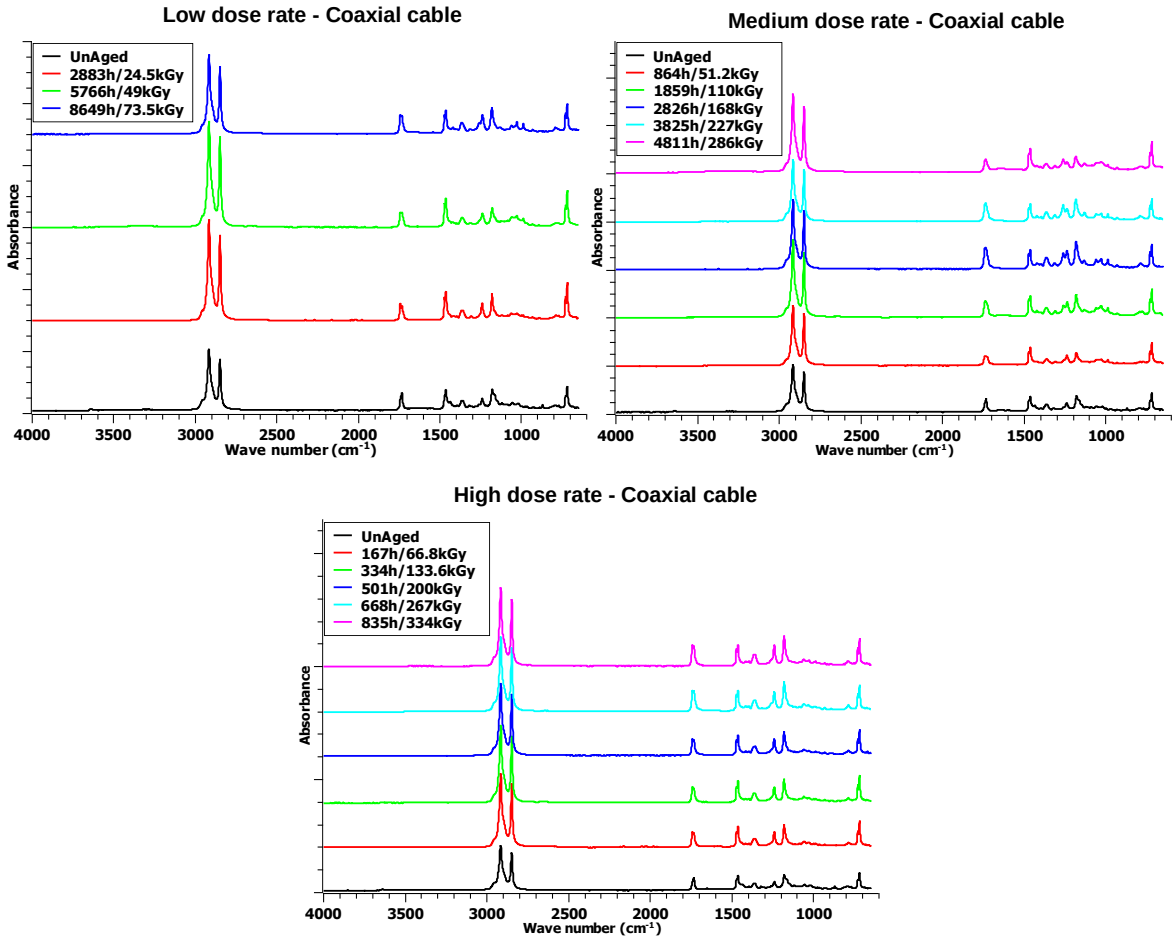

Figure 72 FTIR spectra for the coaxial cable as a function aging. (a) Low dose rate, (b) Medium dose rate, (c) High dose rate.

Figure 73-74 depict the FTIR spectra of the outer surface and the bulk of the insulating layer, respectively. As already presented, the reported spectra refer to three specific spectral regions: (a) between 3500 and 3800 cm^{-1} (hydroxyls), (b) 1600 and 1850 cm^{-1} (carbonyls), and (c) between 900 and 1500 cm^{-1} (esters).

In the carbonyl region (Figure 73.a,d,g), it is possible to observe a single IR absorption peak at 1737 cm^{-1} for the unaged material, likely linked to the carbonyl groups of the two antioxidants. With aging, two new peaks can be found in the same region at 1720 cm^{-1} and 1742 cm^{-1}. In the case of medium and low dose rates, the two peaks show an initial decrease during the first aging period, followed by an increase of the carbonyl peak with aging. On the contrary, in the case of high dose rate, the peaks own similar height for the first three aging periods, while further aging brings to the growth of the carbonyl band followed by a stabilization (4^{th} and 5^{th} aging periods).

With regards to the hydroxyl region (Figure 73.b,e,h), a single and small IR absorption band is observed at 3640 cm^{-1} for the unaged material. This band is likely to be assigned to the phenol group of the phenolic antioxidant. This band disappears on the insulation surface during the

first aging time for all the cases here analyzed, probably due to a significant chemical consumption of the primary antioxidant.

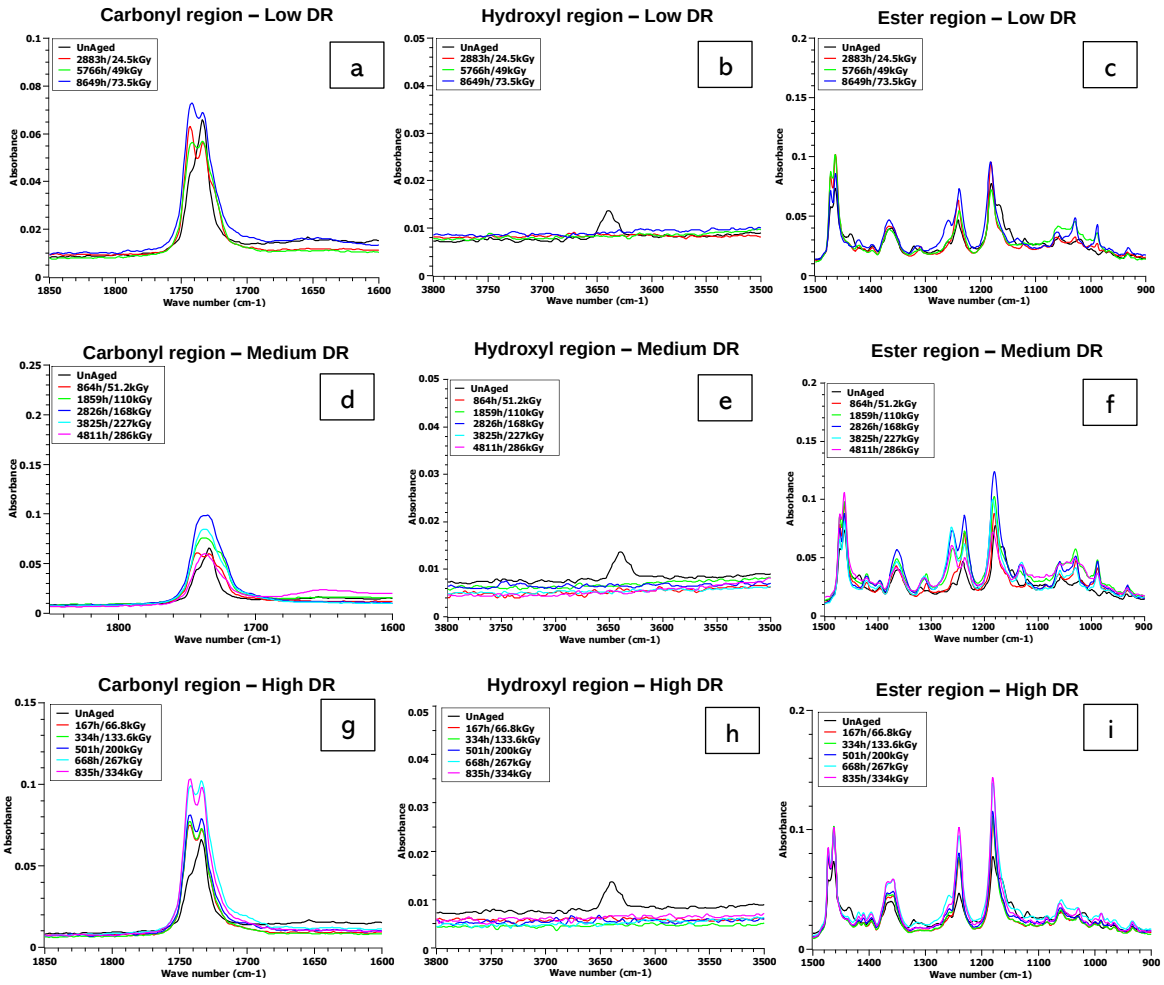

Figure 73 FTIR spectra for the coaxial cable with aging. (a, d, g) Carbonyl region, (b, e, h) Hydroxyl region, (c, f, i) Ester region, for the low, medium and high dose rate respectively.

Finally, in the region between 900 and 1500 cm^{-1} (Figure 73.c,f,i), the IR absorption bands at 1366, 1262, 1238, 1186, and 1085 cm^{-1} are observed for the unaged sample and likely imputable to the C-O bonds of the ester groups of both antioxidants. The amplitudes of these peaks follow the increase of aging period. Moreover, other IR absorption bands appear at 1028, 1046, 1131, and 1313 cm^{-1} on the insulation surface, which may be assigned to the oxidation products of thioether antioxidant (in particular, sulfoxide and sulfone species) formed during aging.

Figure 74 shows the changes in the FTIR spectrum of the carbonyl region obtained in the bulk of the insulating layer. The same observations can be made as previously reported, referring to the presence of a single IR absorption band at 1737 cm^{-1} for the unaged sample. The evolution of this peak with aging is different among the different aging environments. In particular, it does almost not vary with aging in the case of the lowest aging stresses, suggesting that no significant variation in terms of concentration occurs. For the higher dose

rates, an initial increase of the peak is then followed by a decreasing phase. It is worth pointing out that the last aging level of the highest dose rate aging causes an abrupt increase of this peak probably due to the huge amount of oxidized species caused by the stressors.

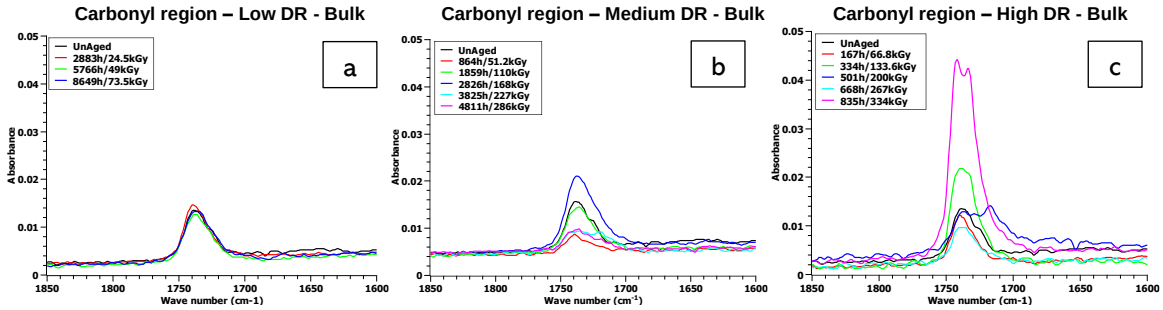

Figure 74 Carbonyl region FTIR spectra in the bulk of the material with aging. (a) Low dose rate (b) Medium dose rate (c) High dose rate. Coaxial cable.

As presented in § 2.3.7, the ester index is a quantity which is often used for the evaluation of the concentration of oxidized species from ATR-FTIR. Calculation of the ester index is carried out following equation reported in § 3.4.4. It is worth pointing out that only the peak at 1742 cm^{-1} is considered for calculation of the ester index, since it does not change its shape e.g., turning into a shoulder of a bigger peak or being overlapped by other peaks, for all the conditions considered. Therefore, Figure 75 reports the trend of the ester index as a function of aging time for the three aging environments considered. The black line refers to the quantity monitored on the surface of the material, while the blue line refers to the measurements done in the bulk of the material. In this latter case, slightly no variation can be evaluated so that the ester index can be considered as constant in the bulk, exception given for the last aging period of the high dose rate. The constant ester index could be related to two main reasons: oxidation mainly occurs in the surface of the material, due to the presence of oxygen in the environment, and the antioxidant products arising to the polymer surface. In this latter case, the variation in terms of concentration of ester bonds can be compensated, thus showing no difference, as it will be described in further details in the following Chapter.

On the surface, low and medium dose rates cause an initial decrease of the ester index followed by an increase and/or stabilization with aging. The initial decrease can be likely related to the migration of the antioxidants on the surface, while the stabilization and increase can be related to the conversion of the antioxidants into their degradation products and the formation of new oxidized species.

In the case of high dose rate, the decreasing part is not present probably due to the particularly harsh conditions which enhance and catalyze the antioxidant chemical consumption. For this reason, the ester index shows an initial increase and a stabilization.

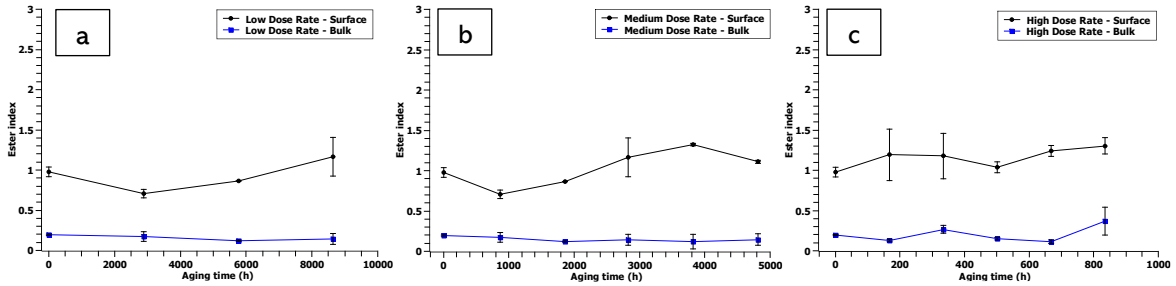

Figure 75 Ester index of the coaxial cable as a function of aging time for the three different aging conditions considered. (a) Low Dose Rate, (b) Medium Dose Rate, (c) High Dose Rate

4.5.2 Twisted pair non-filled cable

The FTIR spectra coming from analyses on the twisted pair non-filled cable are quite different from the one presented for the coaxial cable, even if the compound of the primary insulation is the same. It is worth recalling that, due to the different geometries of cables, the actual aging stressors are attenuated in the case of the twisted pair cable.

Figure 76 depicts the trend of the FTIR spectra, obtained on the polymer surface, over the entire set of chosen wave numbers for the twisted pair non filled cables.

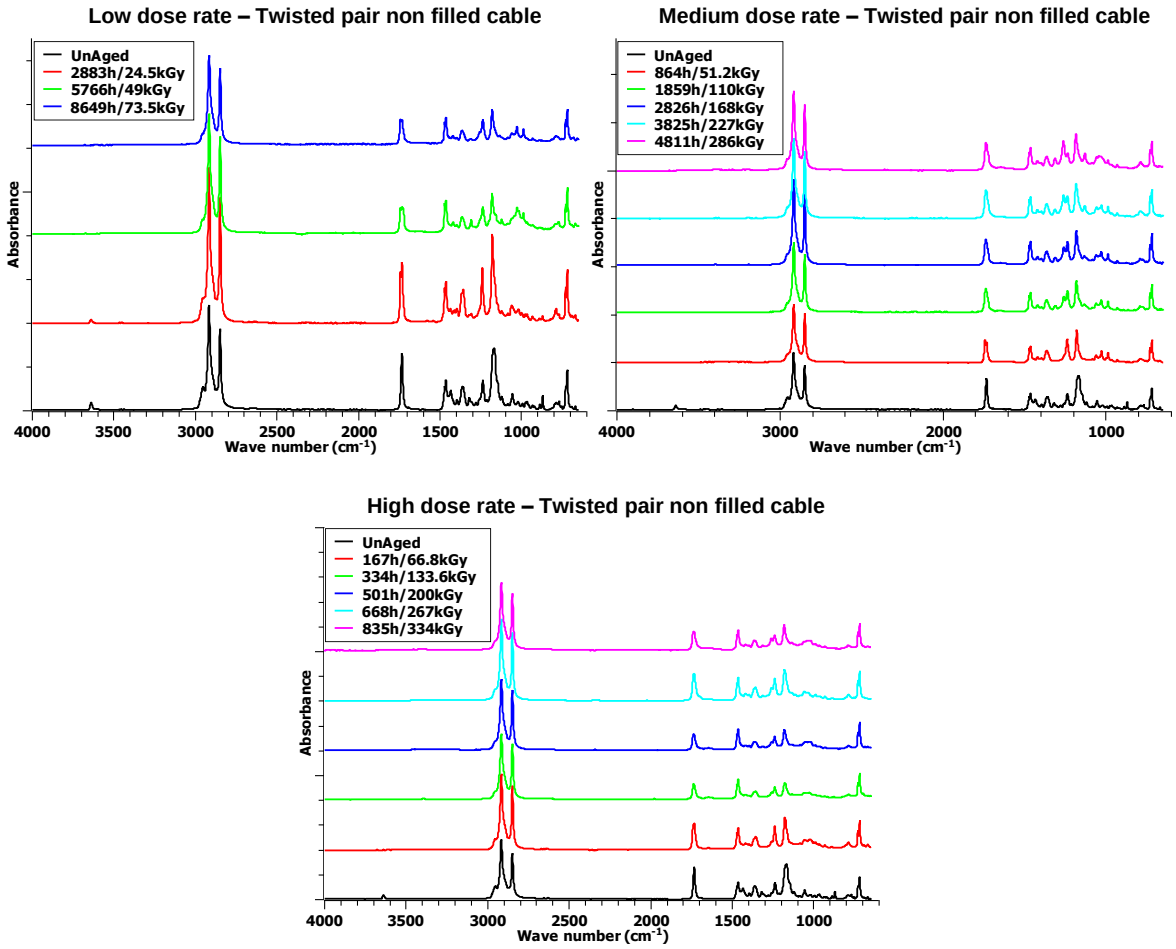

Figure 76 FTIR spectra for the twisted pair non filled cable as a function aging. (a) Low dose rate, (b) Medium dose rate, (c) High dose rate.

Figure 77-78 report the trend of the FTIR spectra for the three regions analyzed in the introduction to this paragraph on the surface and in the bulk, respectively.

Focusing on the carbonyl region FTIR spectra (Figure 77.a,d,g) on the surface, in all the aging conditions analyzed, the initial IR absorption band at 1737 cm^{-1}, which is attributable to the antioxidants ester groups, shows an initial decrease with aging. Referring to the high and medium dose rates, the initial decrease is followed by a slight increase of the considered peak imputable to the conversion of the antioxidants into their degradation products. In the case of low dose rate, only the initial reduction is reported probably due to the softer aging conditions.

In the hydroxyl region (Figure 77.b,e,h), a single and small IR absorption band was observed at 3640 cm^{-1} for the unaged material. This band was assigned to the phenol function of the phenolic antioxidant. It disappears on the insulation surface and no new peak appears in the case of medium and high dose rates. For low dose rate, the peak is kept, with a lower amplitude, in the first aging period considered, suggesting that phenol antioxidants are still present in significant concentration.

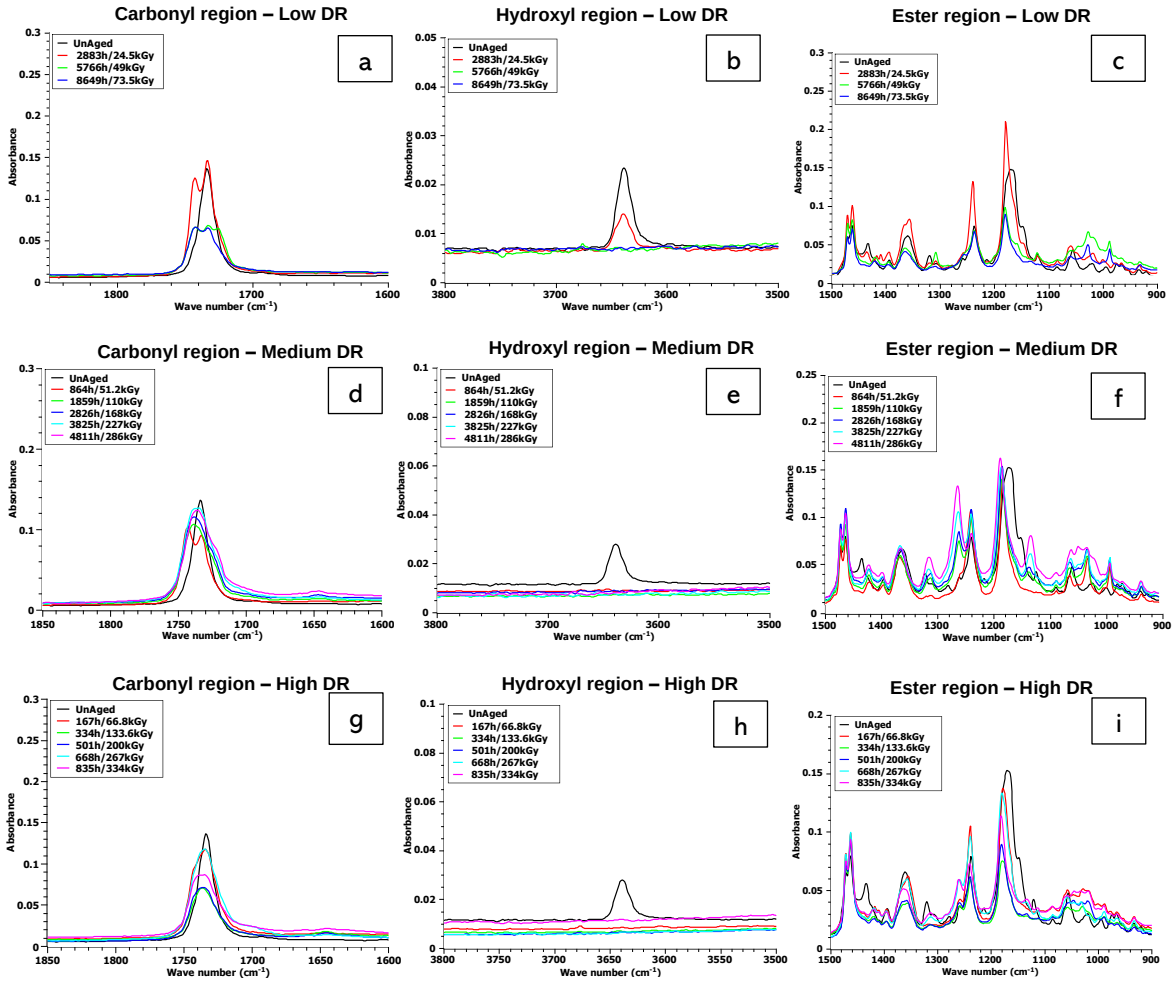

Figure 77 FTIR spectra for the twisted pair non-filled cable with aging. (a, d, g) Carbonyl region, (b, e, h) Hydroxyl region, (c, f, i) Ester region, for the low, medium and high dose rate respectively.

Finally, in the region between 900 and 1500 cm^{-1} (Figure 77.c,f,i), the IR absorption bands at 1366, 1262, 1238, 1186, and 1085 cm^{-1} initially observed for the unaged sample are likely related to the C-O bonds of the ester groups of both antioxidants. The trend with aging follows the one described for the carbonyl bands. Moreover, as already presented, new IR absorption bands appear at 1028, 1046, 1131, and 1313 cm^{-1} on the insulation surface, which might be related to the thioether antioxidant products (e.g. sulfoxide and sulfone species).

Figure 78 shows the changes in the FTIR spectrum obtained in the bulk of the insulating layer (exclusively in the carbonyl region). The same observations can be made as previously reported, referring to the presence of a single IR absorption band at 1737 cm^{-1} for the unaged sample. Then, this band seems to slightly increase during the first aging period to finally diminish with aging.

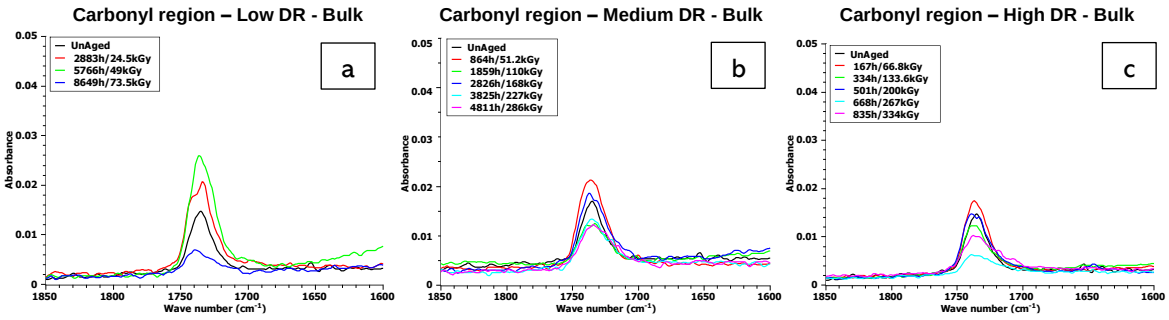

Figure 78 Carbonyl region FTIR spectra in the bulk of the material with aging. (a) Low dose rate (b) Medium dose rate (c) High dose rate. Twisted pair non-filled cable.

Figure 79 displays the behavior of ester index (absorbance ratio between the 1733 cm^{-1} ester peak and the reference peak at 1472 cm^{-1}) with aging time in the bulk (blue dots) and on the outer surface (black dots) of the insulation, for the three aging conditions considered.

In all the cases analyzed, an initial decrease of the ester index is shown on the surface of the material. It can be noticed that the dose rate plays a significant role in the definition of the duration of the decreasing phase. As a matter of fact, the reduction of the ester index lasts for the initial two (small and high dose rates) and one (medium dose rate) aging periods.
After the initial decrease, one can observe a stabilization of the ester index on the surface followed by a slightly increase, likely associated with the conversion of the antioxidants into their degradation products and with an initial oxidative state of the polymer surface.

In the bulk, the variation of the ester index is almost negligible suggesting a very weak modification of the ester content, which is mainly occurring on the surface, as discussed above.

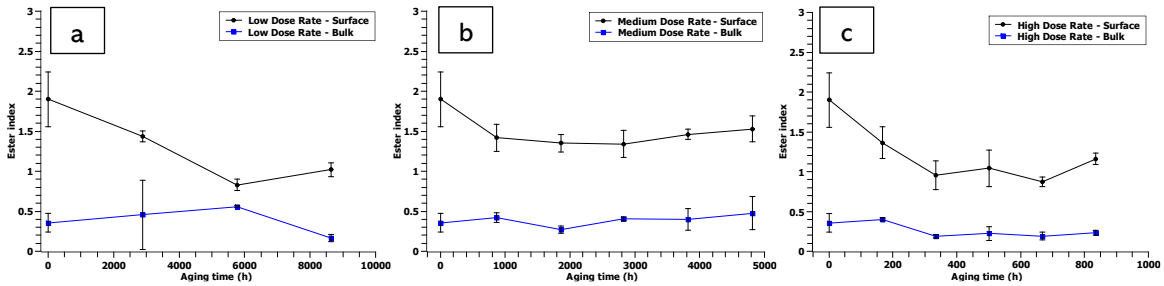

Figure 79 Ester index for twisted pair non-filled cable as a function of aging time for the three different aging conditions considered. (a) Low Dose Rate, (b) Medium Dose Rate, (c) High Dose Rate

4.5.3 Twisted pair filled cable

Figure 80 reports the trend of FTIR spectra for the different aging conditions analyzed, in the case of the twisted pair filled cable. Measurements have been performed on the surface of the polymer.

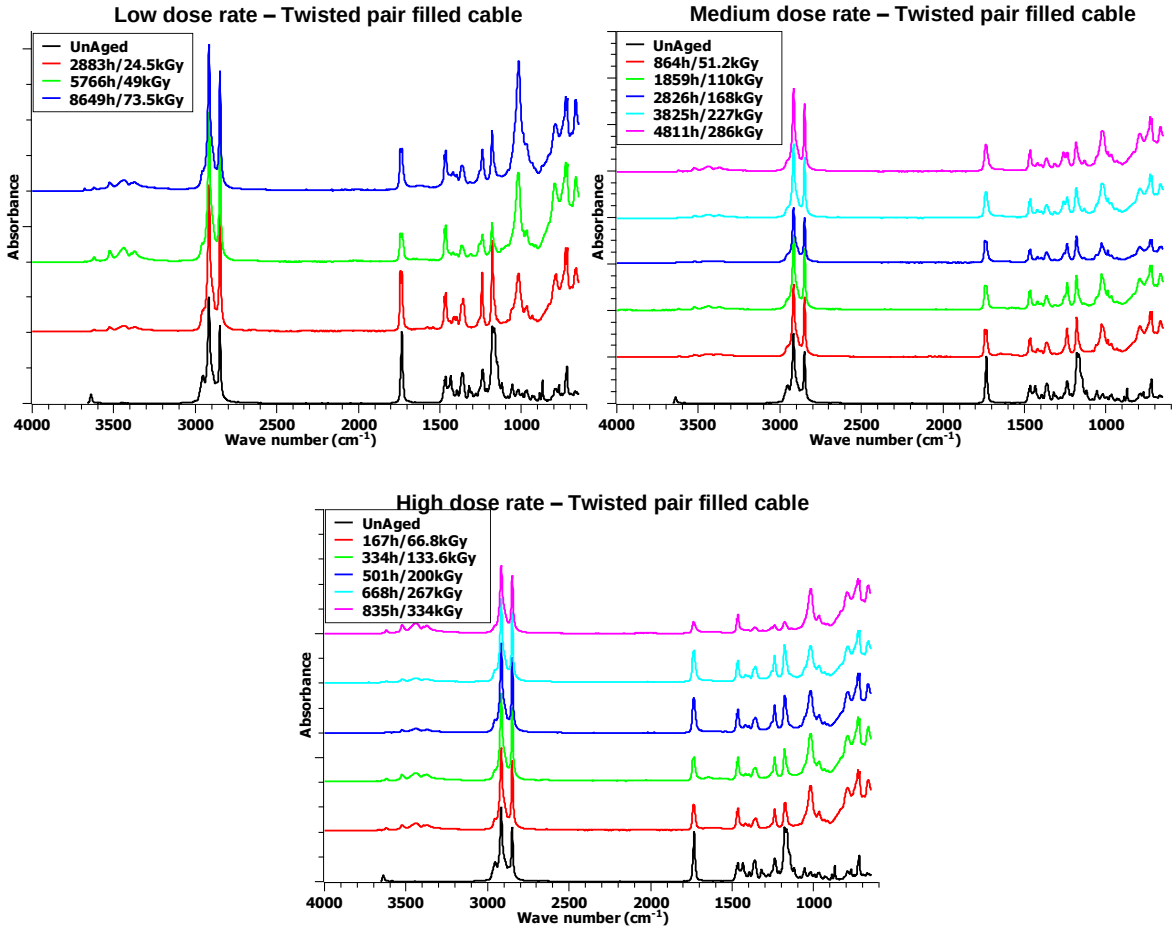

Figure 80 FTIR spectra for the twisted pair filled cable as a function aging. (a) Low dose rate, (b) Medium dose rate, (c) High dose rate.

Similarly to what has been reported above, in the following only FTIR spectra obtained for the three analyzed regions are reported and discussed (Figure 81-82).

In the carbonyl region (Figure 81.a,d,g) on the surface, a single IR absorption band was initially observed at 1737 cm^{-1} for the unaged material, attributed to the ester groups of both phenol and thioether antioxidants. Then, two new bands appear in this spectral region during the first aging period: a shoulder at 1720 cm^{-1} and another main band at 1742 cm^{-1}. These latter two peaks firstly decrease with exposure time on the insulation surface and then increase. The amplitude of these variations is deeply influenced by the environmental stress severities. As a matter of fact, low and medium dose rates show a little increase only during the last aging period, while the high dose rate reveals a further decreasing phase which can be imputable to the possible specimen inhomogeneity.

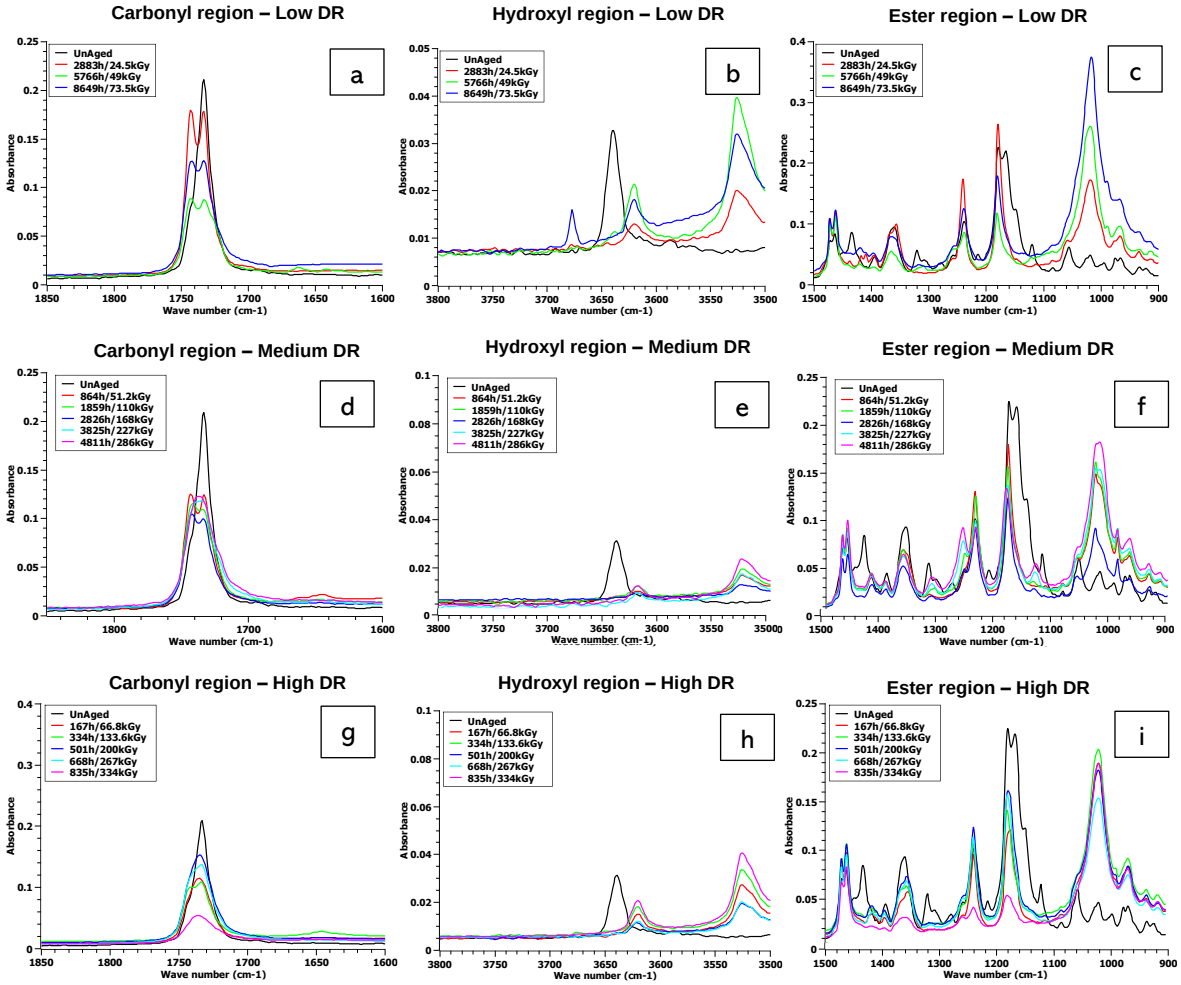

Figure 81 FTIR spectra for the twisted pair filled cable with aging. (a, d, g) Carbonyl region, (b, e, h) Hydroxyl region, (c, f, i) Ester region, for the low, medium and high dose rate respectively.

Focusing on the hydroxyl region (Figure 81.b,e,h), it is difficult to single out the contribution given by the ATH, which exhibits -OH bond, from the hydroxyl molecules arising with the oxidation of the polymer matrix. However, it is worth pointing out that a single and small IR absorption band is observed at 3640 cm^{-1} for the unaged material. This band could be assigned to the phenol function of the phenolic antioxidant as seen from the compound #1

materials. Further aging causes the disappearance of the peak from the surface of the insulation, suggesting a chemical consumption of the antioxidant molecules with aging time.

Finally, in the region between 900 and 1500 cm^{-1} (Figure 81.c,f,i), the IR absorption bands at 1028, 1046, 1131, and 1313 cm^{-1} might be assigned to the oxidation products of thioether antioxidant (in particular, sulfoxide and sulfone species) formed during the stabilization reactions involving the secondary antioxidant. These peaks generally increase with aging time in all the considered exposure conditions except for the highest value of total dose for the high dose rate, where all the peaks show an abrupt decrease, similarly to what described for the carbonyl region.

Figure 82 shows the changes in the FTIR spectrum obtained in the bulk of the insulating layer (exclusively in the carbonyl region). In all the aging conditions considered, IR absorption band at 1737 cm^{-1} initially increases and finally decreases with aging time, likely due to the antioxidant chemical consumption in the bulk or migration towards the outer surface.

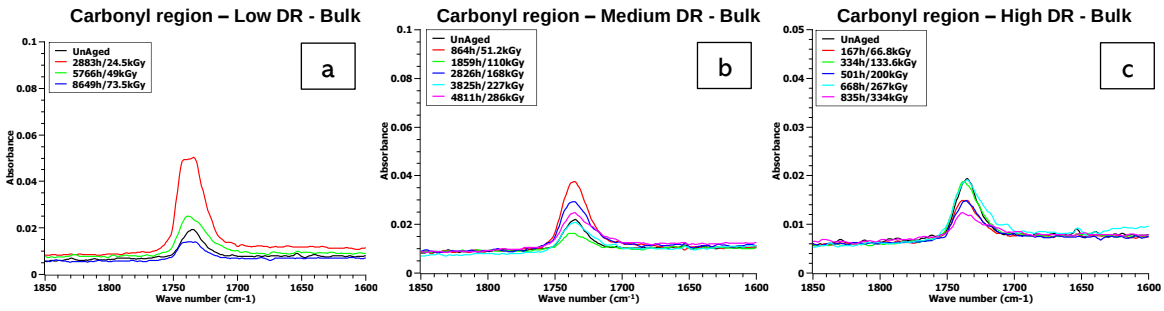

Figure 82 Carbonyl region FTIR spectra in the bulk of the material with aging. (a) Low dose rate (b) Medium dose rate (c) High dose rate. Twisted pair filled cable.

Figure 83 depicts the trend of the ester index as a function of the different aging conditions considered both in the bulk (blue dots) and on the outer surface (black dots). Similarly, to the case of the twisted pair non-filled cable, the ester index shows an initial decrease in all the aging environments considered. As already presented, this behavior is likely imputable to a possible decrease of the concentration of antioxidants on the surface and lasts differently among the different conditions suggesting a dependence on both aging time and dose exposure. Further aging causes a stabilization and/or an increase of the ester index value, as seen in previous cases. It is worth pointing out that the last aging period of the high dose rate shows an atypical decrease of the ester index (as already seen when describing the FTIR spectra), which could be imputable to possible inhomogeneity of the specimen, as described above.

To conclude, the variation of the ester index is almost negligible in the bulk, suggesting a very weak modification of the ester content, which is primarily occurring on the surface.

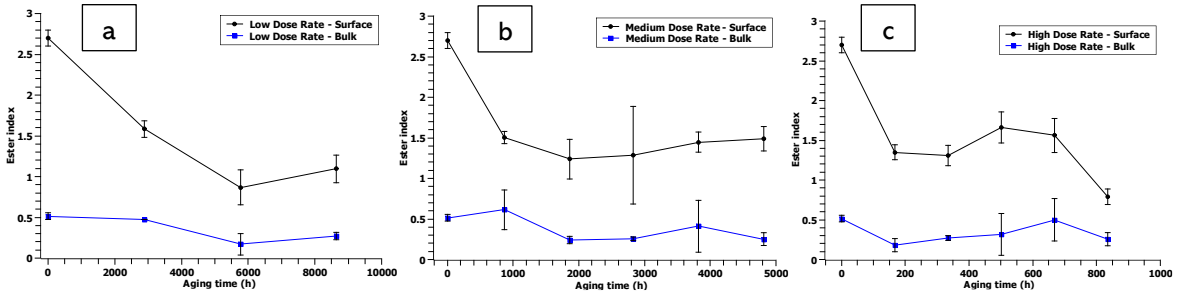

Figure 83 Ester index for twisted pair filled cable as a function of aging time for the three different aging conditions considered. (a) Low Dose Rate, (b) Medium Dose Rate, (c) High Dose Rate

4.6 TENSILE STRESS MEASUREMENTS

Tensile stress tests have been performed by UJV Rez (Czech Republic), one of the Project's partners. From these tests, it is possible to obtain the values of tensile strength (maximum stress that a material can withstand while being stretched or pulled before breaking) and the values of elongation-at-break (maximum value of elongation obtained by the specimen before it breaks). Results are obtained following equations reported in § 2.3.2. Data dispersion is derived considering a 98% confidence interval.

4.6.1 Coaxial cable

Figure 84 depicts the trend of the elongation-at-break as a function of the different aging time and conditions. It is worth pointing out that, due to very degraded polymer, in some cases (some low dose rate and combined aging withdrawals) it was not possible to remove the inner conductor from the primary insulation without damaging the primary insulation, hence it was not possible to perform the mechanical tests on the relevant cable insulation.

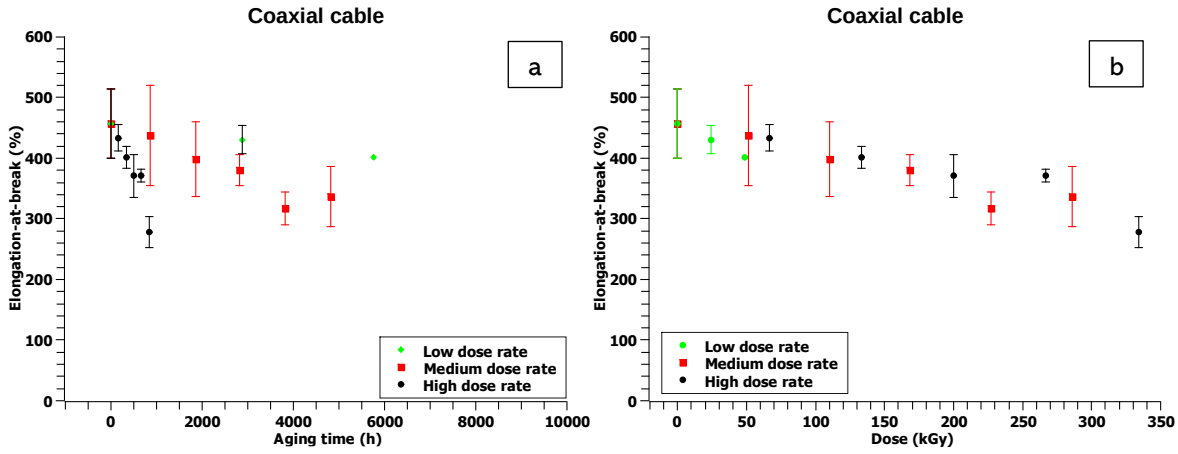

Figure 84 EaB trend as a function of (a) aging time, (b) dose. Coaxial cable.

In all the conditions considered, EaB decreases in comparison to the non-aged material, as expected. The decreasing trend over time is very similar, almost linear, between the different aging conditions, suggesting a gradual degradation of the polymer, which brings to an only 60% reduction of the initial EaB value. The severity of the aging condition impacts the

mechanical response of the material over time. As a matter of fact, even if the trend is similar, the time needed to cause the same mechanical degradation level is very different. As an example, the lowest value of EaB for the medium dose rate, corresponding at 4810 h of aging, is reached after about 500 h in the case of the high dose rate.

Focusing on the mechanical response over the total absorbed dose (Figure 84.b), it is possible to point out that the EaB reduction is very similar among the different aging conditions, particularly for the medium and high dose rates. Contrary to what explained for the tensile response with aging time, the stressor severity over total absorbed dose has no impact on the material mechanical response. This behavior is already known in literature [52], [54], according to this, equivalent absorbed dose causes equivalent damage on the insulation under test.

Similarly, the tensile stress value decreases during aging, as expected (Figure 85). In fact, the more degraded is the polymer, the lower is the load it can bear before breaking. Here again, the different dose rates do not impact on the response over the total absorbed dose, as presented for the elongation-at-break. On the contrary, the response over the aging time is not similar due to the effect of different degradation period and aging stressors, as presented above. As presumed, harsher aging stressors brings to faster degradation of the tensile properties.

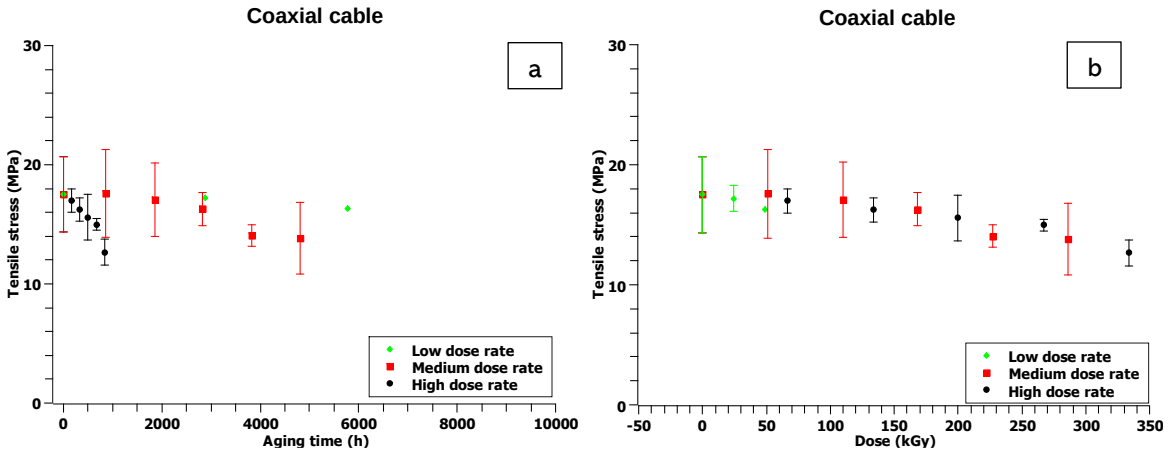

Figure 85 Tensile stress trend as a function of (a) aging time, (b) dose. Coaxial cable.

4.6.2 Twisted pair non-filled cable

Figure 86 reports the twisted pair non-filled cable trend of EaB as function of aging time for the different aging conditions considered.

The initial value of EaB showed to be higher than in the case of the coaxial cable even if the polymeric compound is the same (compound #1). This suggests that the different manufacturing process together with various geometries, hence design of tubular specimens, can have an impact also on the mechanical behavior of the polymer.

With aging time, except for the high dose rate where one can observe a significant reduction over the entire aging time, the decay of the EaB is very little in the case of small and medium dose rates for the first three aging periods. Further aging causes a significant reduction of the EaB which is kept constant for additional aging periods (step-like behavior).

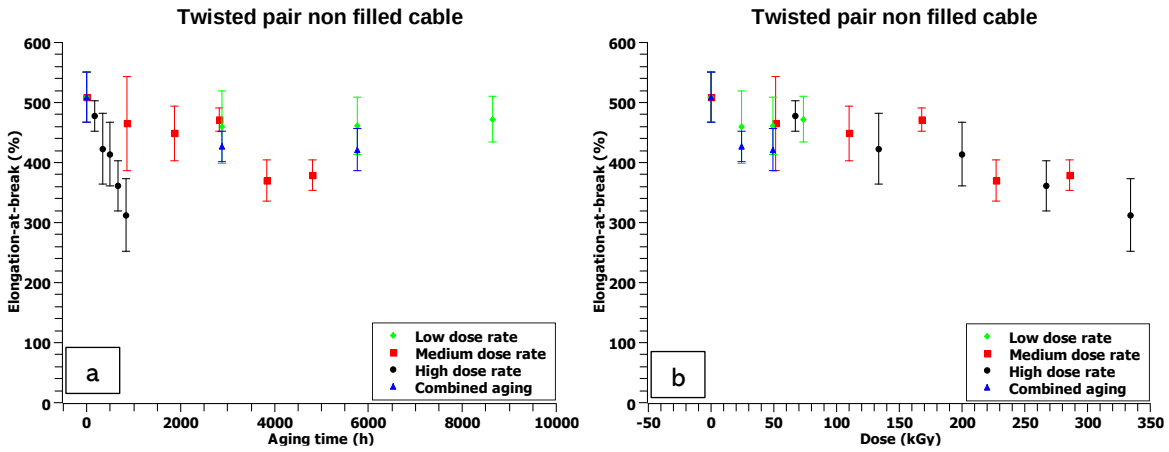

Figure 86 EaB trend as a function of (a) aging time, (b) dose. Twisted pair non-filled cable.

With the addition of thermal stress, as expected, the combined aging condition causes a shifting downwards of the EaB in comparison to the radiation-only aging (low dose rate), due to the synergic effect of the two environmental stresses.

Focusing on the EaB response with the total absorbed dose (Figure 86.b), one can observe an initial correspondence among the different aging environments up to 75 kGy. Higher doses result into a divergence of the decreasing trends probably due to the different severity conditions. Indeed, with the same absorbed dose, the lower the dose rate the higher the ultimate elongation-at-break of the material.

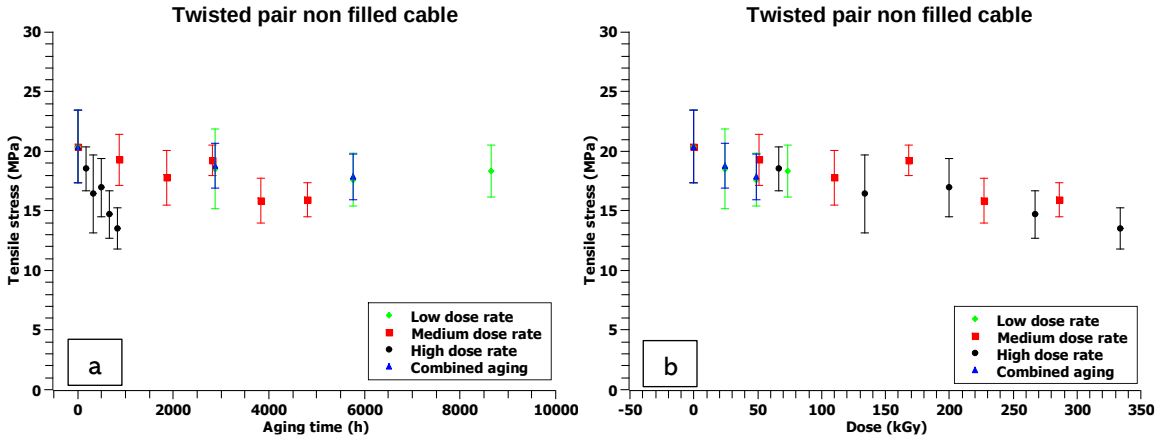

Figure 87 Tensile stress trend as a function of (a) aging time, (b) dose. Twisted pair non-filled cable.

Figure 87 reports the trends of the tensile stress as a function of aging time (a) and total absorbed dose (b) for the different aging severities analyzed. The initial value of tensile stress is slightly higher than in the case of coaxial cable, however inside the confidence bar. As

expected, even in this case, the value of tensile stress is reduced over aging periods. The severity of the environmental stresses plays a major role, resulting in almost halving the initial value of tensile stress in less than 900 hours of aging, in the case of the high dose rate. On the contrary, lower dose rates do not significantly impact the tensile stress keeping tensile strength always higher than 15 MPa. Similarly, the mechanical response with dose shows an initial stabilization of the tensile stress, as seen for the EaB, followed by a more significant reduction in the case of higher dose rates.

4.6.3 Twisted pair filled cable

The evolution with aging of EaB for the twisted pair filled cable is reported in Figure 88.
It can be observed that the initial value of EaB is much lower than the above cases (compound #1), probably due to the presence of inorganic fillers inside the polymer matrix.

High dose rate results into a constant decrease of the EaB over time. On the contrary, the other aging conditions show a step-like decreasing law: an initial reduction followed by the stabilization of the EaB value (up to more than 8500h in the case of the low dose rates), and a further decrease and stabilization, in the case of the medium dose rate. It is noticeable that the first aging period of the low dose rate exhibits an EaB higher than the one showed for the unaged material. This phenomenon, quite unusual, could be imputed to the specimen inhomogeneity and it could be considered as an outlier.

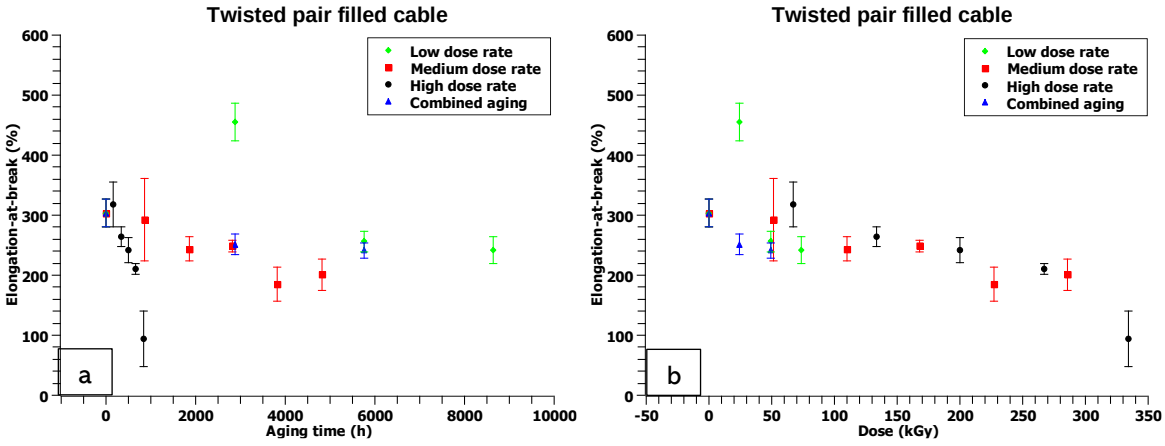

Figure 88 EaB trend as a function of (a) aging time, (b) dose. Twisted pair filled cable.

Focusing on the EaB response as a function of the absorbed dose, the behavior is similar to the one just described. The high dose rate environment causes a countinous decrease of the property which leads to values close to 100% absolute elongation. Other dose rate conditions keep much higher EaB values (around 200%). Even in this case, the response over dose is similar among the different conditions untill about 300 kGy where a divergence between the harshest and other aging environments occurs.

The tensile stress results (Figure 89) depict a similar behavior. The initial value is lower compared to the one presented for compound #1, likely imputable to the addition of fillers. The reduction of the tensile stress with high dose rate is linear while for the other aging conditions is much slower, so that it can be considered almost stable over the aging time here analyzed.

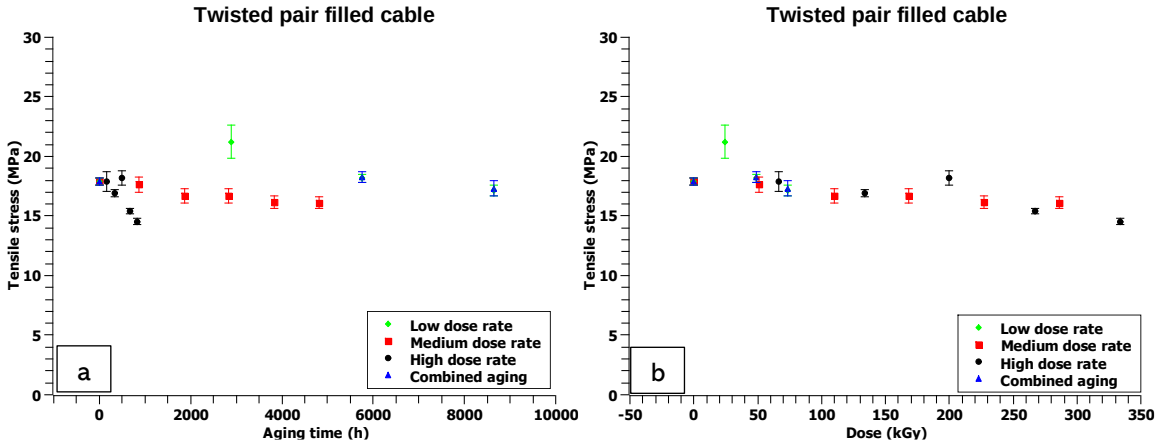

Figure 89 Tensile stress trend as a function of (a) aging time, (b) dose. Twisted pair filled cable.

CHAPTER 5
DISCUSSION

5.1 INTRODUCTION

In the previous Chapter, it has been shown how aging can deeply modify the response of a cable throughout its service life. In particular, it has been reported that the severity of aging conditions may significantly influence properties of the insulating material.
Moreover, it has been shown how several different properties, e.g. chemical, mechanical and electrical, are tightly related each other, opening up the possibility to correlate them taking into account different polymer characteristics investigated by a particular technique.

At first instance, it is significantly important to consider the microscopical chemical modifications occurring inside the polymer during aging, in order to better understand the variation of macroscopical properties like, e.g., electrical and mechanical behavior. This is particularly crucial in the case of low-voltage cable systems where a major part of the polymeric compound is given by additives which deeply impact on the response with aging of the polymer matrix e.g. delaying the oxidation due to the presence of antioxidants.
On the other side, the possibility to correlate the different techniques allows the chance to scale the actual monitoring techniques for cable diagnostics up without losing the expertise gained in several years of application of these approaches.

As presented in Chapters 1 and 2, the most widely accepted criterion for the evaluation of the health of low voltage cable systems inside nuclear power plants is based on the tensile technique, mainly the ultimate elongation at break (EaB). The advantage in using EaB lays in its effective correlation with aging, which also allows the comparison of the results obtained with different stress levels.

In order to study the evolution of the material properties in a reasonable time, accelerated aging is required. Empirical and mathematical models able to correlate accelerated test results with aging in real operation conditions have been already developed focusing on the use of EaB.
Under these circumstances, it is evident that the possibility to correlate the different properties with the EaB is a key feature in order to proceed with the proposed widening of the actual state of the art for cable monitoring.

Besides this, tensile tests are destructive local measurements so that they may be not representative of the entire cable system under test and, in addition, they are not always easy to perform due to the possible difficulties in reaching some parts of the cables, usually the most stressed ones.

The non-destructiveness is for sure a key property to be evaluated in developing a new monitoring technique. Other requirements for a non-destructive testing technique could be summarized as follows [22]:

- Tests should be performed *in situ* with limited interruption of the plant operation.
- Test should be easily replicable with very low error dispersion.
- The chosen condition indicator should demonstrate a monotonical variation with aging.
- Tests should be referred to the bulk of the material since it is usually difficult to access significant sections of the cable.
- If not possible, the local cable tests should be performed evenly in the accessible part of the considered cable.
- There should be a universal acceptance criterion which is used as a warning alarm for scheduling of the cable maintenance.

In recent years, among the various techniques, dielectric spectroscopy gained more and more importance in the extruded cable science research field. As a matter of fact, this technique is non-destructive, it is capable to assess the health of the entire cable system and has shown to have monotonous variation of the measured property, depending on the analyzed frequency. Unfortunately, up to date, it lacks in enough knowledge to allow this technique to be fully operational in the actual industry.

The discussion Chapter is divided into two main parts: one related to the radio-chemically aged cables, which includes the correlation among different micro and macroscale properties, and one related to the thermally aged cables which is limited to the discussion on the electrical behavior of those cables, as reported in the previous Chapter.

5.2 Dielectric spectroscopy as a condition monitoring technique

As described in Chapter 3, the frequency region investigated by means of the Novocontrol Alpha Dielectric Analyzer is between 10^{6} and 10^{-2} Hz.
Based on the already discussed division of dielectric spectrum as a function of different polarization mechanisms (§ 2.3.8), it is possible to split the investigated frequency region into two zones:

- **10^{-2}-10 Hz** which corresponds to the highest frequency zone of the interfacial polarization.

- **10^3-10^6 Hz** which represents the low-frequency part of the dipolar polarization.

The first one is related to interfacial or Maxwell-Wagner-Sillars polarization (as seen in Chapter 4), it is caused by limited diffusion of space charges inside the dielectric by means of applied electric field. These charges may settle next to interfaces or discontinuities inside the dielectric itself. As recognized, interfaces can be at least of two different types:

- **Chemical interfaces** between two materials of different chemical composition, for instance in a multilayer structure (inter-layers interface) and in composite materials (fiber/matrix interface).
- **Physical interfaces** between materials of the same chemical composition but of different physical state, for instance amorphous/crystal interface in semi-crystalline polymers.

It is important to recall at this point that the interfacial polarization shares the characteristic frequencies with Q-DC conduction, as already discussed in § 4.2.1. Hence, it could be difficult to single the two phenomena out when free ions and/or radicals are present inside the material under test.

The high-frequency region is related to dipolar polarization of large dipolar species. These ones, e.g. oxidized polymer groups, are often created through action of aging factors, like e.g. high temperature and radiation, which catalyze oxidative reactions mainly responsible for the degradation of polymers.

In § 1.4, it has been reported that main consequence of radio-chemical aging is chain scission. Mainly coming from the decomposition of hydroperoxide species. The resulting free radicals are very unstable and tend to react with other free radicals and polymer substrate in order to form non-reactive species, or with oxygen. In this latter case, the resulting molecule is characterized by a big size and strong dipolar moment due to the presence of oxygen. Thanks to this, under an AC electric field, the molecule responds electrically in the dipolar polarization area. Due to the bandwidth limitation given by the instrumentation, one can observe only the low-frequency branch of this kind of polarization. In particular, this area is the most interesting one since it represents the response of big-sized dipolar molecules such as the ones given by oxidized polymer groups or products of antioxidants.
Among the two frequency regions, it is evident that the most suitable for following the development of aging is the latter one due to the ability of this area to analyze the presence of degradation products given by aging, hence it is suggested to be used as an aging marker.

On the contrary, various works [91], [92] suggests the use of the very low frequency range as an aging marker for diagnostics. These results are mainly focused on the use of this technique for medium and high voltage cables, whose primary insulation is characterized by a very pure compound. In the cases here investigated, the crosslinking process through silane is used only

on low voltage cable systems due to the presence of various impurities produced by this technique, implying moisture curing. Additives could also enhance the presence of interfaces, which may deeply influence the low frequency dielectric response so that it could be not easy to distinguish the interfaces created by the multilayer structure from the ones related to the microscale such as interfaces among different macromolecules and interfaces created by aging species. Moreover, the low frequency electrical response can be affected by Q-DC conduction phenomenon which is usually predominant over the interfacial polarization (§ 4.2.1), making the analyses very complex and possibly misleading. As a further confirmation, it has been reported and discussed in Chapter 3 that low-frequency dielectric response does not exhibit a monotonous increase of the property with aging, probably due to the presence of these different concurrent phenomena.

Under these circumstances, it has been chosen to use the high frequency, i.e., 100 kHz, dielectric response to follow the development of aging process on the considered cables. Furthermore, it has been correlated to different physical-chemical techniques in order to prove the ability of dielectric spectroscopy to assess global cable aging.

5.3 The impact of antioxidants and their products on the dielectric spectrum

Antioxidants are dipolar species and are incorporated into the polymer to prevent oxidation and, consequently, early degradation of the insulating material.

The addition of antioxidants inside the base polymeric material may have an impact on the physical-chemical properties of the unaged material. It has been shown in literature that the introduction of additives can worsen both the electrical, due to the dipolar properties of these molecules e.g. antioxidant, and mechanical properties of the material with respect to the unfilled one [124].

Furthermore, it is widely known that one substance can be mixed inside another one as far as their solubility parameters are compatible. Focusing on the polymeric materials, solubility plays an important role in the behavior of incorporating many additives inside a polymeric matrix. Limited solubility of additives in a given polymer may lead to problems e.g. agglomeration and/or ineffective additives [125].

Focusing on antioxidants, chemical measurements performed on the cable specimens showed that the maximum fractions of Irganox® 1076 and PS802 antioxidants inside the considered silane crosslinked matrix is around 0.9 phr and 1 phr, respectively [66], [126]. This means that any higher amount than this value results into non-efficiently dissolved molecules. However, no evidence on the threshold value is reported in the case when two antioxidants are simultaneously present.

Obviously, due to the industrial manufacturing of these cables, the concentration might not be exactly the one claimed by the specifications. Moreover, the actual amount can vary from one

zone to another one due to a non-homogenous dispersion of the additives. Further chemical measurements on Project samples claimed that the actual concentration of antioxidants inside the polymeric matrix is slightly higher than 1 phr per each antioxidant type, leading into a non-complete dispersion of additive molecules.

It has been shown in [59], [66] that the non-dispersed antioxidant molecules, as dipolar species, may have an impact on material electrical properties. In particular, they can migrate to the surface of the material due to diffusion phenomena and arrange themselves into crystals. The amount of crystals could increase with aging time if aging temperatures are close to the melting temperature of the antioxidant, since they result into an easier migration of these molecules from the bulk to the surface of the material. If these crystals are homogenously dispersed, so that it could be possible the percolation of free charges, they could create a sort of conductive layer which can impact the electrical behavior of the insulating material. Indeed, the accumulated antioxidant molecules can act as induced dipoles following the applied alternating electric field even at high frequencies, similarly to ionic polarization which may occur in crystals causing the raise of dielectric losses in the high frequency region.

A complementary technique used to confirm the assumption of the migration of antioxidants from the bulk to the insulation surface is optical microscopy.
In our previous work [59], the insulation surface was examined by optical microscopy in reflection mode in order to evaluate any possible formation of antioxidants crystals. A huge quantity of polyhedral crystals, due to the exudation of antioxidants from the insulation, are shown to be formed on the insulation surface. Example of pictures coming from the microscopical analyses are reported in Figure 90.

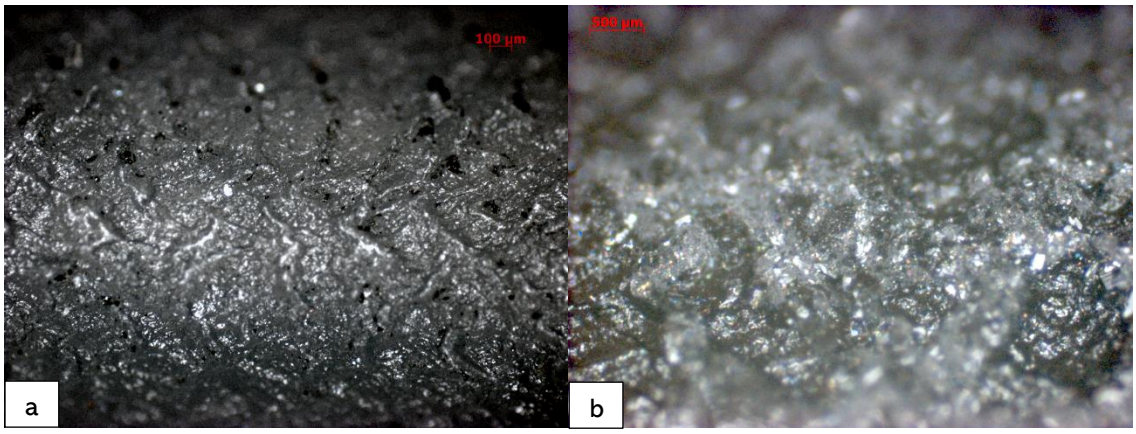

Figure 90 Micrographs of the polymer surface. Unaged coaxial cable. Magnification (a) 50x (b) 200x.

Despite their limitations, antioxidants are required inside the polymeric compound in order to prevent degradation and oxidative phenomena to occur. Briefly summarizing what is reported in § 1.4, the severity of the aging conditions (γ-rays) accelerates degradation, i.e. consumption and physical loss of antioxidants. When the antioxidants are completely depleted, the polymer

undergoes oxidation i.e., chain scission and chemi-crystallization (main causes of the loss of mechanical performance of the polymer matrix).
When antioxidants are present, as reported in Chapter 1, they react with free radicals to form non-reactive species, namely degradation products. As far as antioxidants endure, no oxidation can occur and only conversion of antioxidants into their degradation products takes place.

As stated in Chapter 2 and 3, OIT measurements are used to evaluate the concentration of remaining antioxidants in the polymer matrix [122]. In particular, the higher the value of the OIT the higher the level of stabilization of the material and consequently the concentration of antioxidants. It is evident that the consumption of antioxidants causes the reduction of the OIT values and the formation of new degradation products. These molecules own the same ester bond of the initial antioxidant molecules so that the two phenomena (antioxidant consumption and degradation products formation) can be difficulty singled out through FTIR measurements due to possible compensation of concentration of the ester bonds leading to the flattening of the ester index trend with aging.

However, different kinetics of the antioxidant conversion reactions can help defining borders among the different degradation phases.
This can be evaluated taking into account the trend of the ester indexes (Figure 75, 79, 83) over the aging time together with the variation of OIT values (Figure 68-70). In all the considered cases, the ester index on the surface shows a significant decrease during the first aging periods. The duration of this descending phase is linked to the severity of the aging stressors. It is shown that, in some cases, the low dose rate aging requires more than two aging periods to complete the decreasing phase. Similarly, the OIT values show a significant reduction of its value during the first aging periods followed by a slower variation over time.
This trend suggests that these two quantities are strictly related each other and, in particular, that the ester index on the surface could be related to the actual OIT value, hence to the antioxidant concentration. Therefore, it is possible to claim that on the unaged samples many antioxidant molecules rise to the surface of the material, due to diffusion phenomena. This gives birth to the above-mentioned antioxidant crystals melting during aging and preventing oxidation to occur [66]. Thus, they are expected to contribute to the initial high OIT value, together with the dispersed antioxidant fraction in the polymer matrix.

The first aging period causes both the physical loss and chemical consumption of antioxidant molecules, hence their conversion into degradation products. The physical loss, in particular, could be the main cause of the abrupt decrease of OIT values during the initial aging, to which it corresponds the reduction of the ester index on the surface. As stated above, if chemical consumption of antioxidants only had been present, the ester index value would have been

roughly constant, since antioxidant products have the same ester bond of the initial antioxidant molecule.

From the trend of the ester indexes over time, it can be noticed that further aging causes, in most analyzed cases, stabilization of the chemical quantity over time due to the abovementioned conversion of antioxidants into their degradation products.

After the stabilization phase, an increasing phase of ester index occurs during aging. This is likely imputable to the arise of new oxidized species which are no more related to antioxidant kinetics. Indeed, since all the antioxidants have been consumed (OIT~0 min), thus converted into antioxidant degradation products, the oxidation of polymer chains starts during radio-chemical aging, resulting in new oxidized molecules which are characterized by the carbonyl bond.
Obviously, the concentration of these new oxidized species raises with the increase of aging time due to the incessant environmental stresses which continue enhancing degradation mechanisms. Hence, it is possible to claim that there is a relationship between the concentration of ester groups, represented by the ester index, and the aging time. Unfortunately, this trend can be evaluated only once all the antioxidants have been consumed so that it is possible to investigate the actual oxidation occurring inside the polymer.

In the bulk, the variation of the ester index is almost negligible suggesting a very weak modification of the ester content, which is mainly occurring on the surface, as stated above.

Focusing on the electrical behavior, in most cases, one can observe an increase of the dielectric losses with aging time. Thanks to the dipolar properties of antioxidant molecules, these latter can be easily analyzed through the dielectric spectroscopy technique. However, as mentioned before, due to their reduced molecular size, their dielectric relaxation peak is placed outside the frequency region here investigated so that it is possible to investigate only the low-frequency branch of the additive response. With aging, antioxidants react with macromolecular free radicals giving birth to bigger molecules (e.g. hydroperoxide and antioxidant-grafted polymer chains) which can respond electrically inside the frequency region analyzed. For these reasons, antioxidants and their conversion into degradation products may be linked to the increase of the 10^5 Hz dielectric losses and, consequently, to the aging of the polymer matrix. Contextually, dielectric spectroscopy is able to evaluate the concentration of other dipolar species inside the material e.g. oxidized species which are chemically related to the ester bonds in FTIR spectra. As a matter of fact, various works correlate the increase of the ester index after the antioxidant chemical consumption to the increase of the dielectric losses at high frequencies [48], [59]. Indeed, the same chemical species may have their electrical response placed in the high frequency region (around 10^5 Hz) and they are, hence, linkable to the presented changes in the material chemistry.

5.4 CABLE RESULTS DISCUSSION

5.4.1 Coaxial cable

The coaxial cable is the simplest geometry analyzed in this Thesis. Its multilayer structure is presented in Figure 34. From this, it is possible to observe that a polymeric film is placed between the primary insulation (XLPE) and the external copper braid; this is used in order to protect the primary insulation during the processing operations. Electrical analyses, due to the experimental setup employed, take into account the presence of this film whose interface between the copper braid and the insulation is prone to charge accumulation. This gives rise to the polarization peak at lower frequencies (Figure 49) which also appear for the whole set of specimens considered (both unaged and aged samples).

As seen from Figure 49, 51, the low frequency region shows to be not usable for the evaluation of the development of aging conditions. Indeed, it is seen an overlapping and a mixing of the various curves suggesting that the variations with aging are almost negligible in that area probably due to the multilayer structure and conduction phenomena, which leads the low-frequency dielectric response.
On the contrary, the high frequency region well describes the development of aging conditions, due to the increase of the dipolar species (e.g. antioxidant degradation products and oxidized polymer species) as presented above.

However, the variation of the dielectric losses with aging time are not always monotonously increasing due to different occurring phenomena. As presented in Chapter 1, the oxidative degradation is directly proportional to the concentration of free radicals, which is related to the severity of the aging stressors. If the aging stressor i.e. irradiation dose rate is very significant, the concentration of free radicals is high and environmental oxygen is rapidly chemically consumed by free radicals. Hence, the oxygen molecules bond themselves only on the outer layer of the insulation, preventing the oxygen to diffuse in the bulk. Under these circumstances, one can observe a localized degradation in the outer part of the insulation while the bulk of the material remains non-oxidized and, consequently, not aged. This phenomenon in known in literature as Diffusion Limited Oxidation (DLO) [32]–[34], [127]. It is worth recalling that dielectric spectroscopy is a bulk measurement thus it is not possible to evaluate the localized superficial degradation. As a result, if DLO phenomenon is occurring, the dielectric losses amplitude increasing over time is reduced at higher dose rates in comparison to lower ones (Figure 50).

As stated in the introduction, a first significant correlation to be made is between dielectric and tensile measurements. Figure 91 reports the crossplot of EaB versus the dissipation factor at 100 kHz for all the aging conditions and materials analyzed.

In this crossplot, the last high dose rate value of tanδ is not considered since it is believed to be an outlier, as previously reported in Chapter 4. From Figure 91, it can be observed that the reduction of EaB corresponds to the increase of the dissipation factor. As commented for the EaB trend (Figure 84), analyzed aging conditions showed to be not sufficient to cause a significant reduction of EaB. Similarly, the dielectric loss variations result into a little modification from the initial aged value. Therefore, only the initial part of the correlation can be displayed at this stage.

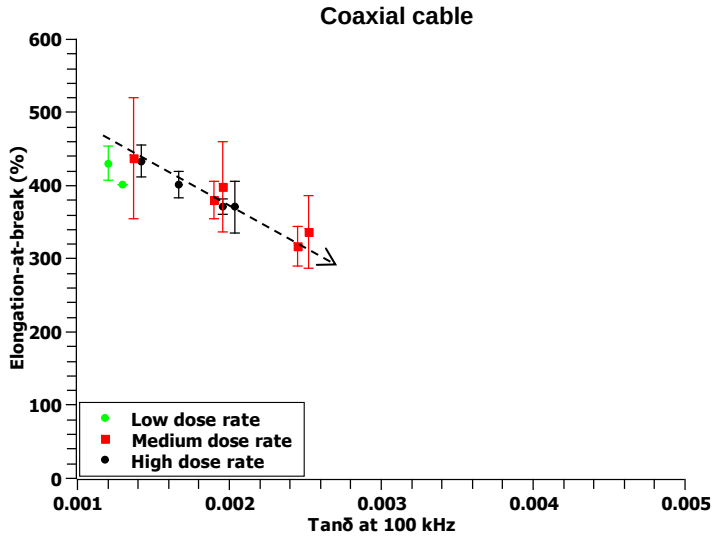

Figure 91 Elongation at break as a function of the dissipation factor for all the aging conditions analyzed. Coaxial cable.

It is important to point out that both the analyzed quantities could be considered as representative of the aging conditions of cables. It is widely known in literature [48], [50], [124], that both EaB and dielectric losses have a monotonous variation with aging time due to the degradation process occurring in the polymer. Due to the presence of antioxidants, the variation of both properties with aging time is reduced or delayed due to the protection by these additives against oxidation. In respect to FTIR (Figure 75) and OIT (Figure 68) measurements, it is possible to claim that the oxidation process is likely to be started in the last aging period for all environmental conditions analyzed. Therefore, at the present stage, no significant oxidation has occurred in the polymer and this results into a significant but still small variation of both EaB (which decreases by 40%) and tanδ.

Under these circumstances, the major variations occurring during aging derives mainly from the change at the microscale. Investigated chemical properties indicate very significant variation with aging time, mainly related to the effect of antioxidants, in the case of the coaxial cable.

It has been discussed that antioxidants, due to the effect of thermal stress and diffusion, can arise to the surface of the material changing their spatial configuration and turning themselves

into crystals. FTIR analyses highlighted the migration of antioxidants from the bulk to the insulation surface with the appearance of new absorption bands of ester (at 1720 and 1742 cm^{-1}) and phenol functions (at 3580 and 3609 cm^{-1}) (see Figure 73). These new bands could be assigned to different crystalline structures of antioxidants formed on the insulation surface. This phenomenon called polymorphism have already been observed in literature for several phenol antioxidants [66], [128].

Nevertheless, it is worth commenting that, for cables here investigated, aging conditions do not yield to a significant oxidation of the primary insulation as shown by physico-chemical analyses. As it can be seen in Figure 68, OIT decreases with aging in all the conditions considered but it reaches almost null values only during the last aging periods, for all the conditions analyzed. Crystallinity ratio also does not display significant variation during aging (see Figure 65), meaning that very small changes in the macromolecular network of XLPE have occurred.

The radical decrease of the dielectric losses observed during the first aging period (Figure 49) could be due to the chemical consumption of antioxidants. Indeed, OIT drastically drops during this first period (Figure 68) while the active functions of phenolic antioxidants disappear (at 3640 cm^{-1}) and those of thioether antioxidants are converted into sulfoxide and sulfone functions (at 1028, 1046, 1131 and 1313 cm^{-1}) (Figure 73).

As presented in the previous paragraph, a significant amount of antioxidant molecules can arise to the surface of the material due to diffusion phenomena, impacting on the dielectric properties of the insulation.
This huge amount of antioxidant molecules in the unaged material is also confirmed by the FTIR measurements, in particular by ester index (Figure 75) which shows an initial high value of the quantity followed by a reduction, likely imputable to the additive chemical consumption.

The chemical consumption of antioxidant results into the conversion of these molecules into their degradation products (§ 1.4), whose concentration increases with aging. The decrease of the antioxidant concentration can be evaluated through the OIT trend (Figure 68) but not by the ester index trends where one can observe a flattening of the ester index with aging time (Figure 75). This is likely imputed to the fact that the antioxidant degradation products own the same ester bond, so that no modification of the chemical bond intensity is registered. On the contrary, dielectric spectroscopy is capable to investigate the antioxidant conversion. Indeed, the antioxidant degradation products are larger dipolar species, hence, their dielectric response is shifted to lower frequencies than the ones typical of smaller polar molecules. It has been shown [117] that 100 kHz represents a good value for the evaluation of the increase of the antioxidant products, whose concentration is, obviously, directly proportional to the degradation of the polymeric material.

After the running out of antioxidants, the high frequency dielectric response is led only by the oxidized species created during aging, which cause the increase of the dielectric losses. The formation of these species can also be evaluated through FTIR measurements (Figure 73) in which one can observe the continuous increase of the oxidized species-related wavenumbers. Similarly, the ester index (Figure 75) shows an increase during the last aging periods which could be likely imputable to the formation of these oxidized species. The duration of the increasing phase of the ester index is dependent upon the harshness of the aging conditions. As a result, the high dose rate aging causes a more significant increase of the ester index on the surface with aging in comparison to the other two conditions. This would have corresponded to the increase of the dielectric losses but, due to the particularly severe conditions, DLO effect can influence the dielectric spectroscopy trend resulting into a non-direct correlation between the two properties.

It is interesting to highlight that the last aging period of the high dose rate condition is confirmed to be an outlier for different measurements techniques. Focusing on the dielectric response, the tanδ curve is placed in between the 2nd and 3rd aging period (Figure 49), so that the increasing law over aging time is not followed. Similarly, the OIT value of the same specimen shows a singular value (7 min) which is way higher than the one related to the previous aged specimen (4 min).

Figure 92 depicts the crossplot of the ester index, after the running out of antioxidants, as a function of the tanδ values. Unfortunately, only few points are reported in the plot due to the lack of further withdrawals. In particular, only two points are shown for the high dose rate which reports a declining trend due to the abovementioned non-homogenous degradation hence no correspondence can be evaluated between the electrical bulk measurement and the superficial chemical one in this case. Anyway, it is observable that the low and medium dose rate conditions show a linear increase of the two factors, confirming the correlation among each other. This correlation is significantly important since it further confirms the ability of the dielectric spectroscopy to investigate the arising of oxidized species hence the possibility to use this technique to examine the aging development of the insulating material.

In conclusion, it could be summarized that the antioxidant migration and accumulation on the insulation surface could be the cause of the initial very high value of OIT and of the dielectric losses. With aging, the value of tanδ shows an abrupt reduction imputable to the huge antioxidant chemical consumption as confirmed by the OIT measurements. After the complete conversion of the antioxidant molecules, tanδ showed to be feasible to be correlated with the increase of oxidized species and, consequently, to assess the changes in polymer properties with aging.

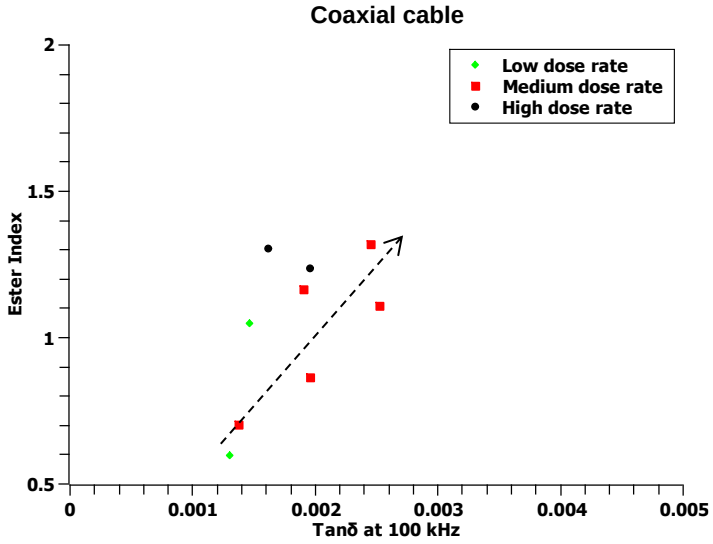

Figure 92 Crossplot of the increase of the ester index as a function of the dielectric losses. Coaxial cable.

5.4.2 Twisted pair non-filled cable

The considered different geometry implies the change in the connection scheme for the dielectric spectroscopy measurements. Despite the similar trend over frequency of tanδ (Figure 54) with the one described for the coaxial cable, in this case, the interfaces arising by the analysis are different. Indeed, no polymeric film is placed between the input and output connection plugs, but interfaces are located between the two wires which are twisted together, creating a massive interface throughout all the length of the twisted pair cable. The dielectric losses at low frequencies (Figure 56) show negligible variation with aging time at least at low doses. Indeed, at high absorbed doses, the variation is appreciable probably due to enhanced Q-DC conduction phenomena, but no monotonous trend can be evaluated. On the contrary, the behavior of tanδ at high frequency well follows the increase of both aging time and absorbed dose (Figure 55).

It is important to recall at this stage that, despite the same polymeric compound, the behavior of the various properties of twisted pair non-filled specimens with aging can be slightly different from the one described for the coaxial cable, due to different geometries. Indeed, the primary insulation is covered by several different layers, among which there are two copper layers (Figure 35), which could partially reduce the actual dose reaching the insulation. In addition, air is present between the two wires, leading to an easier oxidation with aging.

Similarly to what already discussed for the coaxial cable, early variations in the polymer properties with aging time are linked to the antioxidant chemical consumption and conversion into their degradation products. Indeed, the OIT trend (Figure 69) depicts an initial abrupt decrease likely imputable to the physical loss and chemical consumption of antioxidant during the first aging period. This decrease is again linked to the decrease of the ester peak height (Figure 79) on the surface of the material.

It is worth indicating that in this case the early decreasing phase of the ester index (Figure 79) is lasting more aging periods probably due to the abovementioned reduced effective dose. This is particularly evident in the case of the first periods of the low dose rate, which is the mildest condition analyzed. Here, the OIT value remains quite high (in comparison with other aging), suggesting that antioxidants are still present in very high concentration, as confirmed also from the high value of the ester index and from the hydroxyl region of the FTIR spectrum (Figure 77), that is the only case in which the hydroxyl peak related to the phenol antioxidant does not disappear during the first aging condition.

Focusing on the electrical behavior, one can observe that the dielectric losses linearly increase over the absorbed dose at high frequencies (Figure 55), showing two main differences in comparison to the coaxial cable case: the first aging period does not cause the reduction of the tanδ value and the dielectric losses keep increasing for all the conditions analyzed, also for the highest dose rate analyzed.
The lower initial tanδ value could be imputed to the presence of a lower amount of antioxidant in the twisted pair non-filled specimens, as confirmed by an OIT starting value about 20% lower than in the case of the coaxial cable (Figure 69). As a consequence, the arising of the antioxidant molecules and crystals towards the surface is reduced and the antioxidant related peak in the dielectric spectrum may not be evaluated in the frequency region investigated.

Furthermore, it is possible to believe that DLO effect is avoided in the case of twisted pair cables. As abovementioned, this could be related to two main causes: the weaker aging stresses reaching the primary insulation due to the geometry of the cable and the presence of air between each cable pair, avoiding the possible oxygen deficit (see Figure 10).

Focusing on the trend of the ester index with aging time, it is similar to the one already presented in the coaxial cable case, it is made up of a non-varying and an increasing phase, to which it corresponds the rise of the dielectric losses.

Figure 93 depicts the values of the third increasing phase of the ester index as a function of tanδ. From the plot, it is possible to point out that, for all the aging conditions, there is a direct dependence between the two factors. Different dose rates own different increasing slopes. In particular, the high dose rate condition is characterized by a slower increase of the ester index, despite the more significant increase of the dielectric losses, expected due to the severer stressors. This could be imputable to the effect of aging time which is significantly reduced in the case of the high dose rate. On the contrary, the other two dose rates show similar slope but different magnitudes possibly due to the different absorbed doses.

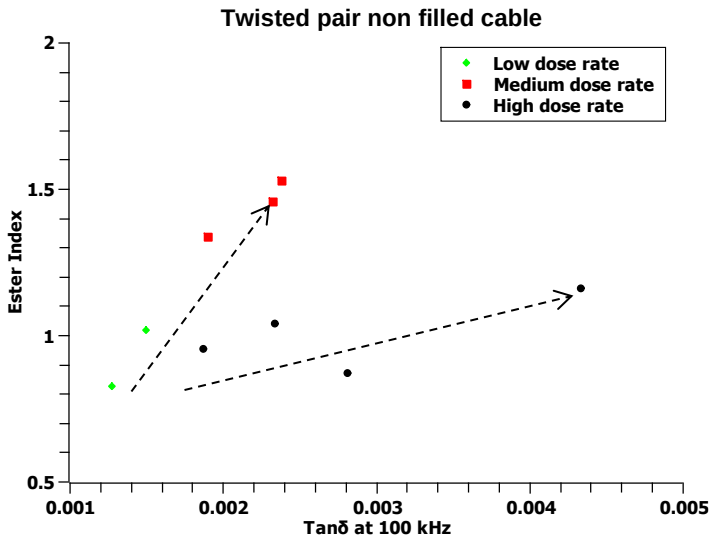

Figure 93 Crossplot of the increase of the ester index as a function of the dielectric losses. Twisted pair non-filled cable.

Focusing on the mechanical behavior of the twisted pair non-filled cable, Figure 94 depicts the trend of the elongation at break as a function of the dielectric dissipation factor. As discussed above, the aging conditions show to be not enough to cause the failure of the cable according to the actual standard, blocking the reduction at about 40% for the harshest condition. Though, as the EaB decreases, tanδ increases following an almost linear law.

Here again, due to the presence of antioxidant additives the degradation of the polymeric material is delayed and, as seen from the FTIR and OIT measurements, very little oxidation can be appreciable at this stage of aging. Under these circumstances, only the initial part of correlation between the electrical and mechanical behavior of the investigated twisted pair cable is shown and no end-of-life point, in terms of electrical properties, can be derived.

It is worth underling that the dependence is almost linear until the 4th aging period of the high dose rate aging. The 5th (last) aging period causes an abrupt increase of the dielectric losses without a significant variation of EaB value. Thus, this aging point could be related to the initial stage of oxidation as seen from a steep increase of the ester index to which it also corresponds a significant increase of tanδ (Figure 93). However, this oxidation level seems to be not sufficient to cause significant reduction in terms of mechanical properties, owning an EaB ~300%.

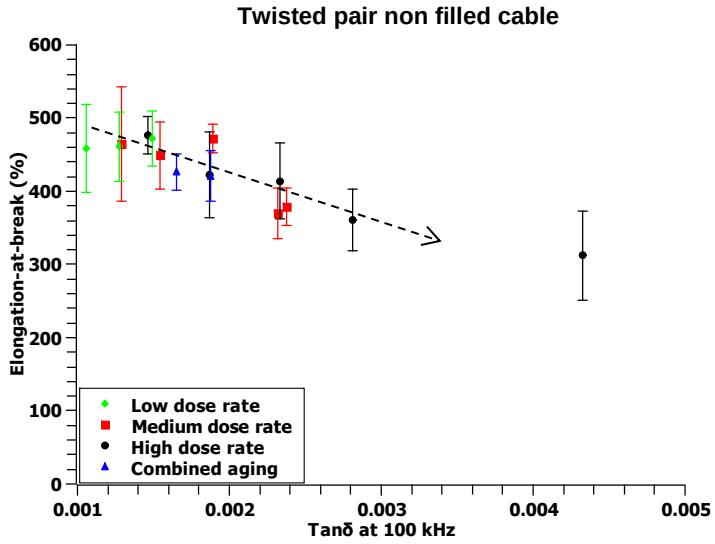

Figure 94 Elongation at break as a function of the dissipation factor for all the aging conditions analyzed. Twisted pair non-filled cable.

5.4.3 Twisted pair filled cable

Twisted pair filled cables are characterized by compound #2 as primary insulation. The presence of flame retardants (ATH) in such high concentration (50 phr) showed to deeply influence both the chemical and electrical properties, other than the mechanical ones.

Inorganic fillers e.g. ATH ($Al(OH)_3$) are placed in the amorphous phase of the polymer matrix where they can easily agglomerate if their concentration is enough to rearrange themselves into clusters. In Figure 95, it is possible to observe a image from X-ray tomography showing the difference between the cross section of the unfilled (a) and filled (b) material. One can notice a different distribution of polymeric chains (dark grey) due to the presence of the fillers (white dots).

Microscopically, fillers have an impact on both the chemical and electrical properties. As an example, FTIR spectra (Figure 81) showed different new peaks in the hydroxyl region due to the chemical formula of these fillers (presence of -OH bond), a slightly reduction of the initial OIT value, hence of the concentration of antioxidants (Figure 70), and a significant variation of the crystallinity ratio (Figure 67) compared those measured on compound #1.
In particular, crystallinity shows a different initial value and response with aging time. This is once again imputable to the fact that the presence of fillers changes the morphological distribution between the crystalline and amorphous phases. As a matter of fact, the inorganic filler might act as a kernel around which polymeric chains can crystallize giving rise to the initial crystallinity value. With aging, in all the conditions considered, the trend of the crystallinity increases. This could be imputable to the chemi-crystallization phenomenon (§ 1.4.3) in addition to the increase of the number of broken chains, created by radiation, which crystallize following the abovementioned mechanism.

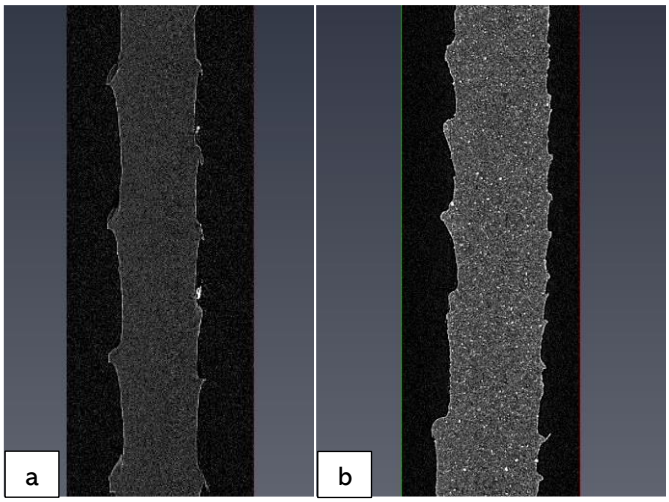

Figure 95 Images from X-ray tomography of the cross-section of the unfilled (a) and filled (b) material. Courtesy of VTT Finland

The dielectric response also is affected by inorganic fillers. The reason for that can be found in the dipolar properties of the filler molecule itself. ATH molecules are characterized by a very high polarity due to the presence of the -OH bond. Electrically, the response of these molecules is placed in the dipolar polarization area making the use of 100 kHz frequency as aging marker difficult (Figure 60). These molecules are usually not affected by the radio-chemical aging; consequently, it could be difficult to distinguish the dipolar response of these molecules from the arising of aging products i.e. antioxidant degradation products and oxidized polymer species.

Moreover, due to the agglomeration of ATH particles, the low-frequency dielectric response also is influenced by the creation of ATH cluster interfaces. From the trend of the low-frequency dielectric response (Figure 61), one can observe an nearly flat behavior of tanδ except for the last aging time of the high dose rate condition. For this reason, it could be tricky to choose a frequency region which could be used as an aging indicator based on dielectric spectroscopy for this kind of material.

Luckily, when the concentration of aging products reaches a threshold value, the variation of tanδ values in the high frequency region could be linked to the increase of polar species given by aging (Figure 60). This threshold is around 2900h in the case of low and medium dose rates, while it is around 500h in the case of high dose rate. This divergence could be related to a possible diffusion limited oxidation phenomenon, which was not considered in the case of the non-filled twisted pair cable. In the case of compound #2, the concentration of the degradable matter (polymer matrix) is way reduced than in the case of compound #1, hence effects of dose rates and related degradation phenomena on the polymer are larger, possibly

causing DLO phenomenon in the twisted pair filled case. From the threshold time, the increase of tanδ values is monotonous and hence usable as an aging marker.

Equivalently to what described for compound #1 materials, the trend of the ester index (Figure 83) is characterized, in all the aging conditions considered, by three phases: an initial reduction, a stabilization and a final increase, except for the last aging period of the high dose rate aging.
The initial reduction corresponds to a significant decrease of the OIT value (Figure 70), thus it could be related to the antioxidant chemical consumption of the accumulated antioxidants molecules on the surface. Electrically, the removal of the antioxidants causes again a reduction of the tanδ value at high frequency (Figure 60).
Further aging causes the stabilization of the concentration of ester bonds which could be likely imputed to the conversion of the antioxidant molecules into their degradation products, also confirmed by the continuous reduction of the OIT values, similarly to what discussed for compound #1 materials. Contextually, the dielectric response shows a flattening (Figure 59), followed by an increase depending on whether the threshold value is reached or not (before this the dielectric response appears to be led only by the ATH molecules).
Finally, after the running out of antioxidants, hence OIT value is nearly zero, both the ester index and the dielectric losses increase with aging probably due to the creation of oxidized species.

Figure 96 reports the values of the increase phase of the ester index as a function of tanδ for all the aging conditions considered.
From this figure, one can observe a direct correspondence between the two factors, except for the last aging time of the high dose rate since it was considered as an outlier for the ester index trend. This behavior again confirms the strict correlation between the increase of the oxidized species and the increase of the dielectric losses.

Focusing on the mechanical behavior with aging of the twisted pair filled cable (Figure 88), it is worth noting that the initial EaB value is way lower than in the case of compound #1 materials. As a matter of fact, the presence of fillers could bring to other two concurrent effects: the reduction of chain mobility and the lowering of the crosslinking grade. On the one hand, smaller crosslinking grade can bring to decreased tensile stress (Figure 89) but higher elongation at break, due to less rigid polymer. On the other hand, reduced polymer chains mobility could reduce elongation-at-break values as reported in Figure 88.

As expected, the mechanical properties continue to worsen during aging under the effect of environmental stressors. Indeed, fillers could also lead to a phenomenon similar to DLO (Figure 10), impacting the mechanical properties of the material. As a matter of fact, ATH can hinder

the oxygen molecules from diffusing through the polymer thickness, acting as physical barriers. This would lead to non-homogenous aging throughout the polymer sample, causing an abrupt reduction of the elongation-at-break, as reported in Figure 88 in the case of high dose rate aging.

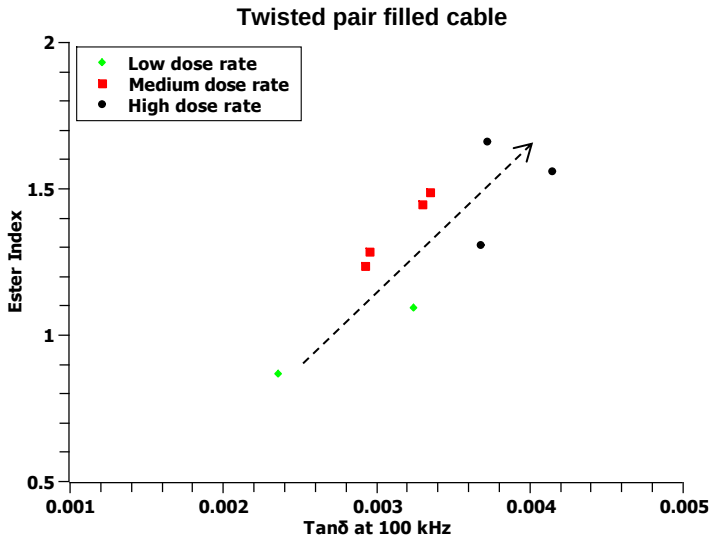

Figure 96 Crossplot of the increase of the ester index as a function of the dielectric losses. Twisted pair filled cable.

Figure 97 reports the trend of the elongation at break as a function of tanδ at 100 kHz. As stated above, due to the influence of ATH fillers on the dielectric spectrum together with a little reduction and huge data dispersion of EaB, it is difficult to point out a correlation between these two parameters.

However, it is worth commenting that a decreasing trend is noticeable at least for the high dose rate aging conditions where the threshold is reached quite early in comparison with the other two stressor environments.

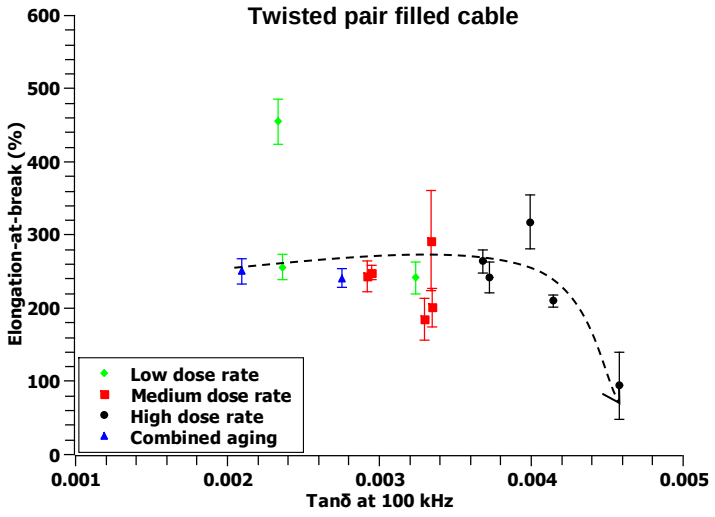

Figure 97 Elongation at break as a function of the dissipation factor for all the aging conditions analyzed. Twisted pair filled cable.

5.4.4 Conclusions

In conclusion, in all the cases analyzed, the tanδ values at 100 kHz from the first aging period well fits the total dose absorbed by specimens during aging. This behavior confirms the strict correlation among the evolution of aging, its products (above all dipolar species), and the dissipation factor at 10^5 Hz. Therefore, tanδ at 100 kHz may be also used as an indicator for development of material dielectric properties with aging other than a marker for aging state of the insulation in the case of the investigated cables.

Referring to the mechanical behavior of cables, correlation with the electrical properties can be done only in the case of unfilled polymeric materials (compound #1). These materials show an almost constant decay of the mechanical properties to which it corresponds an almost linear increase of the dielectric losses at high frequencies. On the contrary, referring compound #2, it is not possible to claim an effective correlation between the two quantities due to the overwhelming influence of inorganic fillers on mechanical properties of the material. These latter, from the mechanical point of view, cause a significant reduction of the ultimate elongation during the first aging period due to the formation of clusters, the value of EaB does not further vary except for very severe conditions. From the electrical point of view, filler dielectric response overcomes the one relatable to oxidation products, so that it is difficult to distinguish the two contributions from the dielectric spectra at least during early aging states.

Ester index successfully follows the concentration of oxidized species which show a characteristic carbonyl bond. Unfortunately, due to the overlapping of wavenumbers, it is not possible to single out from FTIR spectra the bands referred to the antioxidant molecules from the ones related to macromolecular oxidation products. For this reason, it is possible to correlate the polymer aging with the ester index only after the running out of antioxidants, hence with the increase in concentration of the oxidized polymer species. It has been demonstrated that the correlation with the increase of tanδ at 100 kHz with the ester index is possible only after the complete running out of antioxidants in order to avoid the contribution of the conversion of these molecules into their degradation products. However, due to the very early stage of degradation of the material under test, only few points for this correlation are available.

5.5 Data analysis – comparison between compounds

In this section a more complete data analysis is reported, considering, at the same time, all the materials and aging conditions analyzed. Big attention is given to the different behaviors of the two compounds and geometries (coaxial and twisted pair), in order to better understand the influence of these factors on the actual depletion of the polymer properties with aging.

Thanks to the similar behavior over aging of the different materials under test and testing technique homogeneity, it is possible to investigate the aging response through three different levels:

- Antioxidant consumption and conversion
- Arising of oxidized polymer species
- Correlation between mechanical and electrical properties.

5.5.1 Antioxidant consumption and conversion

In order to easily investigate the conversion of antioxidants into their products, it is possible to introduce the Antioxidants Depletion Factor (ADF) defined as:

$$\mathbf{ADF} = \frac{\mathbf{OIT_0} - \mathbf{OIT}}{\mathbf{OIT_0}} \tag{26}$$

where *OIT* and OIT_0 are the respective values for the aged and unaged samples.

As the name suggests, this factor represents the depletion of the antioxidants over the aging time, hence their conversion into antioxidant degradation products.
The association with dielectric losses lays on the fact that both the factors keep into account the contribution of the changes of antioxidant concentration. The dielectric spectroscopy at the analyzed frequencies (around 10^5 Hz) may evaluate the presence and the concentration of antioxidant degradation products (dipolar species). On the other side, as stated above, OIT is directly dependent on the concentration of antioxidants inside the polymer matrix, hence it is associated to the conversion of these molecules into their degradation products.

It has been shown in Chapter 4 that in all the conditions and materials analyzed the OIT value significantly decreases during the first aging time then it slower decreases until a nearly zero value, which claims the total consumption of the antioxidants and the conversion into their products.
As presented in the cable discussion section, the initial different values between the two cables characterized by compound #1 could be imputable to two possible causes: (i) different initial concentration of antioxidants, as confirmed by the different initial OIT values between the two, (ii) different measurement setup used due to the different geometries of samples.

Similarly, the dielectric spectroscopy trends (Figure 49, 54, 59) show an important variation during the first aging period, followed by a slower increase of the dielectric losses with aging time.

The trend of the dissipation factor (tanδ) and the above defined antioxidant depletion factor is reported in Figure 98. It can be assessed for all the aging conditions and analyzed materials,

that after a significant initial variation of ADF, data are placed between the range ADF= 0.8 – 1. In this region, it is possible to build a regression curve which shows an initial exponential branch and it finally tends asymptotically to 1, corresponding to the complete running out of antioxidants (namely when OIT=0 min).

Therefore, in the exponential region, it is possible to define a correlation between the two analyzed quantities and, in particular, it is possible to claim a correspondence between the grade of conversion of antioxidants, hence the increase of antioxidant degradation products, with the raise of tanδ values.

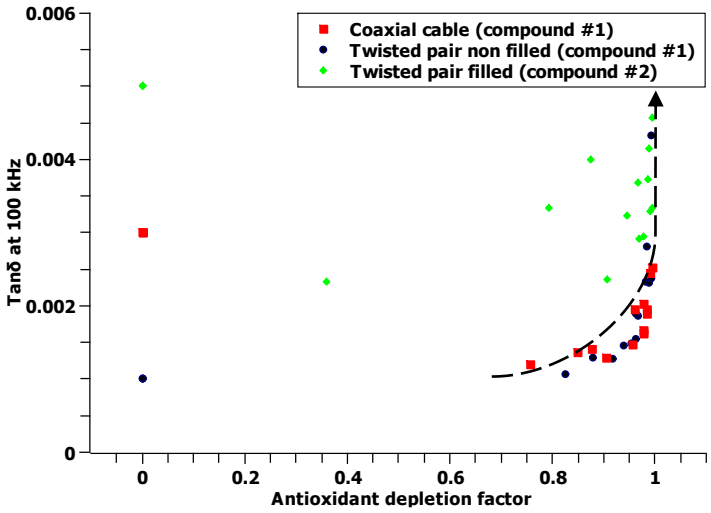

Figure 98 Dissipation factor as a function of the antioxidant depletion factor for the three analyzed cables

Focusing on the compound properties, it is evident how compound #1 materials depict the same tendency behavior with similar dissipation factor values. On the contrary, the introduction of ATH fillers (compound #2) results into the shifting of the abovementioned trend upwards (Figure 98), due to the higher tanδ values.

However, data dispersion is wider in this latter case, due to the difficulty to single out the electrical response of the ATH dipoles from the one related to antioxidants and their degradation products.

Nonetheless, the correlation between tanδ and ADF is possible until the antioxidants are present, hence, when they are fully converted into antioxidant degradation products and no oxidation occurs, so that OIT≠0 min.

Once all the antioxidants are converted (depletion factor = 100%), the thermo-oxidative reactions can take place in the polymer matrix resulting into the formation of new molecules (oxidized polymer species), as described in Chapter 2.

5.5.2 Arising of oxidized species

Literature is plenty of studies [48], [59], [76] correlating the increase of the ester peaks with the aging time, suggesting the possibility to use the ester bands and their amplitude as an aging marker. These studies usually focus on neat highly pure polymers which are, in a certain sense, non-completely representative of the actual industrial application of the material e.g. electrical insulator.

Even in this case, it is important to recall the fact that dielectric spectroscopy is a bulk measurement, so that it could be difficult to keep into account the actual concentration of the antioxidants on the surface. Under these circumstances, it is not possible to directly correlate the dielectric response with superficial ATR-FTIR.
As presented in the previous section, the last aging times for the three aging conditions show an increase of the ester index which is also linked to the minimum value reachable by the OIT measurement, possibly suggesting that oxidation has started and the new esters created are directly referred to the oxidized polymer species.

Figure 99 reports the trend of the dielectric dissipation factor at 100 kHz versus the ester index obtained through FTIR measurements. In order to build this graph, only the values referring to the third phase of the trend of the ester index has been reported (Figure 83), this in order to avoid the contribution of the antioxidants and their consumption and to keep into account only the oxidation of the polymeric material.
As it can be seen from Figure 99, the correlation between the two parameters is well established, confirming the capability of the dielectric spectroscopy to successfully follow the concentration of the oxidized polymer species, hence the degradation of the material.

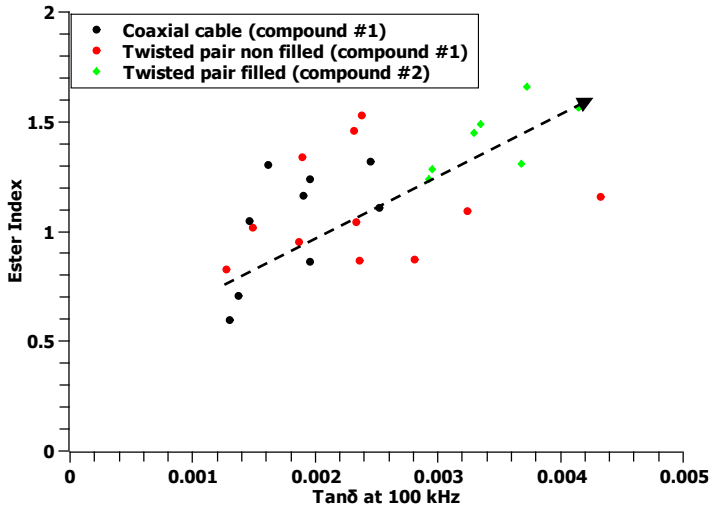

Figure 99 Dielectric losses versus ester index for the three different cables analyzed.

This correlation is a key feature for the assessing of the dielectric spectroscopy as an aging marker since it shows to be able to relate the electrical quantity to the main cause of the polymeric degradation at the microscale: oxidation.

It can be estimated that cables owning the same compound showed similar data displacement in the above plot. Indeed, it is possible to divide available data into two data cluster: one related to cables with compound #1 and the second related to cables with compound #2. In particular, the cluster referred to compound #2 shows the same increasing behavior as compound #1, but it is shifted towards higher values of both quantities, suggesting similar behavior of the two properties with aging.

5.5.3 Correlation between mechanical and electrical properties.

In this section the correlation between the elongation-at-break and dielectric spectroscopy measurements is presented. Trying to correlate these two quantities is very important due to the current use of the EaB as a condition monitoring technique for cables inside NPPs. In particular, the ultimate value of EaB which is widely used as end-of-life criterion is 50% of the absolute value.

The entire set of data depicts a peculiar trend between the two measurements techniques, as shown in Figure 100. Even in this crossplot, two main clusters can be highlighted in the graph: one related to cables characterized by a non-filled primary insulation (compound #1) and the second one representative of the twisted pair filled cable (compound #2). This division is imputable to the presence of the filler clusters which leads, usually worsening, the mechanical behavior of the cables.
Focusing on the electrical properties, the values of the dissipation factor are higher due to the presence of ATH dipoles. These two phenomena, linked together by the filler properties, result into a shifting of the experimental points to a different area.
These data show a unique master-curve among the different materials, depicting a good correlation between the two quantities.

It is evident that no cable reached the end-of-life value of elongation for all the aging conditions analyzed. The lowest value of EaB is equal to about 90% and it is related to the ultimate elongation of the highest dose of the harshest aging condition (high dose rate) for compound #2. Moreover, the decreasing rate of the low dose rate is more significantly impacting the tensile stress measurements, showing a bigger decreasing slope, but at this stage, no sufficient aging periods are present to further investigate this behavior.

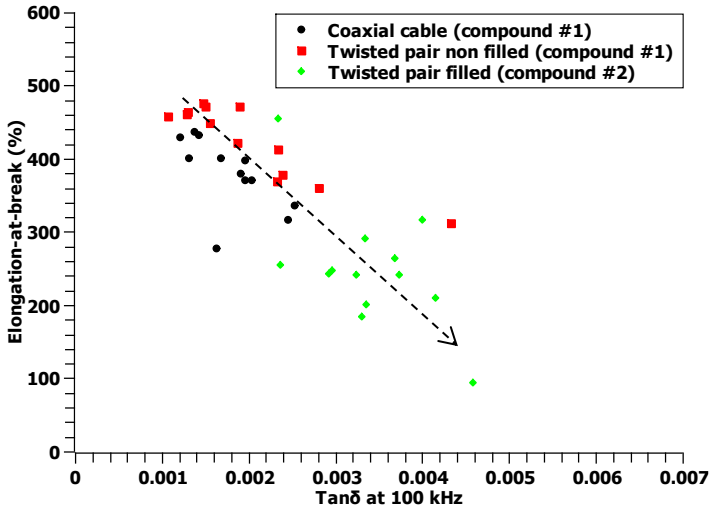

Figure 100 Crossplot of EaB vs dissipation factor at 100kHz

5.5.4 Conclusions

It has been shown that no cable reached the ultimate EaB required by the actual state of the art cable monitoring. The aging conditions, at this stage, are not very strong so that no significant degradation is reached, particularly for the cables with compound #1, since no substantial oxidation occurred inside the polymer. This is also confirmed by the very little duration of the third phase (increase of the ester peaks after the running out of antioxidants) discussed for the ester index. Consequently, the variations in terms of mechanical (e.g. EaB) and electrical properties (e.g. dissipation factor) are only related to microstructural modification inside the polymer, i.e., antioxidants consumption, chain rearrangements. However, it is possible to build preliminary correlations between the different properties, assessing the suitability of dielectric spectroscopy to investigate all phases of the polymer degradation.

Under these circumstances, a modelling approach is needed to evaluate the residual life of the analyzed cables in terms of mechanical endurance and find a corresponding ultimate tanδ value, thus an acceptance criterion, in terms of the electrical property. This could be a substantial step forward for the actual state of the art in cable diagnostics since it could be done in a non-destructive way.

5.6 Discussion on thermally aged cables

5.6.1 Introduction

In this section, discussion on thermally aged cables is reported. The discussion is limited to the dielectric properties of the material due to the lack of other physical-chemical results.

5.6.2 Discussion

Paragraphs § 4.2.1-4.2.3 depict the evolution of the dielectric properties of the analyzed cables subjected to thermal stresses. Three temperatures, namely: 87 °C, 110 °C and 130 °C have been chosen as accelerated aging conditions.
It has been widely discussed that aging temperature deeply influences the dielectric response of the analyzed cables, raising the dielectric losses. On average, the higher the aging temperature the more significant are the changes of dielectric losses with aging time.

In most cases, the first aging period causes a reduction of the dielectric losses in comparison with the unaged material. This behavior has been already reported in the case of radio-chemically aged cables and it could be linked to the antioxidant molecule consumption which weakens the dipolar response.
Further aging periods lead to the increase of tanδ, probably due to the arising of antioxidant product molecules together with the creation of new oxidized degradation species created by aging stresses. It is possible to believe that the very little increase, seen in the coaxial cable samples, could be related to the conversion of antioxidant molecules into their degradation products as discussed for the radio-chemically aged samples. On the contrary, the arising of oxidized species is expected to cause a significant upward shift of the dielectric losses due to the high dipolar properties of these species.
Probably, in the case of 87 °C, the selected aging period together with the chosen aging temperatures are not sufficient to cause the complete running out of antioxidants and, hence, to let oxidation mechanisms take place.
The 110 °C aging condition showed to trigger significant variations of the dielectric property suggesting a complete consumption of antioxidant together with the arise of the dipolar oxidized species.
However, chemical tests (e.g. OIT and FTIR spectroscopy) are needed in order to confirm these speculations.

From the thermographs shown in Chapter 4, it is derived that the melting peak for the tested polyethylene material occurs at around 120 °C. Aging temperatures higher than this value cause a change in the material morphology, melting the entire crystalline part. During the withdrawal phase, polymer is subjected to an abrupt decrease of temperature to ambient temperature (around 25 °C). This process leads to the rapid crystallization of some chains from the amorphous phase (annealing [129]), leading to a different microscopical structure and a substantially lower crystallinity ratio. The structural morphology of the material can affect the macroscopic properties, e.g., electrical ones. In particular, the resulting polymer can differently behave in terms of dielectric response from another aged material with the same chemical

composition and structural arrangement. Under these circumstances, it is possible to claim that the 130 °C aging could not be directly compared with the other two chosen temperatures.
This is particularly evident in the case of the coaxial cable where one can observe an unusual reduction of the electrical property throughout the frequency region under test. On the contrary, tanδ variations with aging are not significant in the case of the twisted pair filled cables, where an initial abrupt increase of the property is followed by a stabilization of tanδ value. However, at this stage, very few withdrawals are available for this aging condition, hence it could be difficult to deliver a complete picture of the microstructural modification occurring in the polymer due to aging.

Focusing on compound #1, it is shown that cable morphology can play a role in the degradation kinetics ruled by high temperatures. In particular, coaxial cable tanδ at low frequencies showed to be slightly higher than the ones related to the twisted pair morphology. This suggests a different interfacial arrangement inside the polymer compound for the two geometries, as expected. Indeed, various cable structure could result into a different interface arrangement, potentially justifying such a behavior.
In the high frequency region, which has been demonstrated to be relatable to aging, almost null differences of tanδ values between the two geometries are reported. This could be considered as a further confirmation that the aging kinetics is the same among the different geometries giving raise to degradation species with the same dipolar properties. However, further chemical tests are needed in order to better understand which kind of dipolar species arise in the different geometries under thermal stress.
Compound #2 tanδ values are significantly higher than in the case of compound #1, due to the introduction of ATH species which enhance the dielectric response due to their dipolar properties.
Moreover, thermally aged compound #2 showed a different tanδ trend with respect to the one described for the radio-chemically aged samples, as already discussed in the case of combined aging conditions and in the previous paragraph. As a matter of fact, the temperature stress deeply influences the dielectric response of the material giving birth to a different tanδ curve shape throughout the investigated frequency range and in an appreciable increase of the electrical property with aging.

5.6.3 Conclusions on thermally aged cables

In this section, the dielectric spectroscopy trends of the thermally aged cables have been reported and discussed. The choosing of three temperatures allow the analysis of the development of the dielectric property with different degradation kinetics.

The conclusions could be summarized as follows:

- Aging temperature deeply influences the dielectric response of the analyzed cables. It has been shown that the higher the aging temperature the more significant are the changing in the dielectric losses with aging time.
- The use of the high frequency dielectric response as an aging marker showed to be suitable also for thermally aged samples, due to its ability to evaluate the changing of dipolar properties of the polymer caused by aging.
- Cable morphology can play a role in the degradation kinetics ruled by high temperatures.
- The variation of the dielectric losses could be linked to the running out of the antioxidants molecules during the first aging periods followed by the arising of oxidized species, which results into a very important increase of the dielectric losses trend.
- In some cases, a stabilization of tanδ is reported. It could be imputed to a constant dipolar property of the material e.g. no increase of oxidized species, suggesting the reaching of the oxidability plateau of the analyzed polymer.
- Compound #2 tanδ values are significantly higher than in the case of compound #1, due to the introduction of ATH species which has been demonstrated to enhance the dielectric response due to their dipolar properties.

CHAPTER 6

MODELLING OF CABLE AGING

6.1 INTRODUCTION

Up to now, the health of NPPs cable systems during aging has been evaluated from their mechanical properties [21], [22], [45], [104], particularly their elongation-at-break (EaB). Indeed, cables must be sufficiently ductile to prevent any deep damage to the cable itself which can lead the breakdown of the insulation and cause its failure.

End-of-life criterion is usually set at 50% absolute value of the elongation-at-break of the cable specimen. This criterion puts its basis in a report issued by EPRI [45] in 2005. In this report dozens of extruded LV cable specimens have been aged and mechanically tested before and after a Loss of Coolant Accident (LOCA) simulation. This simulation is very important and common inside NPPs since it ensures, in specific areas, the possibility of the cable system (particularly safety cables) to deliver signal or data after a nuclear accident. It has been demonstrated that all cables with EaB equal to or higher than 50% absolute value passed LOCA. However, some cables passed the accident simulation with even lower EaB values. For this reason, 50% of absolute EaB is usually used as a conservative value for verifying cable ability to pass the LOCA.
Despite this, other Research institutes and standards (IEC 60216-2) suggest a more conservative approach setting the end-of-life (EoL) criterion at 50% [104], [130] of the relative EaB which can correspond to, e.g. for a PE extruded cable, about 150% of the absolute EaB. However, this criterion, which is the one presented in this study, presuppose the EaB value for the new cable to be known, which is not always available.

In the recent years, electrical properties, in particular dissipation factor (Tanδ), gained more and more interest by some researchers since they appeared to be suitable for the evaluation of health state of the cable during aging in a non-destructive way [2], [48], [83], [115].

This Chapter is divided into two main parts: in the first one the modelling of mechanical and electrical properties is introduced, aiming at a possible scaling up the actual diagnostics methods for cables. In the second one, the current state-of-art life modelling approach is applied to the coaxial cable. Each part is preceded by the theoretical background on mechanical/electrical and lifetime modelling, respectively.

6.2 MODELLING OF CABLE PROPERTIES

6.2.1 Modelling of the mechanical properties

The approach used for modelling the mechanical properties is the one described in § 2.4, issued by IAEA and based on the power law extrapolation method.

This approach allows the building of a curve representing the maximum dose a cable can bare before reaching the crisis of the cable itself, for a given dose rate. In other words, it is made up of points indicating the total doses required to reach a specific end point criterion.
As a result, the curve is built in a log/log plot featuring the Dose Rate (DR) values and the so-called Doses to Equivalent Damage (DED). This latter is defined as the dose, one per each dose rate investigated, at which the EoL point is reached. This plot is found to be linear in a log-log plot for the XLPE insulated cables, enabling extrapolation of DED to lower dose rates. The end point doses are given by

$$\mathbf{DED} = \mathbf{K} \cdot \mathbf{DR^n}\ (\mathbf{kGy}) \tag{27}$$

where *DR* is the dose rate; *K* and *n* are empirical constants specific to the material tested. The constant *n* is usually in the range 0 to 0.3.

In order to draw such plot, an EoL criterion must be assessed. As presented in the introduction, up to date no standard or set rules are available claiming a unique EoL criterion based on EaB. In this work 50% of the relative EaB has been chosen as EoL point for two main reasons: the proximity of $50\%_{relative}$ with the current experimental data and the conservativeness of this approach, which can be recommended for e.g. safety cables.
The model proposed is based on the following assumptions:

- Test data must be obtained in isothermal conditions
- The highest value of analyzed DR is such that homogenous oxidation conditions are achieved
- The dose rates analyzed must be at least three, in order to build a reliable curve.

Among the various limitations this approach can face, such as the extrapolation to dose rates within the thermally dominated aging region, there is the fundamental obstacle that this modelling approach is based on mechanical destructive tests which are usually not representative of the entire cable system and not easy to perform on real cables.

6.2.2 Modelling of the electrical properties

The novelty of this work lays on the possibility to upgrade the actual standard and the ease-of-use (i.e. EaB tests) using nondestructive electrical techniques.

To do so, the trend of the electrical properties, one per each aging condition considered, plotted versus the total absorbed dose, allows the extrapolation of the EoL criterion based on the electrical property. Indeed, the value of tanδ, corresponding to the DED obtained through EaB measurements analyses, will be the end point of the cable dissipation factor. A schematic representation of the used approach is reported in Figure 101.

These tanδ values at a fixed frequency namely: tanδ at DED ($tan\delta_{DED}$), one per each dose rate considered, allows a new tanδ vs DR curve to be built following the inverse power law:

$$\mathbf{tan\delta_{DED}} = \frac{\mathbf{1}}{\mathbf{c \cdot DR^{s}}} \tag{28}$$

Even in this case, *DR* is the dose rate; *c* and *s* are empirical constants specific to the material tested for a given temperature.

Among the frequency values, 100kHz is chosen since it is showed in literature [3, 4] and demonstrated in the previous Chapters, to be representative of the cable aging conditions and, consequently, possibly usable as an aging marker for cables based on electrical non-destructive measurements.
The curve built in this way for a given cable-type could allow the health assessment of the cable insulation, in terms of electrical properties, entirely through non-destructive electrical testing technique.

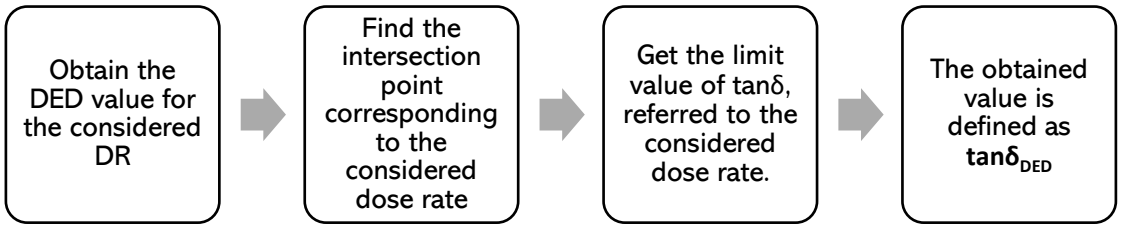

Figure 101 Flow chart for obtaining the $tan\delta_{ded}$.

6.3 Modelling results and Discussion

6.3.1 Mechanical properties

Figure 102-103 display the behavior of the relative EaB, namely EaB/EaB_0, as a function of the total dose for the coaxial and twisted pair filled cable. The case of twisted pair non-filled cable could not be investigated due to the lack of experimental data for the low dose rate aging. Moreover, due to the severe conditions, in some cases it was not possible to remove the primary insulation from the conductor. For this reason, only few points for the tensile measurements referred to the low dose rate condition are reported here.
Relative EaB is calculated by the ratio between the actual EaB and the EaB of the unaged cable.

Once plotted, a linear regression line is built in order to obtain the end-of-life point corresponding to $EaB/EaB_0=0.5$. In order to keep the uncertanty and the confidence intervals coming from these measurements, other two lines are drawn corresponding to the upper and lower limits of the highest and lowest EaB/EaB_0 values obtained, respectively. So that every obtained measurement value results to be placed inside the built confidence interval.

The dose values, and contextually the upper and lower limits, corresponding to $EaB/EaB_0=0.5$, are selected and used for the application of the above described power law method.

As an example, Figure 104 reports the method of graphical extrapolation of the required data for the high dose rate aging conditions on the coaxial cable.

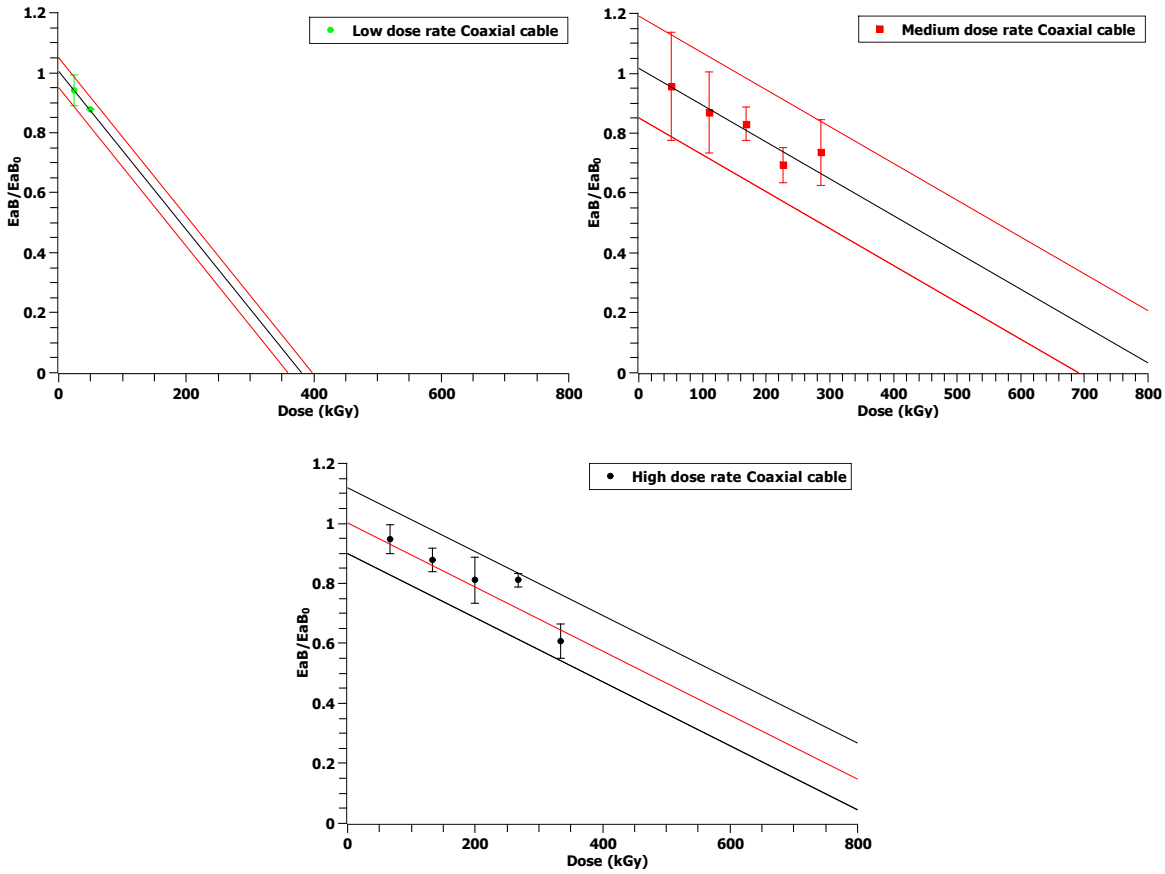

Figure 102 EaB relative values for coaxial cable samples.

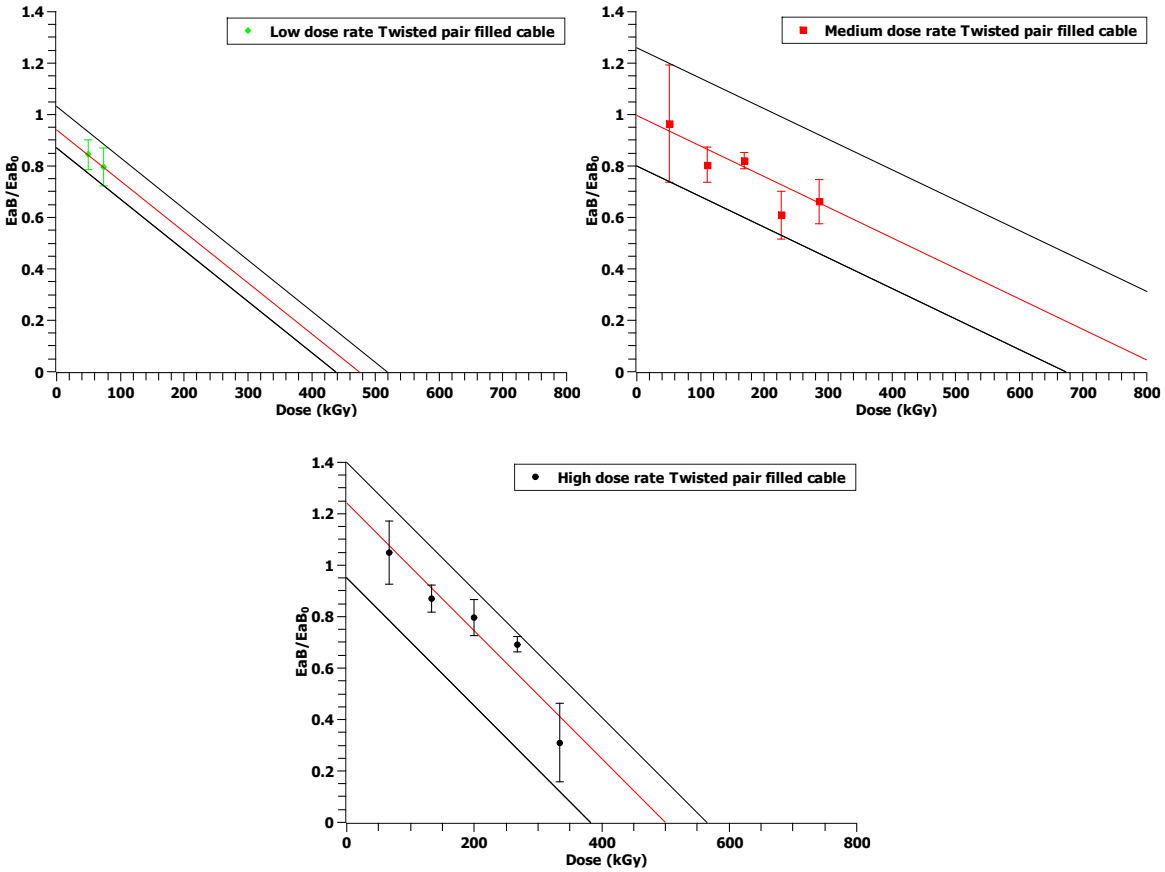

Figure 103 EaB relative values for twisted pair filled samples.

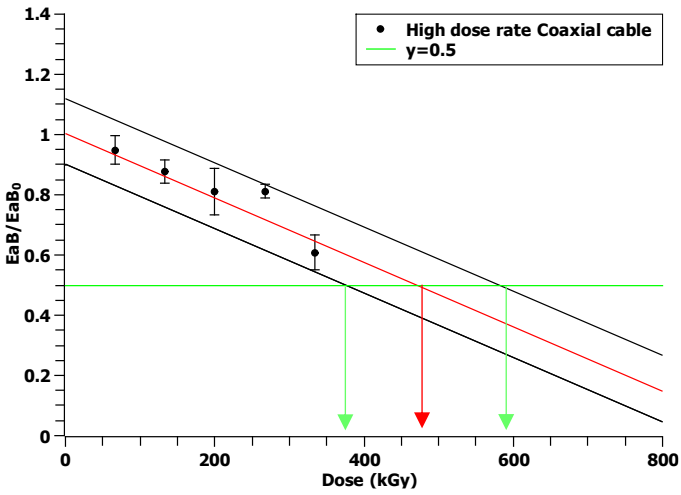

Figure 104 EaB relative value for coaxial cable aged under high dose rate conditions. 50% relative value graphical extrapolation.

Hence, the dose (kGy) values corresponding to the chosen end-of-life criterion, namely the Dose to Equivalent Damage (DED) are reported in Table 3.

Table 3 Dose equivalent to damage (DED) values for the different conditions analyzed.

	Coaxial Cable			Twisted pair filled		
	Regression DED (kGy)	Upper limit	Lower limit	**Regression DED (kGy)**	Upper limit	Lower limit
Low	193	208	171	227	380	189
Medium	422	565	287	419	647	258
High	472	585	377	301	363	184

Therefore, the obtained values are plotted and fitted through a power law equation and finally plotted in a log/log plot (Figure 105-106).

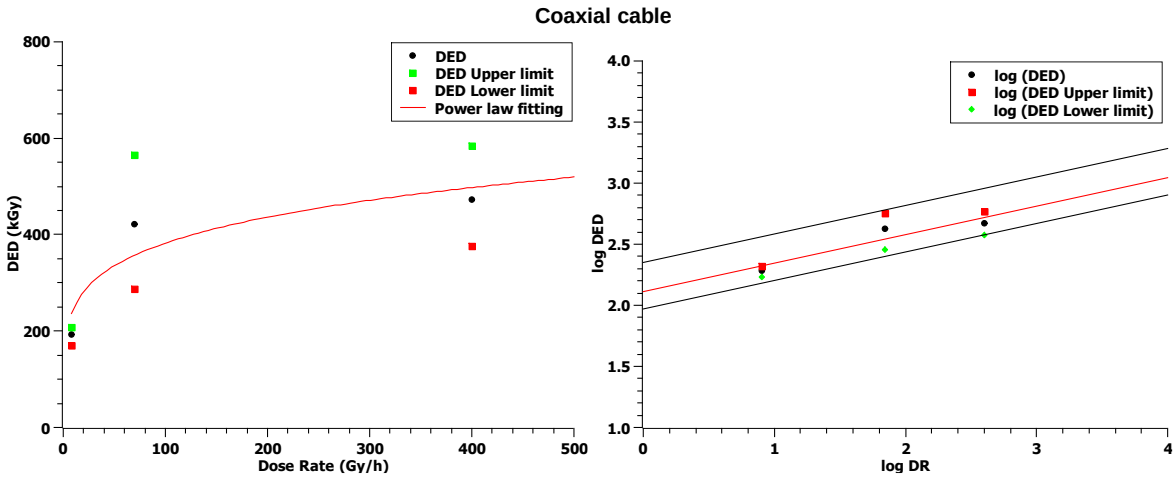

Figure 105 Extrapolation of Dose equivalent to Damage for the coaxial cable.
(a) linear scale, power law fitting (b) log/log scale.

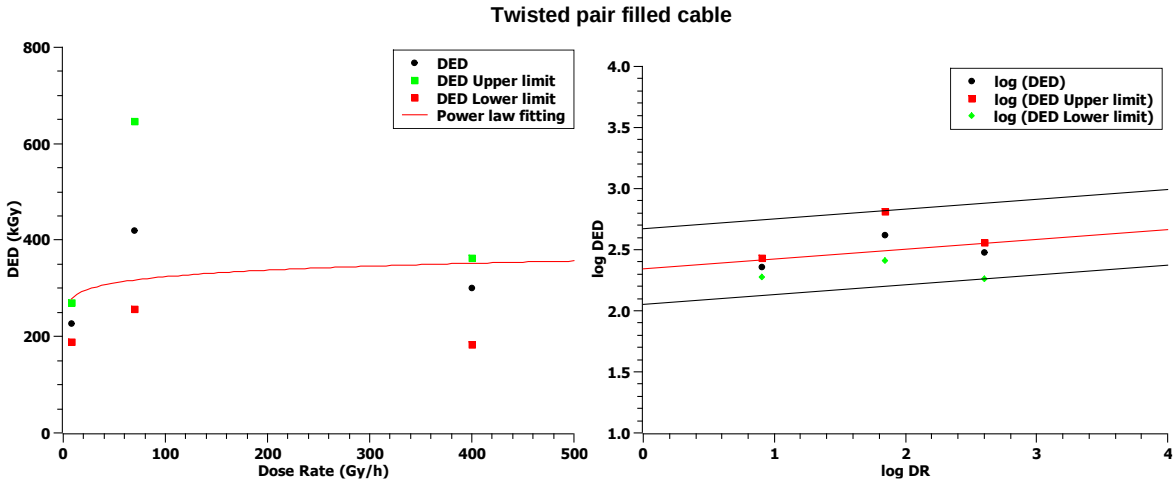

Figure 106 Extrapolation of Dose equivalent to Damage for the twisted pair filled cable.
(a) linear scale, power law fitting (b) log/log scale.

As presented in the introduction to this Chapter, the regression lines, representative of the doses corresponding to the failure of the cable for a given dose rate, are obtained through equation (27).

The values of K and n, for the various configurations analyzed, are reported in Table 4.

Table 4 Power law fitting parameters of mechanical property elongation-at-break

Coaxial Cable		Twisted pair filled	
K	n	K	n
159	0.19	246	0.05

Referring to Table 3, it can be noticed that DED values are similar between the two considered compounds for the low and medium dose rate aging. On the contrary, quite significant differences are appreciable for high dose rate aging. This could be imputed to the different aging kinetics occurring inside the two compounds at high dose rates. Indeed, as presented in § 2.4, one of the limitations of this approach lays on the fact that the polymer has to face a homogenous oxidation in order not to produce cracks and not to early degrade the mechanical properties. The presence of fillers could bring, among others, to two simultaneous effects: the reduction of oxygen diffusion rate and the lowering of the polymer chain mobility. In particular, the former can cause a phenomenon similar to DLO (Figure 10), as already discussed in § 5.4.3. This induces an abrupt reduction of the elongation-at-break, leading to a lower value of DED for compound #2 at high dose rates. As a result, the regression line plotted among the derived doses to equivalent damage is almost flat (slope n-parameter close to 0). On the contrary, compound #1 appears not to be affected by DLO, displaying a higher value of DED provoked by a faster variation of the total absorbed dose, as expected by the theoretical approach. Thus, it could be concluded that the applied modelling approach is more consistent when the presence of additives is reduced.

Focusing on the magnitude of the DED values (K-parameter), compound #2 shows a bigger value of DED at lower dose rates but it poorly varies over the different aging conditions, as reported above. In reverse, for compound #1 materials, the DED values at low dose rates is lower but it significantly increases over the dose rates, reaching higher values than the ones referred to compound #2.

6.3.2 Electrical properties

Figure 107 reports the trend of dissipation factor at 100 kHz for all the analyzed aging conditions and different cable geometries. A linear regression line is built for each considered condition to obtain a tentative value of the electrical property at higher doses. In order to obtain a homogenous trend, tanδ values relatable to DLO effects are removed from the dataset.

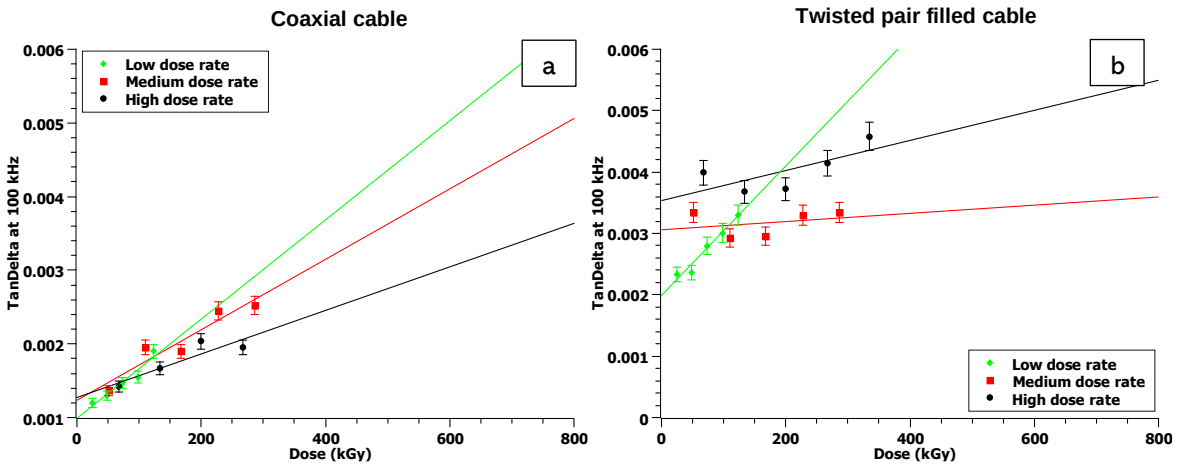

Figure 107 Dissipation factor at 100 kHz as a function of the total dose for the three analyzed cable morphologies. (a) coaxial cable, (b) twisted pair filled cable.

Once DED values are obtained through the above method, it is possible to graphically acquire the end-of-life points in terms of Tanδ, finally providing the values of dielectric losses corresponding to the failure of the material.

As an example, the extrapolation of the dielectric losses values corresponding to the dose equivalent to damage for the case of the coaxial cable aged under low dose rate is reported in Figure 108.

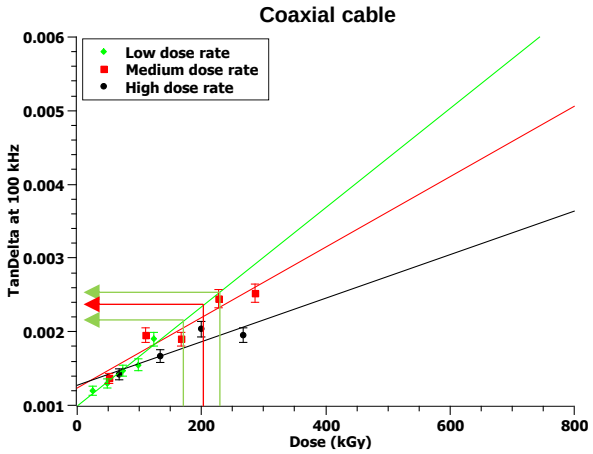

Figure 108 Graphical extrapolation of dissipation factor limit values. Coaxial cable under low dose rate aging.

Even in this case, the values of tanδ corresponding to the upper and the lower limit of the DED ($tan\delta_{DED}$) are obtained and registered in order to take into account the measurements uncertainties. Therefore, the Tanδ values corresponding to the DED are reported in Table 5.

Table 5 Dissipation factor values corresponding to the dose equivalent to damage.

	Coaxial Cable			**Twisted pair filled**		
	tanδ at DED	Upper limit	Lower limit	**tanδ at DED**	Upper limit	Lower limit
Low	0.0023	0.0024	0.0022	0.0044	0.006	0.0039
Medium	0.0032	0.0039	0.0026	0.0033	0.0035	0.0032
High	0.0026	0.003	0.0023	0.0043	0.0044	0.004

The $\tan\delta_{DED}$ values are finally plotted in a tanδ vs DR plot, reported in Figure 109. Note that the values are plotted in a log/log (absolute value) scale since applying the logarithm to the tanδ values result in a negative amount.

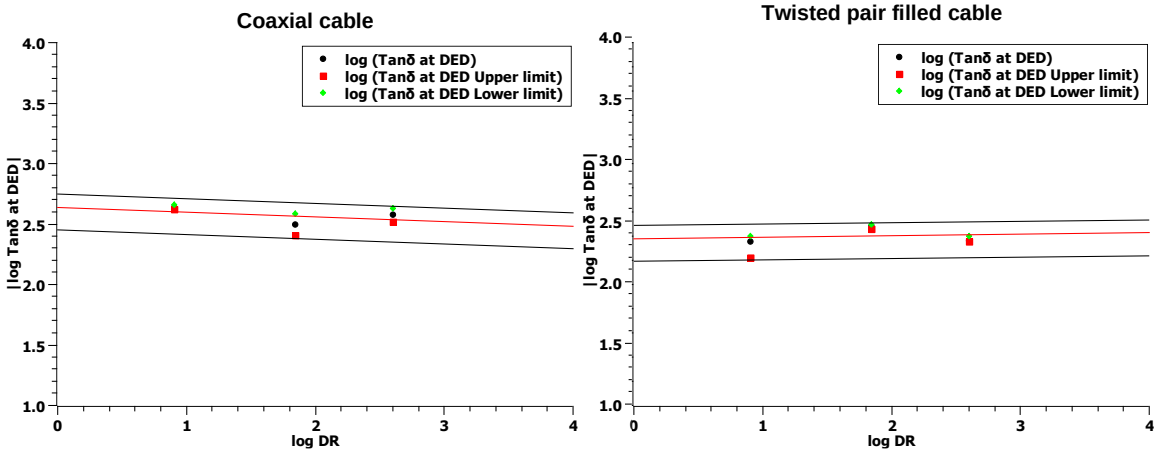

Figure 109 Dielectric losses at DED as a function of Dose Rates (log/log scale).
(a) Coaxial cable, (b) Twisted pair filled cable.

The regression line built represents the values of tanδ the cable owns at DED corresponding to the failure of the cable. Therefore, it is possible to obtain for the cables here considered, the equation representative the tanδ End-of-Life curve is represented by equation (28).

The values of *C* and *s*, for the various configurations analyzed, are reported in Table 6.

Table 6 Power law fitting parameters of electrical property tanδ

Coaxial Cable		Twisted pair filled	
C	s	C	s
423	-0.03	238	0.01

It can be concluded that the above equation describes the end-of-life points in terms of dielectric properties of the analyzed system. Due to this, it is reasonable to claim that if the actual value of tanδ is lower than the one corresponding to DED, precisely if the cable owns an EaB higher than 50%$_{rel,}$ then $\tan\delta \leq \tan\delta_{DED}$ is verified. Consequently, it does not need replacement according to the chosen cable health assessment criterion.

From Figure 109, it is possible to point out that the variation with dose rate of the limit tanδ value is quite small for both the considered compounds. As a result, the slope parameter (s) is close to zero. This interesting behavior suggests that the limit value of the electrical property ($\tan\delta_{DED}$) is not dependent on the aging stress (dose rate) but it is mainly related to the insulation properties e.g. the type of polymeric compound. It is possible to believe that this occurs as far as no diffusion limited oxidation (DLO) effect is present.

On the contrary, C-parameter is significantly different between the two materials. Compound #1 shows a considerable higher value of C. Given the calculation through the absolute value, it reflects a lower limit value ($tan\delta_{DED}$). This is expected due to the weaker polarity of the species, both on unaged and aged polymer, which are inside compound #1.
Compound #2 exhibits higher tanδ values also in the unaged sample since the dielectric spectrum is led by the dipolar properties of ATH molecules throughout the considered aging periods, as discussed in the previous Chapter. This behavior overwhelms the increase of dipolar properties given by oxidized polymer species. As a matter of fact, tanδ values at 100 kHz does not increase with the same slope of compound #1 at medium and high dose rates, resulting into a $tan\delta_{DED}$ value which is close to the early-aged tanδ values. In addition, low dose rate tanδ exhibits a different increasing slope with aging, as reported and discussed in the previous Chapter.

To conclude, given the almost constant trend of $tan\delta_{DED}$, it could be reasonable to consider the electrical property limit values for the two considered compounds as the average of the obtained values (Table 5). Results are reported in Table 7.

Table 7 Limit values of electrical property tanδ

Coaxial Cable $tan\delta_{DED}$	Twisted pair filled $tan\delta_{DED}$
0.0027	0.0042

6.4 AGING MODELLING

6.4.1 Theoretical approach

In the previous section, the limit values of both electrical and mechanical properties have been presented and discussed for the cables under test.
The aim of this section is to illustrate a procedure for lifetime modelling based on electrical diagnostic measurements. To do so, some quantities have to be further defined:

1. **Failure.** Cable failure is achieved once the cable can no longer fulfill its role. If the cable is subjected to aging stresses, the failure is reached once the cable cannot verify the design requirements. This occurs when the cable system reaches the limit value for the considered property (end-of-life criterion).
2. **Lifetime.** It is defined as the time during which the cable can fulfill its role, thus the service time of the cable before reaching failure.
3. **Lifetime curve.** It is a plot representing the life duration as a function of aging stresses, e.g., dose rates in the case of NPPs.

These quantities can be introduced in the following phenomenological aging equation. Referring to [131], the **general aging equation** is defined as:

$$\mathbf{A(t)} = \mathbf{f(p)} = \int_{\mathbf{0}}^{t} \boldsymbol{R(S)dt} \tag{29}$$

where *A* is defined as *aging function*, *S* is a generic *stress*, *t* is the *time* and $p=P/P_0$ is a *property correlated to the cable failure* and $\mathrm{R} = {}^{\mathrm{dA}}/_{\mathrm{dt}}$ is the *aging speed*, which only depends on aging stress.

Once *p* reaches the corresponding limit value p_L, cable failure occurs. Under these circumstances, *aging time t,* becomes *lifetime duration L.*

Consequently, from equation (29) it is possible to derive the equation corresponding to the limit value (A_L). This equation is defined as **general life model:**

$$\mathbf{A_L} = \mathbf{f(p_L)} = \int_{\mathbf{0}}^{\mathbf{L}} \mathbf{R(S)dt} \tag{30}$$

Equation (30) represents a curve in a bi-dimensional space: the single-stress life curve. This could be obtained by the intersection of aging function surface with the plane $p=p_L$.

If the stress is constant, like the case here considered, equations become:

$$\mathbf{A(t)} = \mathbf{f(p)} = \mathbf{R(S)\ t} \tag{31}$$

$$\mathbf{A_L} = \mathbf{f}(\boldsymbol{p_L}) = \mathbf{R(S)\ L} \tag{32}$$

It is noteworthy that $\mathbf{A} = \mathbf{f(p)}$ linearly depends on time. In particular, even if the chosen property can non-linearly change with time, there would be a function of the same property which linearly varies with time. This is usually verified since the property affected by aging stress should monotonously vary with time.

If we divide equation (31) by (32), it is possible to make the dependence between *A* and time explicit. Specifically:

$$\mathbf{A(t)} = \mathbf{A_L}\left({}^{\mathbf{t}}/_{\mathbf{L}}\right) \tag{33}$$

This could be directly linked to Miner's *damage* [131], but, while the *damage* varies from 0 to 1, the *aging function A* varies from 0 to A_L.

6.4.2 Application to Coaxial cable

Once defined the theoretical basis of cable lifetime modelling, in this section the application of this approach to the coaxial cable electrical properties is reported. Modelling could not be applied to the twisted pair cable due to the negligible variation of the considered electrical property with aging for medium dose rate.

In order to apply the modelling method to the coaxial cable, some assumptions have to be made:

1. We do not take into account the abrupt drop of the electrical property between the neat and early aged cable. As a matter of fact, as seen in Chapter 4, the first aging period is mainly relatable to microstructural modifications of the cable, such as antioxidant migration, which do not cause significant aging.
2. We deny the contribution of possible DLO effects. To do so, we remove from the plot the non-increasing values e.g., last tanδ value of high dose rate.
3. From Figure 50 it is possible to notice that the function of the property, which is linearly dependent on aging, is the property itself. However, in order to verify all the requirements, we define *A(t)* as the variation of the property (tanδ) with respect to the value corresponding to the first aging period ($\tan\delta_1$), according to hypothesis #1. Consequently, the y-axis (*reduced time*) is given by the subtraction of the initial aging time (t_1) from the variable time (t). This in order to relate the initial tanδ value ($\tan\delta_1$) with *reduced time* equal to zero.

$$\mathbf{A(t) = \tan\delta - \tan\delta_1 = R(S) \cdot (t - t_1) \text{ with } t \geq t_1} \quad (34)$$

Through equation (34), it is possible to verify all the requirements demanded in the previous paragraph, e.g., *A(t)=0* for $t=t_1$, *A(t)* linearly varies with aging time.
The value of $\tan\delta_1$ has been chosen as constant among the different dose rates. This should be usually verified since the initial value of aging of the cable depends only on the insulating compound. However, in this case, this brings to a negligible upward shift of *A(t)* for medium dose rate, probably due to the late withdrawal with respect to the start of the aging phase.

As reported in § 6.4.2, the value of tanδ corresponding at the cable crisis is defined as $\tan\delta_{DED}$ (Table 7):

$$\mathbf{\tan\delta\ (L) = \tan\delta_{DED}} \quad (35)$$

Hence, A_L can be derived as:

$$\mathbf{A_L = \tan\delta_{DED} - \tan\delta_1 = R(S) \cdot (L - t_1)} \quad (36)$$

Figure 110 shows the plot of the above defined aging function versus the reduced aging time. Lines stop at $A(t)=A_L$. From this graph it is possible to point out that, as expected, the slope of the life curve is directly proportional to the aging severity and, consequently, the lifetime reduces as aging stresses increase.

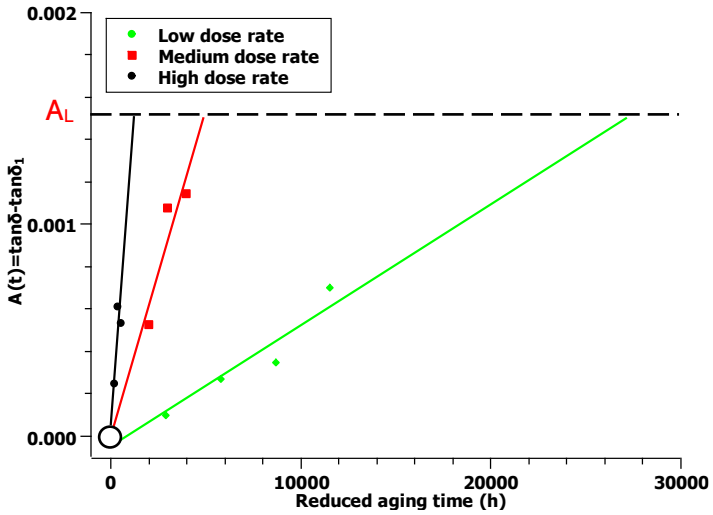

Figure 110 Aging function versus reduced aging time for the three radio-chemical aging conditions considered.

Moreover, it is also possible to evaluate the level of degradation of the considered cable for a given aging stress e.g., dose rate and its aging evolution until failure. Otherwise stated, it would be possible to define the aging the cable have been subjected to and, consequently, the one the cable can withstand before reaching the limit value A_L (failure).

Given (37) and the limit value of tanδ ($\tan\delta_{DED}$), the maximum lifetime (L) can be derived per each considered dose rate. Lifetime values are reported in Table 8.

Table 8 Lifetime values for the three dose rates. Coaxial cable.

	$L-t_1$ (h)	L (h)
Low	27,090	29,970
Medium	4,830	5,700
High	1,230	1,400

Finally, the life curve (Figure 111) relates the lifetime with dose rate at constant temperature. The curve depicts a decreasing trend whose slope is function of the system endurance. As expected, a severer aging stress causes a shorter lifetime. Ideally, if the stress is zero, the insulation is not subjected to radiation aging, hence its lifetime is nearly infinite. Actually, the system is also subjected to other stresses given by the environment e.g., environmental temperature cycles which further reduce the cable expected lifetime.

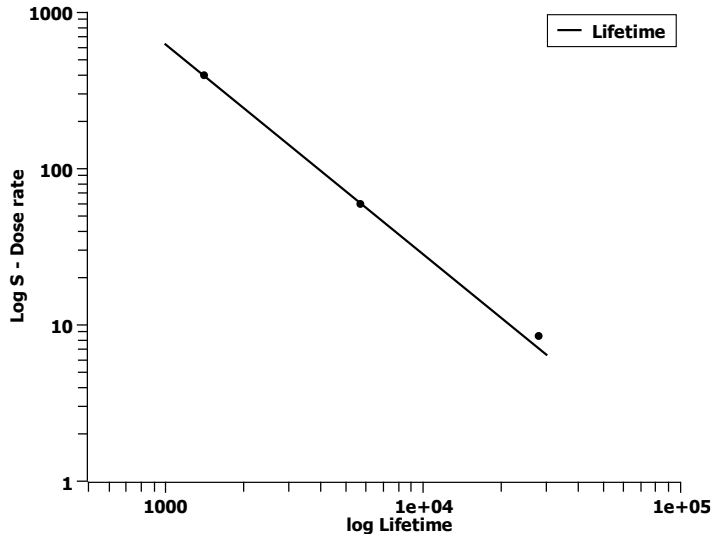

Figure 111 Life curve of coaxial cable for three different dose rates. Lines stop at obtained limit value (L).

As shown in Figure 111, the life curve follows an inverse power law (IPL). Making lifetime (*L*) explicit, the equation can be written as (37). Table 9 reports the values of IPL factors.

$$\mathbf{L} = \mathbf{L_0} \cdot \left(\frac{\mathbf{DR}}{\mathbf{DR_0}}\right)^{-\mathbf{n}} \tag{37}$$

Table 9 Power law coefficients

L_o	n
127,460	0.75

where L_O and n are exponential factors, DR_O is the reference dose rate fixed to a very low value, in this case equal to 1 Gy/h. Factors L_O and n are only function of the considered cable properties e.g. chemical compound, geometry, and additives. Specifically, L_O is the intersection between the life curve and the lifetime-axis. In other words, it is the lifetime corresponding to a very low dose rate stress e.g., equal to the reference one ($DR=DR_O$),

Equation (37) relates the maximum lifetime of the considered cable as a function of the stress the cable is subjected to, namely the dose rate. Furthermore, it is now possible to perform a parametric study varying the stress level, i.e., dose rate. Resulting graph is reported in Figure 112.

As an example, the built parametric curves could be significantly helpful during cable condition monitoring. Indeed, the calculation of *A(t)*, achieved through tanδ measurements, together with the current service time of the cable, would allow the evaluation of the actual dose rate the cable is subjected to and the residual life. As a matter of fact, the presence of dose bursts during cable lifetime, together with a possible different dosimetry of the cable through its length, could result into a different effective dose rate than the designed one. Hence, online

monitoring would allow the selection of the real dose rate curve and the assessment of the expected lifetime of the cable under test, scheduling maintenance in an efficient way.

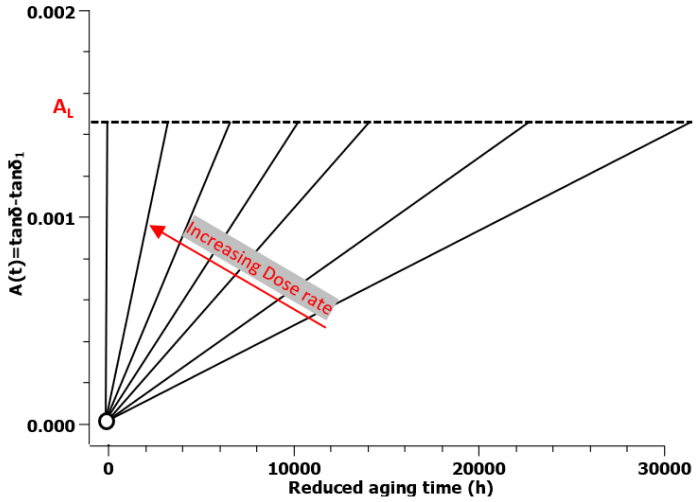

Figure 112 Example of application of life curve. Coaxial cable.

6.5 Modelling conclusions

The electrical modelling approach presented in this Chapter could be considered as a rough procedure of setting an end-of-life criterion based on non-destructive techniques, which can be a substantial improvement of the actual cable management inside NPPs. It allows the evaluation of the dissipation factor corresponding to the crisis of low voltage cables for NPPs applications, for a given dose rate. Furthermore, it permits the estimation of the life of the cable only through non-destructive testing techniques, upgrading the actual standard for cable monitoring, which uses destructive testing techniques, e.g., tensile test, that are often not easy to perform on site and are not always representative of the entire cable system.

In addition, electrical tanδ measurement, as a bulk technique, takes into account the entire cable system giving information about the global health and the electrical applicability of the analyzed polymer insulation.

Mechanical modelling results showed that the trend of DED exhibit an almost negligible variation of the parameter over different dose rates for compound #2, while it considerably varies in the case of compound #1.

On the contrary, $tan\delta_{DED}$ trend resulted to be not affected by dose rate intensities for both the cable geometries. In such circumstances, it could be concluded that the limit value of the electrical property is only dependent on the polymeric compound.

The second part of this Chapter presents the theoretical basis and the application to the coaxial cable of life modelling. Specifically, quantities used for evaluation of the service life and related equations have been reported and discussed.

The life modelling approach has been built starting from the limit value of the electrical properties obtained in the previous section. The introduction of the *aging function* has raised the opportunity to monitor the aging development of the cable when it is subjected to constant stress e.g., dose rate. This function relates the aging time with the cable status through electrical properties. Once the *aging function* reaches its limit value, i.e., A_L, the cable faces failure. The time corresponding to failure is defined as the maximum service time or lifetime of the cable.
It has been observed that the life durations and the *aging function* slopes are function of the aging severity. Specifically, higher dose rates bring to reduced lifetime, as expected.

Ideally, the possibility to build a life curve, which relates the aging stress with expected lifetime, for each cable system could provide a rough estimation of the residual life of cable insulation systems under investigation. It is worth pointing out that the life curve and related life equation for the coaxial cable have been achieved only by the means of electrical nondestructive techniques as only initial value of the property ($\tan\delta_1$) and aging conditions are required for analyses. Moreover, the possibility to perform these tests onsite allows a better evaluation of the remaining life since it would be possible to adjust the life curve in the case of variations of external aging conditions e.g., dose rate bursts due to accidents.
Further development of this approach will include the introduction of aleatory stresses given by e.g., accidental conditions through a Bayesian-based model.

CHAPTER 7
CONCLUSIONS

In this Thesis, a wide investigation of property changes of XLPE-based insulated cables due to aging has been performed. It aimed at analyzing and investigating how typical aging stressors inside NPPs, i.e., radiation and high temperature, can impact the physico-chemical and electrical properties of I&C low-voltage cables. To do so, accelerated aging tests have been performed on several cables through both radiation and high temperature in order to successfully simulate typical NPP environments.

The analyzed cables display two different geometries, commonly used in NPPs, namely: coaxial and twisted pair cables. Moreover, the effect of additives inside polymeric compounds has been taken into account considering two different chemical mixtures, i.e., antioxidant-stabilized XLPE without fillers, and antioxidant-stabilized XLPE filled with flame-retardants.
It has been shown that environmental stresses can deeply influence the analyzed material properties, leading to degradation of the primary insulation which can result into an early failure of the cable system.
The aging conditions considered in this Thesis showed to be not sufficient to cause significant degradation inside the polymer. In particular, in many cases, the lifetime end point is not reached according to the actual state-of-art monitoring technique for LV cables, showing an EaB/EaB0 ratio higher than 50%.

In order to evaluate the capability of dielectric spectroscopy to assess aging, dielectric losses have been correlated with different physico-chemical techniques, starting from the mechanical properties (above all EaB). This aimed at investigating the possibility to upgrade the current state-of-the-art for LV cable monitoring by means of NDTs. Since only one cable reached the chosen end-of-life criterion, variations in terms of mechanical properties have been mainly related to microstructural modification inside the polymer, e.g., antioxidant consumption.

The polymer property changes with aging resulted to be directly dependent on the additives and fillers. Specifically, radio-thermal aging caused an important chemical consumption of antioxidants (showed by OIT measurements) to which it corresponds the decrease of the dissipation factor (tanδ) during the early aging periods.
The initial variations in polymer degradation are mainly related to the antioxidant depletion kinetics, which delay the oxidative reaction kinetics. Antioxidant molecules are gradually consumed under the effect of environmental stresses and new molecules, namely antioxidant

degradation products, arise. These latter are characterized by the same ester bond as the base antioxidant. Hence, the two phenomena (antioxidant chemical consumption and antioxidant degradation products formation) can be difficulty singled out through FTIR measurements as they could keep constant the global concentration of ester bonds, leading to no change in the ester index.

On the contrary, the arising of antioxidant degradation products could be highlighted through dielectric spectroscopy as they are characterized by strong dipolar properties. For this reason, they may be directly linked to the increase of the high frequency dielectric losses and, consequently, to the aging of the polymer. The introduction and the analysis of the antioxidant depletion factor (ADF) allowed relating the conversion yield in antioxidants into degradation products with the dissipation factor (tanδ) at 100 kHz.
As far as antioxidants are present, the two properties are closely correlated each other, claiming the ability of dielectric spectroscopy to follow the antioxidant conversion into degradation products.

After the running out of antioxidants, oxygen is free to bond with the polymer chain. This results into an increase in the IR absorbance of the ester bonds together with the raise of the dipolar properties of the material. It has been reported that both FTIR and dielectric spectroscopies can adequately follow the aging state of the polymer, relating the ester index increase with tanδ.
Under these circumstances, it has been concluded that the dissipation factor (tanδ) at high frequency could be used as an aging marker since it has been demonstrated to properly follow the degradation mechanisms occurring during all the aging phases of the insulating material i.e., antioxidant consumption and polymer oxidation.

The last part of the Thesis focused on the building of a predictive model of mechanical and electrical properties and a life model for NPP LV cables.
The proposed predictive modelling approach puts its basis on an approach firstly issued by IAEA (international Atomic Energy Agency). This model relates the decay of the mechanical properties with the limit dose a cable can withstand without inducing failure. The available model underlines some limitations e.g., it is based on destructive mechanical measurements, tests are often not easy to perform on site and they are not always representative of the entire cable system. The proposed predictive modelling method is based on electrical NDT, which can be a substantial upgrade of the actual cable managements inside NPPs. This allows the evaluation of the dissipation factor corresponding at the failure of low voltage cables for NPPs applications, for a given dose rate and it permits the estimation of the lifetime of the cable only through non-destructive testing. Moreover, tanδ measurements take into account the entire cable system giving information about the health and the electrical applicability of the

analyzed polymer insulation. To conclude, ideally, the possibility to build a life curve for each cable system could allow the diagnostic of cable systems in an easy and nondestructive way.
In addition, a life modelling approach has been presented and discussed. This allowed the evaluation of the *aging function* which relates the aging stresses with the cable expected lifetime, allowing an efficient scheduling of the cable maintenance through electrical measurements.

Further development could consider the analysis of polymeric plate specimens, which would result into more significant variations of the material properties. In doing so, it would be possible to reach the chosen the end-of-life criterion and evaluate the enhanced oxidative degradation occurring in the polymer matrix. Together with that, it could be possible to combine an advanced chemical kinetics analysis of oxidative reactions.
Likewise, local oxidation extend could be evaluated by the means of micro-indentation measurements which would allow the evaluation of the local brittleness of the material surface due to oxidation.
Finally, the modelling approach could be further developed introducing random aging stresses, simulating what could occur inside typical NPP environments e.g., during accidents. This could be taken into account implementing a Bayesian approach which could give birth to a stress-strain model for reliability estimation of aged LV cables used in NPP.

REFERENCES

[1] F. Yu, "A Review of Nondestructive Evaluation Technologies for Cable System Integrity," *Electr. Power Res. Inst. EPRI*, p. 82, 2013.

[2] L. Verardi, "Aging of nuclear power plant cables: in search of non-destructive diagnostic quantities," *PhD Thesis*, p. 128, 2014.

[3] "IEEE Guide on Shielding Practice for Low Voltage Cables," *IEEE Std 1143-2012 Revis. IEEE Std 1143-1994*, pp. 1–91, Mar. 2013, doi: 10.1109/IEEESTD.2013.6471984.

[4] C. Zhou, H. Yi, and X. Dong, "Review of recent research towards power cable life cycle management," *High Volt.*, vol. 2, no. 3, pp. 179–187, 2017, doi: 10.1049/hve.2017.0037.

[5] W. F. Powers, "The basics of power cable," *IEEE Trans. Ind. Appl.*, vol. 30, no. 3, pp. 506–509, May 1994, doi: 10.1109/28.293692.

[6] Subudhi, "Literature review of environmental qualification of Safety-related electric cables," *US Nucl. Regul. Comm.*, 1996, Accessed: Mar. 24, 2020. [Online]. Available: https://www.nrc.gov/docs/ML0314/ML031480454.pdf.

[7] M. Walter, "Overview of Flame Retardants Including Magnesium Hydroxide," p. 9.

[8] E. D. Weil and S. V. Levchik, "Flame Retardants in Commercial Use or Development for Polyolefins," *J. Fire Sci.*, vol. 26, no. 1, pp. 5–43, Jan. 2008, doi: 10.1177/0734904107083309.

[9] D. Tabuani, F. Bellucci, A. Terenzi, and G. Camino, "Flame retarded Thermoplastic Polyurethane (TPU) for cable jacketing application," *Polym. Degrad. Stab.*, vol. 97, no. 12, pp. 2594–2601, Dec. 2012, doi: 10.1016/j.polymdegradstab.2012.07.011.

[10] G. Beyer, "Organoclays as flame retardants for PVC," *Polym. Adv. Technol.*, vol. 19, no. 6, pp. 485–488, 2008, doi: 10.1002/pat.1087.

[11] A. A. Sener and E. Demirhan, "The investigation of using magnesium hydroxide as a flame retardant in the cable insulation material by cross-linked polyethylene," *Mater. Des.*, vol. 29, no. 7, pp. 1376–1379, Jan. 2008, doi: 10.1016/j.matdes.2007.05.008.

[12] H. Azizi, J. Barzin, and J. Morshedian, "Silane crosslinking of polyethylene: the effects of EVA, ATH and Sb2O3 on properties of the production in continuous grafting of LDPE," *Express Polym. Lett.*, vol. 1, no. 6, pp. 378–384, 2007, doi: 10.3144/expresspolymlett.2007.53.

[13] D. Liu *et al.*, "Interactions between a phenolic antioxidant, moisture, peroxide and crosslinking by-products with metal oxide nanoparticles in branched polyethylene," *Polym. Degrad. Stab.*, vol. 125, pp. 21–32, Mar. 2016, doi: 10.1016/j.polymdegradstab.2015.12.014.

[14] N. Fuse, H. Homma, and T. Okamoto, "A new degradation model with critical antioxidant concentration concept for safety cables," in *2012 IEEE International Conference on Condition Monitoring and Diagnosis*, Sep. 2012, pp. 153–156, doi: 10.1109/CMD.2012.6416398.

[15] U. H. Nilsson, R. C. Dammert, A. Campus, A. Sneck, and H. Jakosuo-Jansson, "Morphology of polyethylene for power cable insulation: effects of antioxidant and crosslinking," in *ICSD'98. Proceedings of the 1998 IEEE 6th International Conference on Conduction and Breakdown in Solid Dielectrics (Cat. No.98CH36132)*, Jun. 1998, pp. 365–367, doi: 10.1109/ICSD.1998.709301.

[16] J. W. Ray and A. B. Reynolds, "Effect of Antioxidants on Radiation Stability of Polymers Used for Electric Cable Insulation," *Nucl. Technol.*, vol. 91, no. 3, pp. 394–403, Sep. 1990, doi: 10.13182/NT90-A34460.

[17] G. Botelho, A. Queirós, and P. Gijsman, "Thermooxidative studies of poly(ether-esters) 1. Copolymer of poly(butylene terephthalate) and poly(ethylene oxide)," *Polym. Degrad. Stab.*, vol. 67, no. 1, pp. 13–20, Jan. 2000, doi: 10.1016/S0141-3910(99)00109-3.

[18] C. Armstrong, M. A. Plant, and G. Scott, “Mechanisms of antioxidant action: the nature of the redox behaviour of thiodipropionate esters in polypropylene,” *Eur. Polym. J.*, vol. 11, no. 2, pp. 161–167, Feb. 1975, doi: 10.1016/0014-3057(75)90141-X.
[19] M. Kanegami *et al.*, “Relationship between remaining antioxidant content and radiation-thermal degradation in crosslinked polyethylene,” in *Proceedings of 2011 International Symposium on Electrical Insulating Materials*, Kyoto, Sep. 2011, pp. 448–450, doi: 10.1109/ISEIM.2011.6826309.
[20] P. Gijsman, “Polymer Stabilization,” in *Handbook of Environmental Degradation of Materials*, Elsevier, 2018, pp. 369–395.
[21] R. A. Assink, K. T. Gillen, and R. Bernstein, “Nuclear Energy Plant Optimization (NEPO) final report on aging and condition monitoring of low-voltage cable materials.,” SAND2005-7331, 875986, Nov. 2005. doi: 10.2172/875986.
[22] S. W. Glass, L. S. Fifield, G. Dib, J. R. Tedeschi, A. M. Jones, and T. S. Hartman, “State of the Art Assessment of NDE Techniques for Aging Cable Management in Nuclear Power Plants FY2015,” PNNL--24649, M2LW--15OR0404024, 1242348, Sep. 2015. doi: 10.2172/1242348.
[23] Bruno Fayolle, E. Richaud, X. Colin, and J. Verdu, “Review: degradation-induced embrittlement in semi-crystalline polymers having their amorphous phase in rubbery state,” *J. Mater. Sci.*, vol. 43, no. 22, pp. 6999–7012, Nov. 2008, doi: 10.1007/s10853-008-3005-3.
[24] G. Botelho, A. Queirós, and P. Gijsman, “Thermo-oxidative studies of poly(ether-esters) 2. Copolymer of poly(butylene terephthalate) and polybutylene oxide,” *Polym. Degrad. Stab.*, vol. 68, no. 1, pp. 35–42, Apr. 2000, doi: 10.1016/S0141-3910(99)00164-0.
[25] G. Spadaro, “Effect of irradiation temperature and dose rate on the mechanical tensile behaviour of low density polyethylene,” *Eur. Polym. J.*, vol. 29, no. 9, pp. 1247–1249, Sep. 1993, doi: 10.1016/0014-3057(93)90156-A.
[26] S. Ilie and R. Senetscu, “Polymeric Materials Review on Oxidation, Stabilization and Evaluation using CL and DSC Methods,” p. 62.
[27] R. L. Clough, K. T. Gillen, G. M. Malone, and J. S. Wallace, “Color formation in irradiated polymers,” *Radiat. Phys. Chem.*, vol. 48, no. 5, pp. 583–594, Nov. 1996, doi: 10.1016/0969-806X(96)00075-8.
[28] E. M. Kornacka, “RADIATION-INDUCED OXIDATION OF POLYMERS,” p. 10.
[29] E. Suljovrujic, “Post-irradiation effects in polyethylenes irradiated under various atmospheres,” *Radiat. Phys. Chem.*, vol. 89, pp. 43–50, Aug. 2013, doi: 10.1016/j.radphyschem.2013.04.003.
[30] S. V. Suraci, D. Fabiani, and C. Li, “Post-irradiation effect analysis on XLPE-insulated LV cables used in nuclear power plants,” in *2019 2nd International Conference on Electrical Materials and Power Equipment (ICEMPE)*, Apr. 2019, pp. 53–56, doi: 10.1109/ICEMPE.2019.8727281.
[31] S. V. Suraci and D. Fabiani, “Post-irradiation effect investigation on low-voltage XLPE cables through dielectric spectroscopy,” presented at the Jicable, Versailles, 2019.
[32] L. M. Rincon-Rubio, X. Colin, L. Audouin, and J. Verdu, “A Theoretical Model for the Diffusion-Limited Thermal Oxidation of Elastomers at Medium Temperatures,” *Rubber Chem. Technol.*, vol. 76, no. 2, pp. 460–482, May 2003, doi: 10.5254/1.3547754.
[33] J. Wise, K. T. Gillen, and R. L. Clough, “Time development of diffusion-limited oxidation profiles in a radiation environment,” *Radiat. Phys. Chem.*, vol. 49, no. 5, pp. 565–573, May 1997, doi: 10.1016/S0969-806X(96)00185-5.
[34] K. T. Gillen and R. L. Clough, “Rigorous experimental confirmation of a theoretical model for diffusion-limited oxidation,” *Polymer*, vol. 33, no. 20, pp. 4358–4365, Jan. 1992, doi: 10.1016/0032-3861(92)90280-A.
[35] M. C. Celina, “Review of polymer oxidation and its relationship with materials performance and lifetime prediction,” *Polym. Degrad. Stab.*, vol. 98, no. 12, pp. 2419–2429, Dec. 2013, doi: 10.1016/j.polymdegradstab.2013.06.024.
[36] J. Wise, K. T. Gillen, and R. L. Clough, “Quantitative model for the time development of diffusion-limited oxidation profiles,” *Polymer*, vol. 38, no. 8, pp. 1929–1944, Apr. 1997, doi: 10.1016/S0032-3861(96)00716-1.

[37] M. Celina, J. Wise, D. K. Ottesen, K. T. Gillen, and R. L. Clough, "Oxidation profiles of thermally aged nitrile rubber," *Polym. Degrad. Stab.*, vol. 60, no. 2, pp. 493–504, Jan. 1998, doi: 10.1016/S0141-3910(97)00113-4.
[38] "IEEE Standard for Qualifying Electric Cables and Splices for Nuclear Facilities," *IEEE Std 383-2015 Revis. IEEE Std 383-2003*, pp. 1–27, Oct. 2015, doi: 10.1109/IEEESTD.2015.7287711.
[39] M. Villaran and R. Lofaro, "Essential Elements of an Electric Cable Condition Monitoring Program," vol. U.S.NRC-United States Nuclear Regulatory Commission, 2010.
[40] S. V. Suraci, D. Fabiani, J. Cohen, and P.-S. Campus, "In situ defect recognition analysis on long cables through nondestructive reflectometry and dielectric spectroscopy methods: a comparison," p. 4.
[41] S. W. Glass, A. M. Jones, L. S. Fifield, and T. S. Hartman, "Frequency domain reflectometry NDE for aging cables in nuclear power plants," Atlanta, Georgia, USA, 2017, p. 080015, doi: 10.1063/1.4974640.
[42] Z. Kone, "Cable Qualification for Nuclear Power Plants," p. 4, 2017.
[43] V. Plaček, "Cable qualification," presented at the Proceedings of the workshop "Standardization Academic Exchanges for Equipment Qualification in NPP," Beijing, 2015.
[44] E. Yousif and R. Haddad, "Photodegradation and photostabilization of polymers, especially polystyrene: review," *SpringerPlus*, vol. 2, no. 1, p. 398, Dec. 2013, doi: 10.1186/2193-1801-2-398.
[45] G. Thoman, "Initial Acceptance Criteria Concepts and Data for Assessing Longevity of Low-Voltage Cable Insulations and Jackets," p. 126.
[46] J. F. Calmet, F. Carlin, T. M. Nguyen, S. Bousquet, and P. Quinot, "Irradiation ageing of CSPE/EPR control command electric cables. Correlation between mechanical properties and oxidation," *Radiat. Phys. Chem.*, vol. 63, no. 3, pp. 235–239, Mar. 2002, doi: 10.1016/S0969-806X(01)00585-0.
[47] J.-I. Weon, "Effects of thermal ageing on mechanical and thermal behaviors of linear low density polyethylene pipe," *Polym. Degrad. Stab.*, vol. 95, no. 1, pp. 14–20, Jan. 2010, doi: 10.1016/j.polymdegradstab.2009.10.016.
[48] S. V. Suraci, D. Fabiani, L. Mazzocchetti, and L. Giorgini, "Degradation Assessment of Polyethylene-Based Material Through Electrical and Chemical-Physical Analyses," *Energies*, vol. 13, no. 3, p. 650, Jan. 2020, doi: 10.3390/en13030650.
[49] G. Singh, H. Bhunia, P. K. Bajpai, and V. Choudhary, "Thermal degradation and physical aging of linear low density polyethylene and poly(L-lactic acid) blends," p. 8.
[50] N. Bowler and S. Liu, "Aging Mechanisms and Monitoring of Cable Polymers," *Int J Progn. Health Manag.*, vol. 6, 2015.
[51] A. Sriraman, N. Bowler, S. W. Glass, and L. S. Fifield, "Dielectric and Mechanical Behavior of Thermally Aged EPR/CPE Cable Materials," in *2018 IEEE Conference on Electrical Insulation and Dielectric Phenomena (CEIDP)*, Oct. 2018, pp. 598–601, doi: 10.1109/CEIDP.2018.8544855.
[52] V. Plaček, "The influence of mechanical stress on cable service life-time," *Polym. Test.*, p. 7, 2011.
[53] B. Bartoníček, V. Plaček, and V. Hnát, "Comparison of degradation effects induced by gamma radiation and electron beam radiation in two cable jacketing materials," *Radiat. Phys. Chem.*, vol. 76, no. 5, pp. 857–863, May 2007, doi: 10.1016/j.radphyschem.2006.05.011.
[54] V. Plaček and T. Kohout, "Comparison of cable ageing," *Radiat. Phys. Chem.*, vol. 79, no. 3, pp. 371–374, Mar. 2010, doi: 10.1016/j.radphyschem.2009.08.031.
[55] "IEC 60811 501:2012: 'Electric and optical fibre cables – Test methods for non metallic materials – Part 501: Mechanical tests – Tests for determining the mechanical properties of insulating and sheathing compounds.'" .
[56] E04 Committee, "Test Method for Microindentation Hardness of Materials," ASTM International. doi: 10.1520/E0384-17.
[57] G. F. V. Voort and B. Ltd, "Microindentation Hardness Testing," p. 12.

[58] G. Ryge, D. E. Foley, and C. W. Fairhurst, “Micro-indentation Hardness,” *J. Dent. Res.*, vol. 40, no. 6, pp. 1116–1126, Nov. 1961, doi: 10.1177/00220345610400060401.
[59] S. V. Suraci, D. Fabiani, A. Xu, S. Roland, and X. Colin, “Ageing Assessment of XLPE LV Cables for Nuclear Applications Through Physico-Chemical and Electrical Measurements,” *IEEE Access*, vol. 8, pp. 27086–27096, 2020, doi: 10.1109/ACCESS.2020.2970833.
[60] A. C. Tavares, J. V. Gulmine, C. M. Lepienski, and L. Akcelrud, “The effect of accelerated aging on the surface mechanical properties of polyethylene,” *Polym. Degrad. Stab.*, vol. 81, no. 2, pp. 367–373, Jan. 2003, doi: 10.1016/S0141-3910(03)00108-3.
[61] S. Ray and R. P. Cooney, “Thermal Degradation of Polymer and Polymer Composites,” in *Handbook of Environmental Degradation of Materials*, Elsevier, 2018, pp. 185–206.
[62] S. L. Simon, “Temperature-modulated differential scanning calorimetry: theory and application,” *Thermochim. Acta*, vol. 374, no. 1, pp. 55–71, Jun. 2001, doi: 10.1016/S0040-6031(01)00493-2.
[63] I. H. Craig, J. R. White, and P. C. Kin, “Crystallization and chemi-crystallization of recycled photo-degraded polypropylene,” *Polymer*, vol. 46, no. 2, pp. 505–512, Jan. 2005, doi: 10.1016/j.polymer.2004.11.019.
[64] M. S. Rabello and J. R. White, “Crystallization and melting behaviour of photodegraded polypropylene– 1. Chemi-crystallization,” p. 9.
[65] D20 Committee, “Test Method for Oxidative-Induction Time of Polyolefins by Differential Scanning Calorimetry,” ASTM International. doi: 10.1520/D3895-19.
[66] A. Xu, S. Roland, and X. Colin, “Physico-chemical characterization of the blooming of Irganox 1076® antioxidant onto the surface of a silane-crosslinked polyethylene,” *Polym. Degrad. Stab.*, vol. 171, p. 109046, Jan. 2020, doi: 10.1016/j.polymdegradstab.2019.109046.
[67] Shuaishuai Liu, L. S. Fifield, and N. Bowler, “Towards aging mechanisms of cross-linked polyethylene (XLPE) cable insulation materials in nuclear power plants,” in *2016 IEEE Conference on Electrical Insulation and Dielectric Phenomena (CEIDP)*, Oct. 2016, pp. 935–938, doi: 10.1109/CEIDP.2016.7785636.
[68] G. C. Montanari, A. Motori, A. T. Bulinski, S. S. Bamji, and J. Densley, “Application of oxidation induction time and compensation effect to the diagnosis of HV polymeric cable insulation,” *IEEE Trans. Dielectr. Electr. Insul.*, vol. 3, no. 3, pp. 351–360, Jun. 1996, doi: 10.1109/94.506206.
[69] D11 Committee, “Test Method for Rubber--Compositional Analysis by Thermogravimetry (TGA),” ASTM International. doi: 10.1520/D6370-99R19.
[70] E13 Committee, “Practices for General Techniques of Infrared Quantitative Analysis,” ASTM International. doi: 10.1520/E0168-16.
[71] J. Coates, “Interpretation of Infrared Spectra, A Practical Approach,” in *Encyclopedia of Analytical Chemistry*, R. A. Meyers, Ed. Chichester, UK: John Wiley & Sons, Ltd, 2006, p. a5606.
[72] P. Larkin, *Infrared and Raman Spectroscopy*. Elsevier, 2011.
[73] K. Nagamoto, “Theory of Normal Vibrations,” in *Infrared and Raman Spectra of Inorganic and Coordination Compounds*, John Wiley & Sons, Ltd, 2008, pp. 1–147.
[74] G. Socrates and G. Socrates, *Infrared and Raman characteristic group frequencies: tables and charts*, 3rd ed. Chichester ; New York: Wiley, 2001.
[75] K. Grabmayer *et al.*, “Accelerated aging of polyethylene materials at high oxygen pressure characterized by photoluminescence spectroscopy and established aging characterization methods,” *Polym. Degrad. Stab.*, vol. 109, pp. 40–49, Nov. 2014, doi: 10.1016/j.polymdegradstab.2014.06.021.
[76] M. Sugimoto, A. Shimada, H. Kudoh, K. Tamura, and T. Seguchi, “Product analysis for polyethylene degradation by radiation and thermal ageing,” *Radiat. Phys. Chem.*, vol. 82, pp. 69–73, Jan. 2013, doi: 10.1016/j.radphyschem.2012.08.009.
[77] J. V. Gulmine and L. Akcelrud, “FTIR characterization of aged XLPE,” *Polym. Test.*, vol. 25, no. 7, pp. 932–942, Oct. 2006, doi: 10.1016/j.polymertesting.2006.05.014.
[78] A. Schönhals, “Dielectric Spectroscopy on the Dynamics of Amorphous Polymeric Systems,” p. 17.

[79] J. Mijovic and B. D. Fitz, “Dielectric Spectroscopy of Reactive Polymers,” p. 25.
[80] A. K. Jonscher, “Dielectric relaxation in solids,” *J. Phys. Appl. Phys.*, vol. 32, no. 14, pp. R57–R70, Jan. 1999, doi: 10.1088/0022-3727/32/14/201.
[81] J. W. Schultz, “Dielectric Spectroscopy in Analysis of Polymers,” in *Encyclopedia of Analytical Chemistry*, 2006.
[82] J. D. Menczel and R. B. Prime, Eds., “Frontmatter,” in *Thermal Analysis of Polymers*, Hoboken, NJ, USA: John Wiley & Sons, Inc., 2009, pp. i–x.
[83] E. Linde, L. Verardi, P. Pourmand, D. Fabiani, and U. W. Gedde, “Non-destructive condition monitoring of aged ethylene-propylene copolymer cable insulation samples using dielectric spectroscopy and NMR spectroscopy,” *Polym. Test.*, vol. 46, pp. 72–78, Sep. 2015, doi: 10.1016/j.polymertesting.2015.07.002.
[84] G. C. Montanari, G. Mazzanti, F. Palmieri, A. Motori, G. Perego, and S. Serra, “Space-charge trapping and conduction in LDPE, HDPE and XLPE,” *J. Phys. Appl. Phys.*, vol. 34, no. 18, pp. 2902–2911, Sep. 2001, doi: 10.1088/0022-3727/34/18/325.
[85] T. K. Saha and P. Purkait, “Investigation of polarization and depolarization current measurements for the assessment of oil-paper insulation of aged transformers,” *IEEE Trans. Dielectr. Electr. Insul.*, vol. 11, no. 1, pp. 144–154, Feb. 2004, doi: 10.1109/TDEI.2004.1266329.
[86] N. A. M. Jamail, M. A. M. Piah, and N. A. Muhamad, “Comparative Study on Conductivity Using Polarization and Depolarization Current (PDC) Test,” *Electr. Electron. Eng.*, vol. 2, no. 4, pp. 170–176, Aug. 2012, doi: 10.5923/j.eee.20120204.01.
[87] M. A. Dakka, A. Bulinski, and S. Bamji, “Correlation between dc polarization and failure characteristics of XLPE and EPR aged with ac voltage in a wet environment,” *IEEE Trans. Dielectr. Electr. Insul.*, vol. 12, no. 4, pp. 700–708, Aug. 2005, doi: 10.1109/TDEI.2005.1511095.
[88] S. Mouaci, N. Saidi-Amroun, M. Saidi, V. Griseri, and G. Teyssèdre, “The combined effect of gamma and e-beam irradiation on the electrical properties of polyethylene Terephthalate,” in *2016 IEEE International Conference on Dielectrics (ICD)*, Jul. 2016, vol. 1, pp. 561–564, doi: 10.1109/ICD.2016.7547666.
[89] G. C. Montanari, C. Laurent, G. Teyssedre, A. Campus, and U. H. Nilsson, “From LDPE to XLPE: investigating the change of electrical properties. Part I. space charge, conduction and lifetime,” *IEEE Trans. Dielectr. Electr. Insul.*, vol. 12, no. 3, pp. 438–446, Jun. 2005, doi: 10.1109/TDEI.2005.1453448.
[90] D09 Committee, “Test Methods for DC Resistance or Conductance of Insulating Materials,” ASTM International. doi: 10.1520/D0257-14.
[91] J. Liu, D. Zhang, C. Bin, L. Huang, Y. Gao, and X. Li, “A New method of aging assessment for XLPE cable insulation based on dielectric response,” in *2015 IEEE 11th International Conference on the Properties and Applications of Dielectric Materials (ICPADM)*, Sydney, Australia, Jul. 2015, pp. 560–563, doi: 10.1109/ICPADM.2015.7295333.
[92] Y. Wang *et al.*, “Study of dielectric response characteristics for thermal aging of XLPE cable insulation,” in *2016 International Conference on Condition Monitoring and Diagnosis (CMD)*, Xi’an, China, Sep. 2016, pp. 602–605, doi: 10.1109/CMD.2016.7757932.
[93] S. Banerjee, D. Rouison, and A. Mantey, “LOW FREQUENCY DIELECTRIC SPECTROSCOPY AS A CONDITION MONITORING TECHNIQUE FOR LOW VOLTAGE CABLE IN NUCLEAR PLANTS,” presented at the Jicable 2019.
[94] G. Rizzo, P. Romano, A. Imburgia, and G. Ala, “Review of the PEA Method for Space Charge Measurements on HVDC Cables and Mini-Cables,” *Energies*, vol. 12, no. 18, p. 3512, Sep. 2019, doi: 10.3390/en12183512.
[95] G. Mazzanti, G. C. Montanari, F. Palmieri, and J. Alison, “Apparent trap-controlled mobility evaluation in insulating polymers through depolarization characteristics derived by space charge measurements,” *J. Appl. Phys.*, vol. 94, no. 9, pp. 5997–6004, Nov. 2003, doi: 10.1063/1.1616641.
[96] G. Mazzanti, G. C. Montanari, and J. M. Alison, “A space-charge based method for the estimation of apparent mobility and trap depth as markers for insulation degradation-

theoretical basis and experimental validation," *IEEE Trans. Dielectr. Electr. Insul.*, vol. 10, no. 2, pp. 187–197, Apr. 2003, doi: 10.1109/TDEI.2003.1194099.
[97] I. Tamayo-Ávila, J. M. Nieto, J. R. Viteri-Moya, and J. P. Jácome-Jácome, "Influencia del antioxidante sólido y líquido sobre la formación de carga de espacio en el aislamiento de XLPE de cables de media tensión," *DYNA*, vol. 83, no. 198, p. 142, Sep. 2016, doi: 10.15446/dyna.v83n198.50636.
[98] G. C. Montanari and D. Fabiani, "Evaluation of dc insulation performance based on space-charge measurements and accelerated life tests," *IEEE Trans. Dielectr. Electr. Insul.*, vol. 7, no. 3, pp. 322–328, Jun. 2000, doi: 10.1109/94.848908.
[99] N. Nibbio, T. Uozumi, N. Yasuda, and T. Fukui, "The effects of additives on space charge in XLPE insulation-crosslinking reagent and antioxidant," in *Proceedings of 1994 IEEE International Symposium on Electrical Insulation*, Jun. 1994, pp. 559–562, doi: 10.1109/ELINSL.1994.401394.
[100] M. Meunier, N. Quirke, and A. Aslanides, "Molecular modeling of electron traps in polymer insulators: Chemical defects and impurities," *J. Chem. Phys.*, vol. 115, no. 6, pp. 2876–2881, Aug. 2001, doi: 10.1063/1.1385160.
[101] S. Sallem and N. Ravot, "Self-adaptive correlation method for soft defect detection in cable by reflectometry," in *IEEE SENSORS 2014 Proceedings*, Valencia, Spain, Nov. 2014, pp. 2114–2117, doi: 10.1109/ICSENS.2014.6985455.
[102] W. B. Hassen, "Embedded OMTDR Sensor for Small Soft Fault Location on Aging Aircraft Wiring Systems," *Procedia Eng.*, p. 4, 2016.
[103] A. Lelong and M. O. Carrion, "On line wire diagnosis using Multicarrier Time Domain Reflectometry for fault location," in *2009 IEEE SENSORS*, Oct. 2009, pp. 751–754, doi: 10.1109/ICSENS.2009.5398542.
[104] International Atomic Energy Agency, *Assessment and management of ageing of major nuclear power plant components important to safety - Volume 1*, 2000th ed. .
[105] X. Colin, C. Monchy-Leroy, L. Audouin, and J. Verdu, "Lifetime prediction of polyethylene in nuclear plants," *Nucl. Instrum. Methods Phys. Res. Sect. B Beam Interact. Mater. At.*, vol. 265, no. 1, pp. 251–255, Dec. 2007, doi: 10.1016/j.nimb.2007.08.086.
[106] K. T. Gillen, R. Bernstein, R. L. Clough, and M. Celina, "Lifetime predictions for semi-crystalline cable insulation materials: I. Mechanical properties and oxygen consumption measurements on EPR materials," *Polym. Degrad. Stab.*, vol. 91, no. 9, pp. 2146–2156, Sep. 2006, doi: 10.1016/j.polymdegradstab.2006.01.009.
[107] M. Celina, K. T. Gillen, and R. A. Assink, "Accelerated aging and lifetime prediction: Review of non-Arrhenius behaviour due to two competing processes," *Polym. Degrad. Stab.*, vol. 90, no. 3, pp. 395–404, Dec. 2005, doi: 10.1016/j.polymdegradstab.2005.05.004.
[108] R. Clavreul, "Ageing of polymers in electrical equipment used in nuclear power plants," *Nucl. Instrum. Methods Phys. Res. Sect. B Beam Interact. Mater. At.*, vol. 151, no. 1–4, pp. 449–452, May 1999, doi: 10.1016/S0168-583X(99)00100-7.
[109] "Irganox® 1076 Phenolic primary antioxidant for processing and long-term thermal stabilization." BASF - The chemical company.
[110] "Irganox® PS 802 Thiosynergic heat stabilizer." BASF - The chemical company.
[111] "Inotal Aluminium Hydroxides datasheet." Inotal, Accessed: Apr. 28, 2020. [Online]. Available: https://inotal.hu/hydrate/wp-content/uploads/bsk-pdf-manager/Prec-h-specifikacio-20160401-EN_8.pdf.
[112] "ISO 527 1:2012: 'Plastics — Determination of tensile properties — Part 1: General principles.'" .
[113] "ISO 527 2:2012: 'Plastics — Determination of tensile properties — Part 2: Test conditions for moulding and extrusion plastics.'" .
[114] "IEC/IEEE 62582 3:2012: 'Nuclear power plants – Instrumentation and control important to safety – Electrical equipment condition monitoring methods – Part 3: Elongation at break.'" .
[115] E. Linde, L. Verardi, D. Fabiani, and U. W. Gedde, "Dielectric spectroscopy as a condition monitoring technique for cable insulation based on crosslinked polyethylene," *Polym. Test.*, vol. 44, pp. 135–142, Jul. 2015, doi: 10.1016/j.polymertesting.2015.04.004.

[116] C. Zou, J. Fothergill, and S. Rowe, "The effect of water absorption on the dielectric properties of epoxy nanocomposites," *IEEE Trans. Dielectr. Electr. Insul.*, vol. 15, no. 1, pp. 106–117, 2008, doi: 10.1109/T-DEI.2008.4446741.
[117] S. V. Suraci, D. Fabiani, and C. Li, "Additives effect on dielectric spectra of crosslinked polyethylene (XLPE) used in nuclear power plants," *2019 IEEE Electr. Insul. Conf. EIC*, vol. 2019 IEEE Electrical Insulation Conference (EIC), 2019.
[118] D. Fabiani, S. V. Suraci, and S. Bulzaga, "Aging Investigation of Low-Voltage Cable Insulation Used in Nuclear Power Plants," in *2018 IEEE Electrical Insulation Conference (EIC)*, Jun. 2018, pp. 516–519, doi: 10.1109/EIC.2018.8481139.
[119] K.T. Gillen, M. Celina, and R.L. Clough, "Density measurements as a condition monitoring approach for following the aging of nuclear power plant cable materials," *Radiat. Phys. Chem.*, vol. 56, no. 4, pp. 429–447, Oct. 1999, doi: 10.1016/S0969-806X(99)00333-3.
[120] I. L. Hosier, J. E. A. Koilraj, and A. S. Vaughan, "Effect of aging on the physical, chemical and dielectric properties of dodecylbenzene cable oil," in *2016 IEEE International Conference on Dielectrics (ICD)*, Jul. 2016, vol. 2, pp. 812–815, doi: 10.1109/ICD.2016.7547740.
[121] D. Fabiani, G. Montanari, and L. Testa, "Effect of aspect ratio and water contamination on the electric properties of nanostructured insulating materials," *IEEE Trans. Dielectr. Electr. Insul.*, vol. 17, no. 1, pp. 221–230, Feb. 2010, doi: 10.1109/TDEI.2010.5412021.
[122] S. Liu, S. W. Veysey, L. S. Fifield, and N. Bowler, "Quantitative analysis of changes in antioxidant in crosslinked polyethylene (XLPE) cable insulation material exposed to heat and gamma radiation," *Polym. Degrad. Stab.*, vol. 156, pp. 252–258, Oct. 2018, doi: 10.1016/j.polymdegradstab.2018.09.011.
[123] G. Przybytniak, J. Sadlo, M. Walo, N. Wrobel, and P. Zak, "Comparison of radical processes in non-aged and radiation-aged polyethylene unprotected or protected by antioxidants."
[124] S. V. Suraci, D. Fabiani, K. Sipilä, and H. Joki, "Filler impact analysis on aging of crosslinked polyethylene for nuclear applications through dielectric spectroscopy," in *2019 IEEE Conference on Electrical Insulation and Dielectric Phenomena (CEIDP)*, Oct. 2019, pp. 166–169, doi: 10.1109/CEIDP47102.2019.9009787.
[125] C. M. Hansen, "Polymer additives and solubility parameters," *Prog. Org. Coat.*, vol. 51, no. 2, pp. 109–112, Nov. 2004, doi: 10.1016/j.porgcoat.2004.05.003.
[126] A. Xu, S. Roland, and X. Colin, "Thermal ageing of a silane-crosslinked polyethylene stabilised with a thiodipropionate antioxidant," *Polym. Degrad. Stab.*, vol. 181, p. 109276, Nov. 2020, doi: 10.1016/j.polymdegradstab.2020.109276.
[127] C. Sinturel and N. C. Billingham, "A theoretical model for diffusion-limited oxidation applied to oxidation profiles monitored by chemiluminescence in hydroxy-terminated polybutadiene," *Polym. Int.*, vol. 49, no. 9, pp. 937–942, 2000, doi: 10.1002/1097-0126(200009)49:9<937::AID-PI399>3.0.CO;2-8.
[128] J. Saunier, V. Mazel, C. Paris, and N. Yagoubi, "Polymorphism of Irganox 1076®: Discovery of new forms and direct characterization of the polymorphs on a medical device by Raman microspectroscopy," *Eur. J. Pharm. Biopharm.*, vol. 75, no. 3, pp. 443–450, Aug. 2010, doi: 10.1016/j.ejpb.2010.04.014.
[129] S. Roland, G. Miquelard-Garnier, M. Gervais, A. Guinault, and C. Sollogoub, "Controlling the order of triblock copolymer via confinement induced by forced self-assembly," *Mater. Today Commun.*, vol. 6, pp. 37–43, Mar. 2016, doi: 10.1016/j.mtcomm.2015.11.003.
[130] European Standard EN 60216-2:2005, "Electrical insulating materials — Thermal endurance properties — Part 2: Determination of thermal endurance properties of electrical insulating materials — Choice of test criteria." 2005.
[131] L. Simoni, *Resistenza alle sollecitazioni dei materiali isolanti elettrici - Teoria dell'invecchiamento, modelli matematici di vita e valutazione della resistenza alle sollecitazioni elettrica e termica, singole e combinate.*, vol. II. Editrice CLUEB Bologna, 1994.

LIST OF FIGURES

LIST OF TABLES